2023

EXPERIMENTAL AND NUMERICAL ANALYSES OF COUPLED THERMO-HYDRO-MECHANICAL BEHAVIOR IN UNSATURATED SOIL UNDER ONE-DIMENSIONAL HEAT TRANSFER

Nice Kaneza

Recommended Citation

Kaneza, Nice, "EXPERIMENTAL AND NUMERICAL ANALYSES OF COUPLED THERMO-HYDRO-MECHANICAL BEHAVIOR IN UNSATURATED SOIL UNDER ONE-DIMENSIONAL HEAT TRANSFER" (2023). *Civil Engineering Dissertations*. 492.
https://mavmatrix.uta.edu/civilengineering_dissertations/492

EXPERIMENTAL AND NUMERICAL ANALYSES OF COUPLED THERMO-HYDRO-MECHANICAL BEHAVIOR IN UNSATURATED SOIL UNDER ONE-DIMENSIONAL HEAT TRANSFER

BY

NICE KANEZA

Presented to the Faculty of the Graduate School of
The University of Texas at Arlington

In Fulfillment of the Requirements for the Degree of

DOCTOR OF PHILOSOPHY IN CIVIL ENGINEERING

THE UNIVERSITY OF TEXAS AT ARLINGTON

DECEMBER 2023

To God, My Family, and My Friends

ACKNOWLEDGEMENTS

I would like to express my sincere gratitude to Dr. Xinbao Yu, my academic advisor and supervisor, for entrusting me and giving me the opportunity to work on this research project. I am truly thankful to the members of my graduate committee, Dr. Laureano R. Hoyos, Dr. Md Sahadat Hossain, and Dr. Haiying Huang, for the insights and time that have been given to me. I would also like to sincerely thank my colleagues Mehran Azizian and Gang Lei for helping me and enriching my knowledge of heat transfer in unsaturated soil during my research project. I would like to express my appreciation to my colleagues Suman Shrestha, Prachi Saha Rini, Alireza Fakhrabadi, Ayoub Mohammadi, and Taryn DiLorenzo for guiding and assisting me with all the research work that I have conducted at the University of Texas at Arlington.

I am grateful for the Women in Transportation Seminar for their huge support, and Dwight David Eisenhower Transportation Fellowship Program (DDETFP), as well as the United States Department of Transportation (USDOT) and the Federal Highway Administration (FHWA) for supporting me financially during my research.

My deepest gratitude is due to God for His love, grace, and mercy in every single step. My warmest thanks to my parents, Callixte Muzungu and Agnes Mujawayezu, and my siblings Nicole Muhire, Santiana Munezero, and Hervé Niyongabo for their love and cheerfulness. I am also thankful to my friends Yves Rudaseswa Mireille Ishimwe Hope Uwamahoro, Jean de Dieu Mubiligi, Ben Mugabo, Yvette Tuyishime, and Abraham Ishimwe for showing their support and warmth during my studies.

December, 2023

ABSTRACT

Experimental and Numerical Analyses of Coupled Thermo-Hydro-Mechanical Behavior in Unsaturated Soil under One-Dimensional Heat Transfer

Nice Kaneza, E.I.T.

The University of Texas at Arlington

Supervising Professor: Dr. Xinbao Yu

Comprehension of the behavior of unsaturated soil in response to thermal gradients, moisture gradients, and deformation is important in geotechnics. Thermal gradients control fluid density and viscosity and moisture gradients alter thermal properties of unsaturated soil. Similarly, thermal gradients affect the thermal strain of unsaturated soil and changes in porosity influence hydraulic properties of the soil. Thus, thermal, hydraulic, and mechanical properties of unsaturated soil interact with and influence each other; the combination of these interactions form a mechanism called coupled thermo-hydro-mechanical (THM) processes. Although the study of the behavior of coupled THM processes is essential in predicting the performance of geo-structures, complex and lengthy field-scale and laboratory experiments, as well as limitations in existing numerical models of coupled THM processes impede a thorough evaluation of this behavior.

Therefore, this study aims to provide a comprehensive evaluation of coupled TH and THM processes of unsaturated soil experimentally and numerically. A series of soil heating tests were performed to examine the coupled THM and TH processes, and experiments were conducted in different modified soil testing devices of different sizes and configuration, and they equipped with measuring devices will measure key soil properties; i.e. temperature, thermal conductivity, volumetric water content, matric suction, and heat flux. Two soil samples soil samples were tested under various moisture content and temperature conditions. Additionally, an improved mathematical framework was implemented in a multiphysics simulation software to predict the coupling behavior of THM processes.

The study also assesses thermal contact resistance at the soil-structure interface under varying moisture content and density levels using experimental and numerical approaches in a closed-system column testing apparatus. Results show that increasing moisture levels lead to higher temperature differences and reduced thermal contact resistance. Dense soils exhibit higher heat transfer, and loose soils show a correlation between thermal contact resistance and moisture content. Then, this study evaluates the impact of a grout in ground heat exchangers, revealing its effect on heat transfer and suggesting improvements for design. The study also analyzes how moisture migration in soil varies with initial moisture content, affecting hydraulic, thermal, and mechanical properties. Finally, the influence of gravity on moisture migration is examined through heating tests on silty sand with a thermal gradient, considering different initial moisture contents.

Keywords: coupled thermo-hydro-mechanical processes, ground heat exchanger, multiphysics, thermal contact resistance, unsaturated soil.

TABLE OF CONTENTS

LIST OF FIGURES

LIST OF TABLES

CHAPTER 1. INTRODUCTION

1.1 Overview

Geotechnical engineering is a broad field and is highly interconnected with other fields. Recently, energy geotechnics has been applied to geotechnical engineering in the areas of geothermal energy exchange, extraction and storage (Başer et al. 2018; Miao et al. 2016; Zhuang et al. 2014; Zymnis and Whittle 2021), and energy waste disposal (Birkholzer et al. 2023; Börgesson et al. 2001; Nagasaki and Nakayama 2015; Rutqvist et al. 2001, 2011; Sánchez et al. 2012). To understand the concepts of energy geotechnics, it is crucial to identify the geotechnical aspects that constitute unsaturated soil. Unsaturated soil is composed of three components and three phases, as illustrated in Fig. 1-1 (Abed and Sołowski 2017). The three components are pore air, pore water, and solid soil particles, while the three phases are gas, liquid, and solid phases. Water consists of liquid water and water vapor. Dry air and water vapor constitute the gas phase, whereas dissolved air and liquid water constitute the liquid phase. The mechanisms that occur in unsaturated soil include thermal processes, hydraulic processes, and mechanical processes.

In thermal processes, energy (heat) is transferred from warmer solid particles to cooler solid particles through the mode of heat conduction. This is due to thermal gradients occurring in the soil. In addition, buoyancy forces causes warm fluid to move away from the heat source and cooler fluids towards it, through the mode of convection, when a fluid is heated. Besides, in hydraulic processes, differences in hydraulic potential initiate the movement of water and air in the pore space of unsaturated soil. Moreover, mechanical processes involve changes in soil stress and strain, which are the main parameters identified in energy geotechnics. Fig. 1-2 (Sánchez et al. 2016b) portrays the features of the single processes, as well as the interaction of the single processes with other processes, in two directions. While temperature changes in soil alter the fluid density and viscosity of pore water, fluid flow, caused by heat convection, controls the thermal conductivity and specific heat of soil. Temperature changes also modify the strain, and the increase or reduction of porosity affects heat transfer in the soil. On the other hand, the varying porosity influences fluid flow in the pores, and fluid flow, in turn, modifies the effective stress and suction. The combined effects and interaction of these processes produce a paired mechanism called coupled thermo-hydro-mechanical (THM) processes, which are the subject of many studies, including tunneling and deep-level mining stability (Blair et al. 2002; Wu et al. 2017; Zhu et al. 2015), coupled soil heat and water transfer in agronomy (Davis et al. 2014; Heitman et al. 2007b; Zhou et al. 2006), and freeze/thaw cycles behavior in unsaturated soils (Casini et al. 2013; Sweidan et al. 2022; Zhang et al. 2021). This last field involves partially frozen porous media and the phase change of pore water (ice and unfrozen water) needs to be considered. Many studies, such as the present one only consider temperatures above the freezing point.

The purpose of this research is to study experimentally and numerically the behavior of coupled THM processes of unsaturated soil in one-dimensional heat transfer using fully coupled equations. This will be achieved by performing a numerical simulation and verifying the simulation results with experimental results performed in a modified column testing device. The study of coupled THM processes is done as an extension of either thermo-hydro (TH), hydro-mechanical (HM), thermo-mechanical (TM) processes. Under these non-isothermal conditions, it is crucial to conduct an elaborate study of the behavior of unsaturated soil experiencing the combined mechanisms of TH, HM, and TM effects on the gas, liquid, and solid phases of the porous medium.

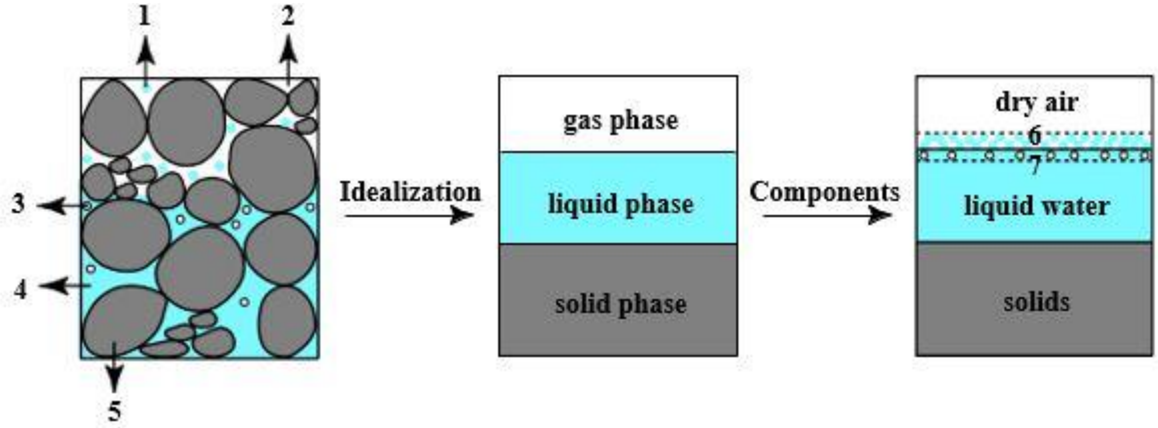

Fig. 1-1. Components and phases of unsaturated soil (Abed and Sołowski 2017).

1 and 6: water vapor; 2: dry air; 3 and 7: dissolved air; 4: liquid water; 5: solid grain.

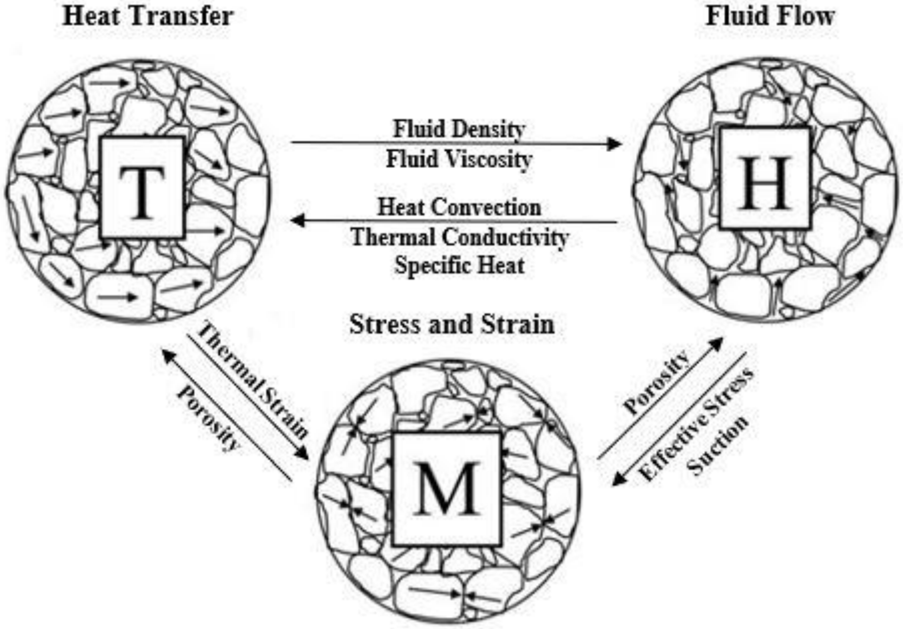

Fig. 1-2. Illustration of the single and coupled THM processes (Sánchez et al. 2016).

1.2 Problem Statement

It is essential to have a sound scientific understanding of coupled THM processes in unsaturated soil for the purpose of geothermal energy extraction/injection and other applications. This task, however, is challenged by various sources of problems, including the complexity of the equipment and mathematical formulations to efficiently study the coupling of THM processes. Experimental studies (Dang 2017; Hedayati-Dezfooli 2016; Heitman et al. 2007a; Zhou et al. 2006) have been conducted to study the coupling of TH processes using developed and improved closed soil column testing devices, but the apparatuses did not include functionality that assess mechanical processes, which are frequently paired with the TH processes. Similarly, numerical studies (Dang 2017; Deru 2003; Philip and de Vries 1957; de Vries 1958) were carried out to establish the full coupling of THM processes, but they missed accounting for non-equilibrium phase change in the heat transfer and water transfer models, that was more recently elaborated by Baser et al. (2018), McCartney and Baser (2017), Moradi et al. (2016), and Smits et al. (2011). In addition, monotonic heating and cooling and cyclic heating and cooling of unsaturated soil were experimentally studied by Faizal et al. (2021), and the researcher found that cyclic heating and cooling is a better alternative for the long-term performance of single energy piles. However, the study lacked evaluating different soil samples of grain sizes, and the imposed temperature boundaries are lower than those sometimes encountered in the field for deep geo-structures or heating/cooling systems combined with heat storage (> 60°C (Gabrielsson et al. 2000; Lottner et al. 2000; Reuss et al. 1997)). Therefore, this research aims to numerically study the fully coupled THM behavior of soil by considering various ranges of soil particle sizes, imposing temperature boundaries typically found in the field for GSHP systems, and considering non-equilibrium phase change in the existing coupled THM formulations, then verify the results using a simple soil column-testing device.

1.3 Objective

The ultimate objective of this study is to evaluate the coupling of TH and THM processes in a simple, modified soil column testing device, by subjecting soil specimens of different gradation to static heating and cooling. In addition, a mock-up model of a geothermal heat exchanger (energy pile surrounded by unsaturated soil) was designed and heating tests were performed to emulate field conditions and study the behavior of coupled TH processes. Accordingly, four tasks are designed to achieve the goal of this study.

(1) Analyzing numerically and experimentally the coupled THM behavior of unsaturated soil in a modified soil cell.

(2) Evaluating the influence of gravity on moisture migration under different direction of thermal gradient.

(3) Determining the thermal contact resistance at the interface of a heated pipe surrounded by unsaturated soil and evaluate how moisture levels and soil density impact this critical parameter.

(4) Assessing the influence of the application of thermal ground around a ground heat exchanger using a combination of experimental and numerical methods.

1.4 Novelty of this Work

This study presents a comprehensive experimental and numerical analyses to examine the coupling behavior of THM and TH processes conducted in simple, well-equipped soil testing devices. In addition, these experiments will serve to verify an improved numerical model that combines and couples the latest findings in the mathematical framework of coupled TH processes with the existing framework of mechanical properties.

The experimental and numerical analyses of this study seek to provide an extension of previous research studies. The consideration of water vaporization as a function of time has been explored in the aforementioned research studies, and it has been shown that non-equilibrium water vapor diffusion is critical to accurately assess the coupling of TH processes. However, this consideration has not yet been applied when the mechanical field is added to and coupled with the thermal and hydraulic fields. This study provides an opportunity to fill this gap and implement this novelty on various types of soil using a laboratory-scale column testing device and a mock-up geothermal heat exchanger model.

1.5 Dissertation Structure

The structure of this thesis is outlined as follows.

Chapter 2 gives a brief overview on geothermal heat extraction, explaining its necessity and its impact on the ecosystem. Additionally, the chapter summarizes past research on the numerical coupling of thermo-hydro-mechanical (THM) behavior in unsaturated soil. It also highlights the current state of the field, points out weaknesses in existing research, and suggests potential improvements.

In Chapter 3, numerical analyses of two soil samples, sandy silt and silty sand, are presented. These samples were tested under different moisture levels at a specific temperature gradient. The chapter proposes an enhanced method for assessing the coupling of heat transfer, moisture movement, and soil deformation. The development of the mathematical framework for this approach is discussed.

In Chapter 4, the study assesses the influence of gravity on the moisture movement in unsaturated soil. Gravity's impact on pore water migration is explored in relation to the direction of the temperature gradient.

Chapter 5 examines how heat and moisture affect the thermal contact resistance at the interface of a heated pipe surrounded by unsaturated soil. Various combinations of moisture levels and soil density states are evaluated, and an improved method for determining thermal contact resistance is discussed.

In Chapter 6, the research evaluates the impact of applying thermal grout around a ground heat exchanger. Tests are conducted to gauge the presence of thermal grout and determine if it enhances or limits heat transfer in the ground heat exchanger system.

Finally, Chapter 7 offers a summary and conclusions for all the research presented in the dissertation. It also provides recommendations for improving future analyses of coupled thermo-hydro-mechanical (THM) and thermal-hydraulic (TH) behaviors.

Each chapter includes a list of references for the cited research.

1.6 References

Abed, A. A., and W. T. Sołowski. 2017. “A study on how to couple thermo-hydro-mechanical behaviour of unsaturated soils: Physical equations, numerical implementation and examples.” *Comput Geotech,* 92: 132–155. Elsevier Ltd. https://doi.org/10.1016/j.compgeo.2017.07.021.

Başer, T., Y. Dong, A. M. Moradi, N. Lu, K. Smits, S. Ge, D. Tartakovsky, and J. S. McCartney. 2018. “Role of Nonequilibrium Water Vapor Diffusion in Thermal Energy Storage Systems in the Vadose Zone.” *Journal of Geotechnical and Geoenvironmental Engineering*, 144 (7): 04018038. American Society of Civil Engineers (ASCE). https://doi.org/10.1061/(asce)gt.1943-5606.0001910.

Birkholzer, J. T., A. Bond, and https://decovalex.org/. 2023. “DEvelopment of COupled models and their VALidation against EXperiments (DECOVALEX).” Accessed March 29, 2022. https://decovalex.org/.

Blair, S. C., S. R. Carlson, K. Lee, and L. Livermore. 2002. *Approved for public release; further* *dissemination unlimited Coupled THM Simulations of the Drift Scale Test at Yucca Mountain*.

Börgesson, L., M. Chijimatsu, T. Fujita, T. S. Nguyen, J. Rutqvist, and L. Jing. 2001. *Thermo-hydro-mechanical characterisation of a bentonite-based buffer material by laboratory tests and numerical back analyses*. *International Journal of Rock Mechanics & Mining Sciences*.

Casini, F., A. Gens, S. Olivella, and G. M. B. Viggiani. 2013. "Coupled phenomena induced by freezing in a granular material." *International Symposium, ISSMGE*, 215: 467–473.

Dang, L. 2017. *Experimental and Numerical Studies of Heat and Moisture Transfer in Soils at Various Conditions*.

Davis, D. D., R. Horton, J. L. Heitman, and T. Ren. 2014. "An Experimental Study of Coupled Heat and Water Transfer in Wettable and Artificially Hydrophobized Soils." *Soil Science Society of America Journal*, 78 (1): 125–132. Wiley. https://doi.org/10.2136/sssaj2013.05.0182.

Deru, M. 2003. *A Model for Ground-Coupled Heat and Moisture Transfer from Buildings*.

Faizal, M., A. Bouazza, and J. S. McCartney. 2021. "Thermohydraulic Responses of Unsaturated Sand around a Model Energy Pile." *Journal of Geotechnical and Geoenvironmental Engineering*, 147 (10): 04021105. American Society of Civil Engineers (ASCE). https://doi.org/10.1061/(asce)gt.1943-5606.0002640.

Gabrielsson, A., U. Bergdahl, and L. Moritz. 2000. "Thermal Energy Storage in Soils at Temperatures Reaching 90oC." *J Sol Energy Eng*, 112: 3–8.

Hedayati-Dezfooli, M. 2016. *DEVELOPMENT OF AN EXPERIMENTAL APPARATUS FOR STUDYING HIGH-TEMPERATURE HEAT AND MASS TRANSFER IN SOILS*.

Heitman, J. L., F. Battaglia, R. M. Cruse, B. K. Hornbuckle, and T. J. Sauer. 2007a. *Measurement of coupled soil heat and water processes*.

Heitman, J. L., R. Horton, T. Ren, and T. E. Ochsner. 2007b. “An Improved Approach for Measurement of Coupled Heat and Water Transfer in Soil Cells.” *Soil Science Society of America Journal*, 71 (3): 872. https://doi.org/10.2136/sssaj2006.0327.

Lottner, V., M. E. Schulz, and E. Hahne. 2000. “Solar-Assisted District Heating Plants: Status of the German Programme Solarthermie-2000.” *Solar Energy,* 69(6): 449–459.

McCartney, J. S., and T. Baser. 2017. “Role of Coupled Processes in Thermal Energy Storage in the Vadose Zone.” *Symposium on Coupled Phenomena in Environmental Geotechnics (CPEG2),* 2–7.

Miao, X. Y., C. Beyer, U. J. Görke, O. Kolditz, H. Hailemariam, and T. Nagel. 2016. “Thermo-hydro-mechanical analysis of cement-based sensible heat stores for domestic applications.” *Environ Earth Sci,* 75 (18). Springer Verlag. https://doi.org/10.1007/s12665-016-6094-3.

Moradi, A., K. M. Smits, N. Lu, and J. S. McCartney. 2016. “Heat Transfer in Unsaturated Soil with Application to Borehole Thermal Energy Storage.” *Vadose Zone Journal*, 15 (10): 1–17. Wiley. https://doi.org/10.2136/vzj2016.03.0027.

Nagasaki, S., and S. Nakayama. 2015. *Radioactive waste engineering and management.* Springer.

Philip, J. R., and D. A. de Vries. 1957. “Moisture movement in porous materials under temperature gradients.” *Transactions of the American Geophysical Union,* 38(2): 222–232.

Reuss, M., M. Beck, and J. P. Muller. 1997. “Design of a Seasonal Thermal Energy Storage in the Ground.” *Solar Energy,* 59(4–6): 247–257.

Rutqvist, J., L. Börgesson, M. Chijimatsu, A. Kobayashi, L. Jing, T. S. Nguyen, J. Noorishad, and C.-F. Tsang. 2001. *Thermohydromechanics of partially saturated geological media:*

governing equations and formulation of four finite element models. *International Journal of Rock Mechanics & Mining Sciences*.

Rutqvist, J., C. Steefel, J. Galindez, J. Birkholzer, and H.-H. Liu. 2011. *Modeling Coupled THM Processes and Reactive Diffusive Transport in Engineered Barrier Systems (EBS)*.

Sánchez, M., A. Gens, and L. Guimarães. 2012. "Thermal-hydraulic-mechanical (THM) behaviour of a large-scale in situ heating experiment during cooling and dismantling." *Canadian Geotechnical Journal*, 49 (10): 1169–1195. https://doi.org/10.1139/T2012-076.

Sánchez, M., A. Gens, M. V. Villar, and S. Olivella. 2016a. "Fully Coupled Thermo-Hydro-Mechanical Double-Porosity Formulation for Unsaturated Soils." *International Journal of Geomechanics,* 16 (6): D4016015. https://doi.org/10.1061/(asce)gm.1943-5622.0000728.

Sánchez, M., A. Gens, M. V. Villar, and S. Olivella. 2016b. "Fully Coupled Thermo-Hydro-Mechanical Double-Porosity Formulation for Unsaturated Soils." *International Journal of Geomechanics,* 16 (6). American Society of Civil Engineers (ASCE). https://doi.org/10.1061/(asce)gm.1943-5622.0000728.

Smits, K. M., A. Cihan, T. Sakaki, and T. H. Illangasekare. 2011. "Evaporation from soils under thermal boundary conditions: Experimental and modeling investigation to compare equilibrium-and nonequilibrium-based approaches." 47: 5540. https://doi.org/10.1029/2010WR009533.

Sweidan, A. H., K. Niggemann, Y. Heider, M. Ziegler, and B. Markert. 2022. "Experimental study and numerical modeling of the thermo-hydro-mechanical processes in soil freezing with different frost penetration directions." *Acta Geotech,* 17 (1): 231–255. Springer Science and Business Media Deutschland GmbH. https://doi.org/10.1007/s11440-021-01191-z.

de Vries, D. A. 1958. "Simultaneous transfer of heat and moisture in porous media." *EOS*

(Transactions, American Geophysical Union), 39: 909–916.

Wu, D., Y. Zhang, R. Zhao, T. Deng, and Z. Zheng. 2017. "A coupled thermal-hydraulic-mechanical application for subway tunnel." *Comput Geotech*, 84: 174–182. Elsevier Ltd. https://doi.org/10.1016/j.compgeo.2016.12.006.

Zhang, G., E. Liu, G. Zhang, and Y. Chen. 2021. "Study thermo-hydro-mechanical coupling behaviors of saturated frozen soil based on granular solid hydrodynamics theory." *Archive of Applied Mechanics*, 91 (9): 3921–3936. Springer Science and Business Media Deutschland GmbH. https://doi.org/10.1007/s00419-021-01987-1.

Zhou, J., J. L. Heitman, R. Horton, T. Ren, T. E. Ochsner, L. Prunty, R. P. Ewing, and T. J. Sauer. 2006. "Method for Maintaining One-Dimensional Temperature Gradients in Unsaturated, Closed Soil Cells." *Soil Science Society of America Journal*, 70 (4): 1303–1309. Wiley. https://doi.org/10.2136/sssaj2005.0336n.

Zhu, W. C., C. H. Wei, L. L. Niu, and S. Li. 2015. "Damage and Unstable Failure of Rock under Coupled THM Conditions during Deep-level Mining." *13th International Congress of Rock Mechanics*. International Society for Rock Mechanics.

Zhuang, X., R. Huang, C. Liang, and T. Rabczuk. 2014. "A coupled thermo-hydro-mechanical model of jointed hard rock for compressed air energy storage." *Math Probl Eng*, 2014. https://doi.org/10.1155/2014/179169.

Zymnis, D. M., and A. J. Whittle. 2021. "Geotechnical considerations in the design of borehole heat exchangers." *Canadian Geotechnical Journal*, 58 (9): 1247–1262. Canadian Science Publishing. https://doi.org/10.1139/cgj-2020-0118.

CHAPTER 2. LITERATURE REVIEW

2.1 Geothermal Energy Extraction

Ground-source heat pumps (GSHP) are widely used in geothermal energy applications to heat and cool buildings during seasonal variations. They are one of the most energy-efficient, economical, and environmentally-friendly conditioning systems, and they make use of renewable energy (Environmental Protection Agency 1993; Toby Couture et al. 2019). The use of GSHP systems increases the potential for greater thermal efficiency, in addition to a significant reduction in energy consumption in comparison to other heating systems. The reduction in energy consumption may attain 44-72 percent, and the associated air pollution emissions are reduced to approximately the same extent (Environmental Protection Agency 1993). Although the capital cost of GSHP systems can be high, their operational cost is low, and a residential building may economize up to 60 percent of annual utility expenses, as compared to conventional heating and cooling systems (Lienau et al. 1995; US Department of Energy 1998). Moreover, they present the best alternative in terms of reducing the production of greenhouse gas (GHG) emissions in relation to other heating, ventilation, and air conditioning (HVAC) systems. For instance, in the United States, using GSHP can produce 2.2 ton/year less than using oil heating and 10.3 tons/year less than electric heating, while in Canada, the savings can reach 2.7 tons/year, 5.3 tons/year, and 3.4 tons/year against the use of natural gas, oil heating, and electric heating, respectively (European Environment Agency. 2008; Government of Canada 2008; US Energy Information Administration 2011).

GSHP systems consist of borehole heat exchangers that transfer heat from earth to (above ground) air and from air to earth. These can be vertical or horizontal closed-loop systems or open-loop systems. The vertical closed-loop systems may include geothermal energy piles. The energy pile systems are drilled shafts that are inserted vertically into the ground down to about 100 m (330 ft.), where the temperature is relatively constant. High-density polyethylene (HDPE) pipes are installed in the borehole heat exchangers and circulate a fluid in the pipes. The fluid typically used is water mixed with anti-freeze agents. In the winter, heat is extracted from the ground and distributed to the building to warm up the building, while in the summer, heat is absorbed from the building and transferred it to the ground to cool down the building.

It is important to properly design GSHP systems to ensure efficient performance of the systems. The long-term performance of energy piles can be affected by unbalanced temperature variations of the soil surrounding the energy piles (Fadejev et al. 2017; Shang et al. 2011; Xiao and Suleiman 2015). At the soil-energy pile interface, heat is transferred from the soil to the energy pile during heat extraction and heat is transferred from the energy pile to the soil during heat injection, as shown in Fig. 2-1 (Gashti et al. 2014). Fast heating of the energy pile can eventually result in a low pile capacity caused by increases in the soil pore water pressure under undrained conditions of the soil (Loveridge et al. 2020). Besides, it was remarked by Akrouch (Akrouch et al. 2016) that the soil surrounding the energy pile dries with continued heat extraction and injection cycles, which also marginally decreases the soil’s thermal conductivity. When unsaturated soil is subjected to temperature changes, as a result of geothermal heat exchanges, thermal gradients control the movement of water inside the soil pores. As pore water moves, the temperature, thermal proprieties, and matric suction in the soil are redistributed (Cahill and Parlange 1998; Jackson 1973). Temperature fluctuations also affects the volumetric strain of the soil surrounding the energy pile (Agar et al. 1986, 1987).

Although a scientific understanding of coupled THM processes in unsaturated soil is essential for the efficient long-term performance of GSHP, the distribution of soil key parameters in the field is transient and difficult to examine. Moreover, despite the importance of the coupling of THM processes, the complexity of the available equipment makes it difficult to effectively study this coupled phenomenon in the laboratory. Additionally, theories have been developed to predict the redistribution of thermal, hydraulic, and mechanical properties, but only a few have been effective for accurately estimating water and temperature distributions in a laboratory setting. In this study, experimental tests will be performed in the laboratory to analyze the coupled THM phenomenon of unsaturated soil, using a modified model of a double column-type testing device developed by Zhou et al. (2006). This study provides an advanced understanding of the coupled THM processes of unsaturated soil on a small scale.

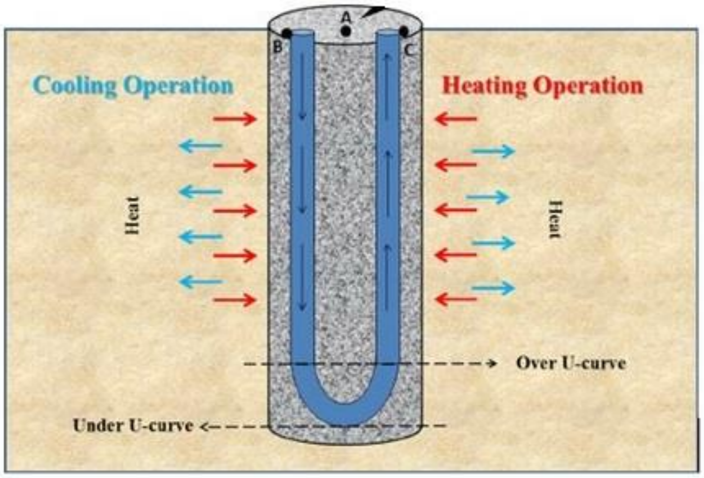

Fig. 2-1. Soil-structure interaction around an energy pile (Gashti et al. 2014)**.**

2.2 Numerical Simulation

Although an experimental analysis can provide a great opportunity to understand the coupling of THM processes, numerical analysis of this coupling is also crucial. Verification and validation of the numerical simulation with experimental results are also as important. Fully coupled THM problems are impractical to study analytically, and this raises the need to study this coupling numerically. First, it is necessary to evaluate the meaning of the terms “fully coupled”. Other terms, such as “uncoupled” or (just) “coupled” will also be defined herein, to better understand the contrast of all these terms.

Since it has been determined that heat and moisture movement are correlated, it would be ineffective to study the two motions separately, and this would be considered as a study of uncoupled TH processes. This uncoupling could lead to neglecting the importance of heat convection, resulting from heating a fluid, for example. An overestimation of the apparent vapor diffusion (Gurr et al. 1952; Taylor and Cavazza 1954) and erroneous estimation of the temperature and water regimes in sandy soil (Shen and Ramsey 1988) could also result from this separation. Moreover, using over-simplified equations that do not represent the actual coupling behavior of TH/THM processes may lead to imprecisions, though these equations are considered coupled. Neglecting the effect of gravity (gravitational equilibrium) (Rees et al. 2001) or neglecting latent heat transfer (Janssen et al. 2002) are examples of over-simplifications. This may also result in underestimation of heat transfer and moisture movement (Cahill and Parlange 1998; Philip and de Vries 1957). Therefore, fully coupled equations take into account all pertinent coupling of TH/THM processes. For instance, considering heat convection and non-equilibrium water vapor diffusion can significantly improve the analysis of coupled TH/THM processes (Smits et al. 2011). Even so, the use of the term "fully coupled" for TH/THM processes does not, and should not, imply closing the door on future opportunities to further improve the coupling of these processes. The following paragraphs briefly summarizes the studies conducted in view of establishing fully coupled equations. The term "coupled THM" will be used in this study to refer to "fully coupled" for brevity.

Originally, moisture movement in unsaturated porous media was estimated by using the fluid flow equation or Richard's equation (Richards 1931). This approach, however, omitted important factors, such as the phase change between liquid and gas and non-isothermal effect on fluid flow (Sullivan 2013). Later on, Taylor and Cavazza (1954) observed that moisture flow in non-isothermal conditions (moisture migration from cooler region to warmer region) occurs largely in the vapor phase. In response, liquid water flows back from the cooler region to the warmer region due to induced potential gradient of moisture flow. These researchers used the air gap technique to detect this moisture flux and noticed that the measured vapor diffusion was 10 times (1 order in magnitude) higher than the diffusion normally obtained from Fick's law of diffusion. Fick's law is used to determine the diffusion coefficient. Thus, they suggested that this discrepancy was a result of the coupling of heat transfer and moisture movement.

Next, Philip and de Vries (1957) developed a model describing liquid water and vapor water flow in porous media under non-isothermal conditions based on an extended version (Penman 1940) of Richard's equation. They expressed water movement (both in the liquid phase and vapor phase) as a function of temperature gradient and volumetric water content, then attempted to determine an enhancement factor (η) of the vapor diffusion to correct the discrepancy between the theoretical and experimental data of vapor diffusion that was previously observed. Their theory was applicable for temperature ranges of 10-30ºC concerning the ratio of the average temperature gradient to the overall temperature gradient and 0-75ºC concerning the thermal conductivity calculations. However, these researchers neglected heat convection, which reduced the total vapor diffusion, and assumed equilibrium phase change, where pore water evaporates instantaneously. Subsequent researchers established a fitting parameter to adjust η (Cass et al. 1984) and included the heat convection that was missing in the previous model (Cahill and Parlange 1998), but omitted to address the fallacious assumption of equilibrium phase change.

Accordingly, Smits et al. (2011) developed a model that accounts for non-equilibrium phase change, where pore water vaporizes gradually with time. The researchers emphasized the importance of vapor transport in coupled TH processes. Additionally, Moradi et al. (Moradi et al. 2016) and McCartney and Baser (2017) extended the model of Smits et al. (2017), integrated a new set of coupled TH constitutive equations, and implemented an approach to determine the enhancement factor of vapor diffusion and the vapor phase change rate. Other recent approaches include those of Deru (2003) and Dang (2017). Deru (2003) developed a two-dimensional model to study coupled TH processes and estimated the heat conductive term to be dominant. Dang (2017) then developed one-dimensional and two-dimensional (axisymmetric) finite-volume methods to verify Deru's (2003) equations and verified the one-dimensional formulation with experimental tests involving high temperature boundary conditions (up to 90°C) and different moisture flow scenarios (vertical and horizontal). The researcher observed a relatively good agreement between the measured and predicted data.

This study will use the model of Moradi et al. (2016) and McCartney and Baser (2017) for fully coupled TH processes, and the model will be extended by coupling the mechanical processes, to establish fully coupled THM processes. Previous researchers established computational models, such as the CODE-BRIGHT (Olivella et al. 1994), ROCMAS (Noorishad and Tsang 1996), FRACON (Nguyen 1996), THAMES (Ohnishi and Kobayashi 1996), ABAQUS-CLAY (AQCLAY) (Börgesson 1996), etc to study coupled THM processes. Principles of finite-element method (FEM) were applied to establish the computational models. The models were predicted prior to the obtention of the corresponding experimental data. Some of these models are only applicable to particular materials; i.e. rock, fractured rocks, expansive clay (bentonite, mixed bentonite). Therefore, for a more general form of the models, fully coupled equations were established in this study and are specifically designed for non-expansive porous media; these equations are described in the next section.

For this study, COMSOL Multiphysics was selected for the numerical simulation of fully coupled THM processes. It is a numerical modelling program that uses the finite element method to simulate real-world designs and fully coupled multiphysics in porous media. The fully coupled equations are solved numerically and simultaneously as partial differential equations. Determining the proper geometry, as well as the correct boundary conditions of the finite element mesh, has a significant influence on the final results of the modelling using COMSOL Multiphysics. The governing equations and constitutive equations used in this study are further detailed in Chapter 3.

2.3 References

Agar, J. G., N. R. Morgenstern, and J. D. Scott. 1986. "Thermal Expansion and Pore Pressure Generation in Oil Sands." *Canadian Geotechnical Journal*, 23: 327–333.

Agar, J. G., N. R. Morgenstern, and J. D. Scott. 1987. "Shear Strength and Stress-Strain Behaviour of Athabasca Oil Sand at Elevated Temperatures and Pressures." *Canadian Geotechnical Journal*, 24: 1–10.

Akrouch, G. A., M. A. Sanchez, and J.-L. Briaud. 2016. "An experimental, analytical, and numerical study on the thermal efficiency of energy piles in unsaturated soils." *Comput Geotech*, 71: 207–220.

Börgesson, L. 1996. "ABAQUS." *Developments in Geotechnical Engineering*, 79 (C): 565–570. Elsevier. https://doi.org/10.1016/S0165-1250(96)80047-2.

Cahill, A., and M. Parlange. 1998. "On Water Vapor Transport In Field Soils." 34 (4): 731–739.

Cass, A., G. S. Campbell, and T. I. Jones. 1984. "Enhancement of thermal water vapor diffusion in soil." *Soil Sci. Soc. Am.*, 48 (1): 25–32.

Dang, L. 2017. *Experimental and Numerical Studies of Heat and Moisture Transfer in Soils at*

Various Conditions.

Deru, M. 2003. *A Model for Ground-Coupled Heat and Moisture Transfer from Buildings*.

Environmental Protection Agency. 1993. "Space Conditioning: The Next Frontier – Report 430-R-93-004."

European Environment Agency. 2008. *Energy and environment report 2008*. European Environment Agency.

Fadejev, J., R. Simson, J. Kurnitski, and F. Haghighat. 2017. "A review on energy piles design, sizing and modelling." *Energy,* 122: 390–407. Elsevier Ltd. https://doi.org/10.1016/j.energy.2017.01.097.

Gashti, E. H. N., V. M. Uotinen, and K. Kujala. 2014. "Numerical modelling of thermal regimes in steel energy pile foundations: A case study." *Energy Build,* 69: 165–174. https://doi.org/10.1016/j.enbuild.2013.10.028.

Government of Canada. 2008. "National Inventory Report 1990–2006:Greenhouse Gas Sources and Sinks in Canada. Canada's Greenhouse Gas Inventory."

Gurr, C. G., T. J. Marshall, and J. T. Hutton. 1952. "Movement of Water in Soil due to a Temperature Gradient." *Soil Sci,* 74(5): 335–346.

Jackson, R. D. 1973. "Diurnal Changes in Soil Water Content During Drying." https://doi.org/10.2136/sssaspecpub5.c3.

Janssen, H., J. Carmeliet, and H. Hens. 2002. "The Influence of Soil Moisture in the Unsaturated Zone on the Heat Loss from Buildings via the Ground." *Journal of THERMAL ENV. & BLDG. SCI,* 25 (4). https://doi.org/10.1106/109719602023683.

Lienau, P. J., T. L. Boyd, and R. L. Rogers. 1995. "Ground-Source Heat Pump Case Studies and Utility Programs." *Geo-Heat Center, Oregon Institute of Technology*.

Loveridge, F., J. S. McCartney, G. A. Narsilio, and M. Sanchez. 2020. “Energy geostructures: A review of analysis approaches, in situ testing and model scale experiments.” *Geomechanics for Energy and the Environment,* 22. Elsevier Ltd. https://doi.org/10.1016/j.gete.2019.100173.

McCartney, J. S., and T. Baser. 2017. “Role of Coupled Processes in Thermal Energy Storage in the Vadose Zone.” *Symposium on Coupled Phenomena in Environmental Geotechnics (CPEG2),* 2–7.

Moradi, A., K. M. Smits, N. Lu, and J. S. McCartney. 2016. “Heat Transfer in Unsaturated Soil with Application to Borehole Thermal Energy Storage.” *Vadose Zone Journal,* 15 (10): 1–17. Wiley. https://doi.org/10.2136/vzj2016.03.0027.

Nguyen, T. S. 1996. “Description of the computer code FRACON.” *Developments in Geotechnical Engineering*, 79 (C): 539–544. Elsevier. https://doi.org/10.1016/S0165-1250(96)80043-5.

Noorishad, J., and C. F. Tsang. 1996. “ROCMAS simulator; A thermohydromechanical computer code.” *Developments in Geotechnical Engineering,* 79 (C): 551–558. Elsevier. https://doi.org/10.1016/S0165-1250(96)80045-9.

Ohnishi, Y., and A. Kobayashi. 1996. “Thames.” *Developments in Geotechnical Engineering,* 79 (C): 545–549. Elsevier. https://doi.org/10.1016/S0165-1250(96)80044-7.

Olivella, S., J. Carrera, A. Gens, and E. E. Alonso. 1994. *Nonisothermal Multiphase Flow of Brine and Gas Through Saline Media*. *Transp Porous Media*.

Penman, H. L. . 1940. “Gas and vapor movement in soil: I. The diffusion of vapors in porous solids.” *J. Agri. Sci.,* 437–462.

Philip, J. R., and D. A. de Vries. 1957. “Moisture movement in porous materials under temperature gradients.” *Transactions of the American Geophysical Union,* 38(2): 222–232.

Rees, S. W., Z. Zhou, and H. R. Thomas. 2001. “The influence of soil moisture content variations on heat losses from earth-contact structures: an initial assessment.” *Build Environ*, 36 (2): 157–165. Pergamon. https://doi.org/10.1016/S0360-1323(99)00063-3.

Richards, L. A. 1931. “CAPILLARY CONDUCTION OF LIQUIDS THROUGH POROUS MEDIUMS.” *Citation: Physics*, 1: 318. https://doi.org/10.1063/1.1745010.

Shang, Y., S. Li, and H. Li. 2011. “Analysis of geo-temperature recovery under intermittent operation of ground-source heat pump.” *Energy Build*, 43 (4): 935–943. https://doi.org/10.1016/j.enbuild.2010.12.017.

Shen, L. S., and J. W. Ramsey. 1988. “An investigation of transient, two-dimensional coupled heat and moisture flow in the soil surrounding a basement wall.” *Int J Heat Mass Transf*, 31 (7): 1517–1527. Pergamon. https://doi.org/10.1016/0017-9310(88)90259-1.

Smits, K. M., A. Cihan, T. Sakaki, and T. H. Illangasekare. 2011. “Evaporation from soils under thermal boundary conditions: Experimental and modeling investigation to compare equilibrium-and nonequilibrium-based approaches.” 47: 5540. https://doi.org/10.1029/2010WR009533.

Sullivan, E. 2013. “Heat and Moisture Transport in Unsaturated Porous Media -- A Coupled Model in Terms of Chemical Potential.”

Taylor, S. A., and L. Cavazza. 1954. “The Movement of Soil Moisture in Response to Temperature Gradients.” *Soil Science Society of America*, 18: 351–358.

Toby Couture, Henner Busch, Flávia Guerra, Teis Hansen, Anna Leidreiter, Hannah E. Murdock, Lea Ranalder, Janet L. Sawin, and Kristin Seyboth. 2019. *Renewables in Cities - 2019 Global Status Report*.

US Department of Energy. 1998. “Geothermal Heat Pump Consortium, Inc.”

US Energy Information Administration. 2011. *Voluntary Reporting of Greenhouse Gases 2009: Summary*.

Xiao, S., and M. T. Suleiman. 2015. “Investigation of Thermo-Mechanical Load Transfer (t-z Curves) Behavior of Soil-Energy Pile Interface Using Modified Borehole Shear Tests.” 1658–1667. https://doi.org/10.1061/9780784479087.150.

Zhou, J., J. L. Heitman, R. Horton, T. Ren, T. E. Ochsner, L. Prunty, R. P. Ewing, and T. J. Sauer. 2006. “Method for Maintaining One-Dimensional Temperature Gradients in Unsaturated, Closed Soil Cells.” *Soil Science Society of America Journal*, 70 (4): 1303–1309. Wiley. https://doi.org/10.2136/sssaj2005.0336n.

CHAPTER 3. EVALUATING THE COUPLED THERMO-HYDRO-MECHANICAL PROCESSES OF UNSATURATED SANDY SILY AND SILTY SAND IN ONE-DIMENSIONAL HEAT TRANSFER

3.1 Introduction

Many researchers have investigated the coupling of TH/HM/THM processes of unsaturated soil experimentally. Generally, soil testing devices differ according to the field of study, and the types of devices that make up the majority of the experimental tests conducted are the closed-system soil testing devices (Type I, Fig. 3-1) and the open-system soil testing devices (Type II, Fig. 3-2). Type I is closed at the top and bottom boundaries, meaning that there is no moisture flux that can be generated at the top and bottom boundary and the side of the device are insulated. This type is mainly used in geosystems applications (Dang 2017; Hedayati-Dezfooli 2016) to simulate the field conditions of geo-structures, for example. It is also used in the soil science applications (Heitman et al. 2007a; b; Zhou et al. 2006). Type II is open at either the top or bottom the device or has two opening at the top and bottom of the device, meaning that a fluid flux can be generated from the openings. This type is essentially used in the study of nuclear waste disposal (Börgesson et al. 2001; Rawat et al. 2019; Saba et al. 2013; Tripathy et al. 2017; Villar et al. 2005) and is more practical when testing expansive clays. The opening are used to infiltrate water into the soil and the infiltrated water represents the water that saturates the backfill clay (barrier) excavated in the host rock (Villar et al. 2005). This is done to simulate the interaction of heat and water occurring in clay barriers placed between the host rock and waste canister in repositories for nuclear waste disposal (Börgesson et al. 2001; Cuevas et al. 1997).

Typically, Type I is equipped with instruments such as thermocouples (TCs), time domain reflectometry (TDR) sensors or thermo-time domain reflectometry (T-TDR) sensors, whereas

Type II is equipped with TCs, relative humidity (RH) sensors, pore pressure sensors, load cells, and pressure transducers. Type I has been used to assess the coupled TH processes only, while Type II has been used to assess the coupled THM processes. Therefore, the testing period for Type I may take up to 5 days, when it may take several months for Type II. A summary of the differences of these two types are summarized in Table 3-1.

The study of Bouyoucos (1915) is among the earliest studies on the paired heat and moisture transfer in soil columns relating to Type I. The researcher developed two separate wooden boxes, each containing cold water (0°C) and warm water (20 and 40°C) and placed 20.3-cm high and 3.8-cm wide columns consisting of various types of soil with different moisture content in the boxes. The soil samples included sandy loam, silt loam, and clay. The researcher concluded that the soil behavior was influenced by the laws of surface tension and viscosity of water in soil until the critical moisture content was attained; thereupon, the soil hydraulic processes were controlled by the strong attractive forces of soil for water. It was also noticed that for the highest temperature gradient (corresponding to temperature boundaries of 40 to 0°C), a greater amount of water was transferred from the warmer to the cooler portion of the soil column. These findings were corroborated by various subsequent researchers (Gurr et al. 1952; Jackson et al. 1965; Kuzmak and Sereda 1957a; b; Maclean and Gwatkin 1953; Taylor and Cavazza 1954). They determined that the quantity of water migrating from warm to cool regions was influenced mainly by the initial moisture content and magnitude of temperature gradients. They also suggested that this migration in unsaturated soil is due to the vapor pressure variations from warm to cool locations in the soil. Temperature gradient is responsible for moisture flow in the vapor phase, while suction gradient is responsible for moisture flow in the liquid phase. Soil properties and initial moisture conditions will determine the extent and direction of the moisture flux.

More recently, Nassar and Horton (1989) developed soil cells that were sealed laterally, but the radial ambient temperature interfered with the imposed axial temperature, which hindered one-dimensional heat transfer. Later, Prunty and Horton (1994) developed other soil cells and attempted to limit this ambient temperature interference (ATI); however, the cells were too small and did not allow ample flexibility for experimental studies. Hence, Prunty (2003) enlarged the soil cells, but this modification did not address the ATI. Therefore, Zhou et al. (2006) developed four configurations of a double soil cell consisting of an inner soil cell containing a control soil specimen and an outer cell containing a buffer soil specimen to impede the ATI. The two soil specimens in both cells were identical. The four configurations were: short-wide (SW), long-wide (LW), short-narrow (SN), and long-narrow (LN). Heitman et al. (2007b) used the SW configuration and further validated one-dimensional heat transfer in the soil cell. Later on, Hedayat-Dezfooli (2016) developed a similar device and Dang (2017) modified it to include plexiglass insulation in the outer soil cell, instead of a buffer soil specimen, and the device was designed for temperatures up to 90ºC.

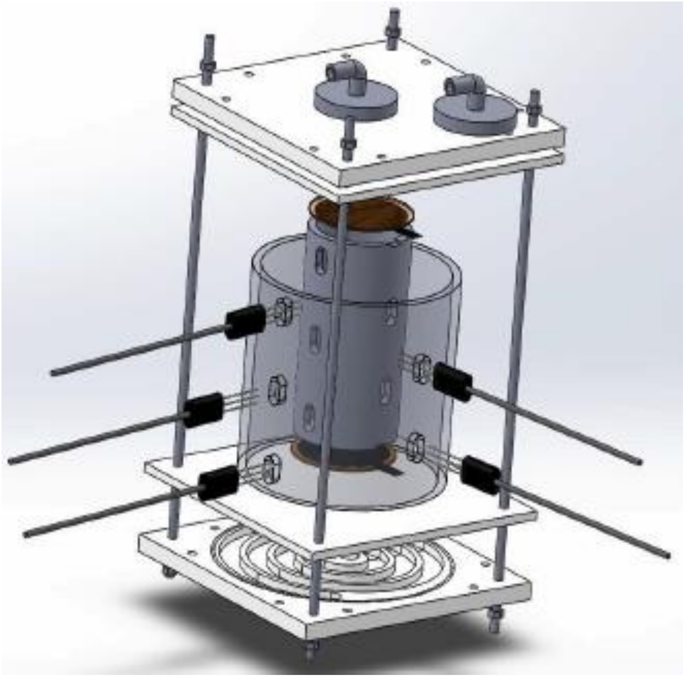

Fig. 3-1. Example of a Type I soil testing device (Hedayati-Dezfooli 2016)**.**

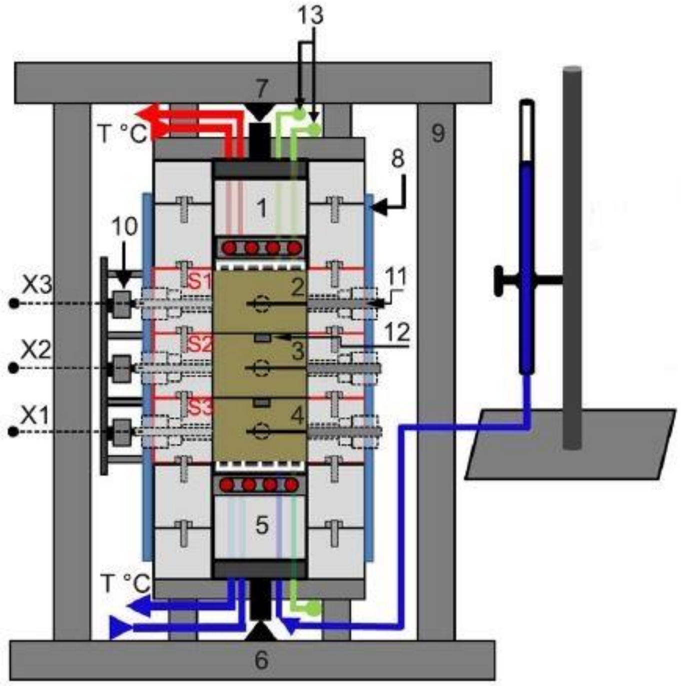

Fig. 3-2. Example of a Type II soil testing device (Rawat et al. 2019)**.**

Table 3-1. Differences in Type I and Type II soil testing devices.

Properties/Features	Soil cell - Type I	Soil cell - Type II
Boundary temperature (warm end)	40 ≤ 60°C (up to 90°C)	≤ 100°C
Boundary temperature (cool end)	10-20°C	≤ 20°C or free (no temperature imposed/initial ambient temperature)
Water intake	None	Some
Test time	A few days (up to 5 days)	Multiple days (up to several months)
Tested soil	Sand, silt, silty clay	Highly expansive clay (bentonite)
Measured properties (*measuring device*)	Temperature (*thermocouples, T-TDR*), volumetric water content (TDR/*T-TDR*), thermal conductivity (*T-TDR*), thermal diffusivity (*T-TDR*), volumetric heat capacity (*T-TDR*)	Temperature (*thermocouples*), volumetric water content (*TDR/T-TDR*), relative humidity *(RH sensors*), pore pressure (*PP sensors*), axial stress (*vertical load cell*), radial stress (*radial load cell*), intermediate pressure (*pressure transducer*)
Columns	Single/Double	Single
Complexity	Low	High
Objective	TH	TH/THM/THMC

The idea behind using a soil column to study the behavior of soil is portrayed in Fig. 3-3. This figure exemplifies the selection of a segment of a clay barrier around a waste canister. In a laboratory setting, a soil column is installed vertically and heated at the bottom and cooled at the top or heated at the top and cooled at the bottom, or even heated on one side and cooled at the other side when the soil column is set-up horizontally; this is done to replicate the field conditions.

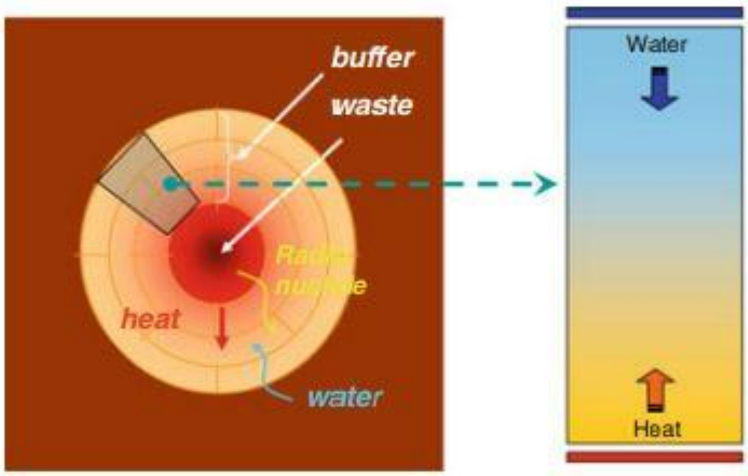

Fig. 3-3. Illustration of a soil column (Schanz et al. 2013)**.**

Other types of experimental apparatuses that have been used to study the coupled TH/THM processes are soil boxes (Alrtimi et al. 2014; Faizal et al. 2021; Moradi et al. 2015; Wang and Su 2010) and are shown in Fig. 3-4. Faizal et al. (2021) developed a soil box, where a model energy pile was installed in the middle; a warm fluid was circulated in the pipe inside the energy pile and the researcher studied the coupled TH processes of the soil under monotonic and cyclic heating. Moradi et al. (2015) also tested soil in vadose zone in a soil box, where the sides of the box were heated, and the heat and moisture migration were monitored using devices installed along the length of the box. Alrtimi (2014) developed two soil columns and placed them on the two sides of a heater installed vertically, so as to simulate soil surrounding an energy pile. Wang and Su (2010) used a similar set-up, but the heater was placed horizontally.

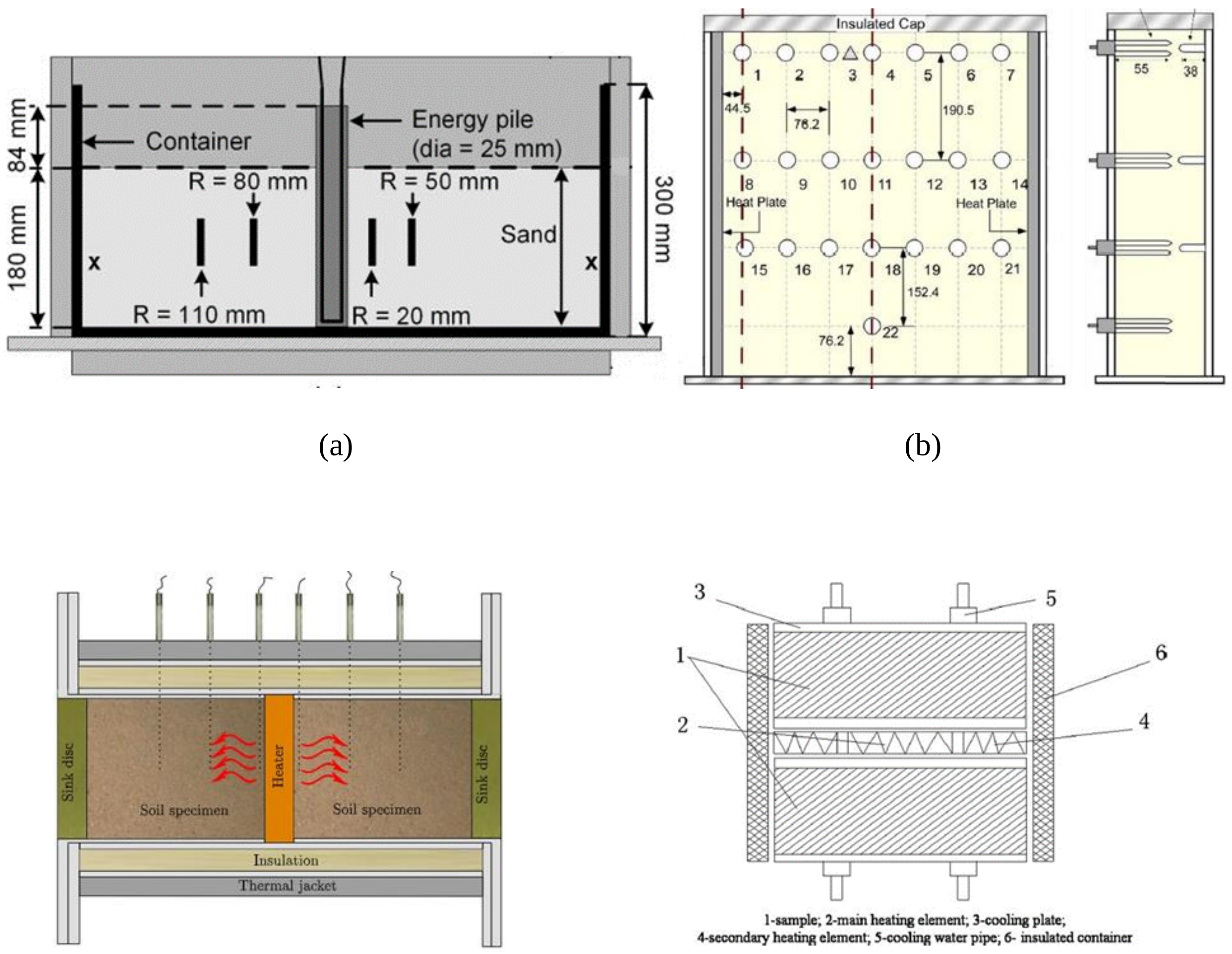

(a)

(b)

(c)

(d)

Fig. 3-4. Alternative soil testing devices (a) Faizal et al. (2021), (b) Moradi et al. (2015), (c) Alrtimi (2014), and (d) Wang and Su (2010).

In order to capture the major key parameters affected by the coupling of THM processes and of the testing, a combination of the features of Type I and Type II soil testing devices was planned. In this study, the LW configuration was selected for the laboratory experiments. This configuration was chosen to allow flexibility in experimental testing. This means that the device will provide enough room for the various instrumentation, so as not to interfere with each other. The modified soil cell will be composed of two heat exchangers, inner and outer soil cells, and other supporting items. The device will be equipped with TCs, T-TDR sensors, tensiometers, pressure transducers, and strain gauges to measure the variations of temperature, moisture, thermal properties, matric suction, pore pressure, and strain, respectively.

3.2 Experimental Procedures

3.2.1 Material Properties

The analysis of soil particle sizes was carried out to characterize two selected soil samples. One soil sample was classified as sandy silt (ML) , and another one as silty sand (SM) based on the Unified Classification System (USCS). The choice of soils with varying gradation/consistency (illustrated in Fig. 3-5) enabled a more extensive examination of the unsaturated soil's response in terms of thermal, hydraulic, and mechanical properties. Additionally, the soil-water retention properties of sandy silt and silty sand were evaluated. For the soil-water characteristic curve (SWCC) test, soil specimens were compacted at 95% of the maximum dry unit weight ($\gamma d,_{max}$) and the optimal moisture content (w_{opt}) determined from standard Proctor test results. Matric suction of the soil was estimated using the pressure plate method for low suction and the filter paper method for high suction. The relationship between the two methods was further explored by constructing a best-fitting curve employing the van Genuchten (1980) model, as illustrated in Fig. 3-6. Ultimately, the residual and saturated volumetric moisture content (θ_{res} and θ_s) were estimated, and empirical parameters from the van Genuchten model (α, n, and m) were determined. The soil particle properties and SWCC properties are summarized in Table 3-2.

Table 3-2. Differences in Type I and Type II soil testing devices.

	D_{60} (mm)	D_{30} (mm)	D_{10} (mm)	G_s (-)	θ_{sat} (m^3/m^3)	θ_{res} (m^3/m^3)	α (m^{-1})	n (-)	m (-)
Sandy silt	0.125	0.004	0.153	2.61	0.232	0.005	0.001	0.396	1.588
Silty sand	0.186	0.064	0.005	2.66	0.300	0.024	4.527	1.246	0.197

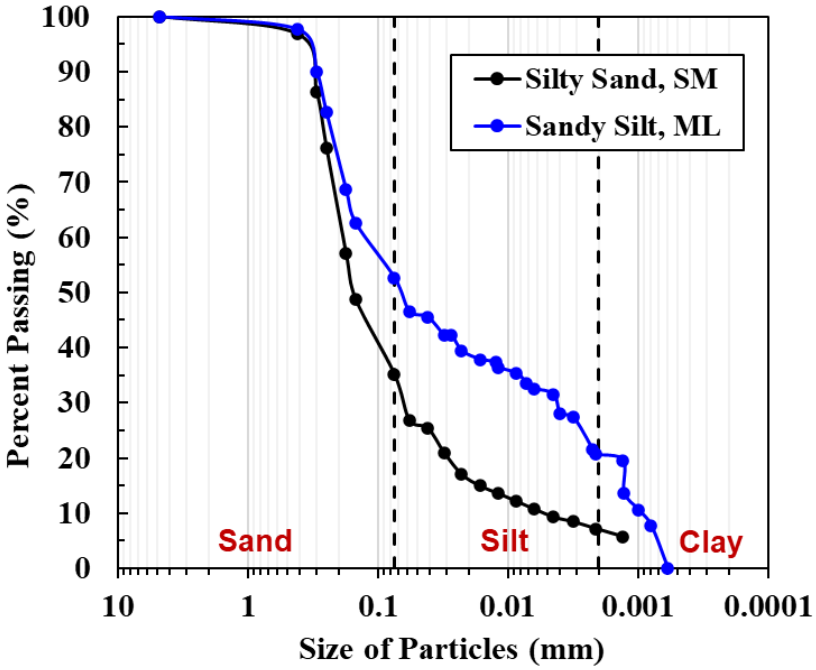

Fig. 3-5. Soil particle size distribution curves of sandy silt and silty sand.

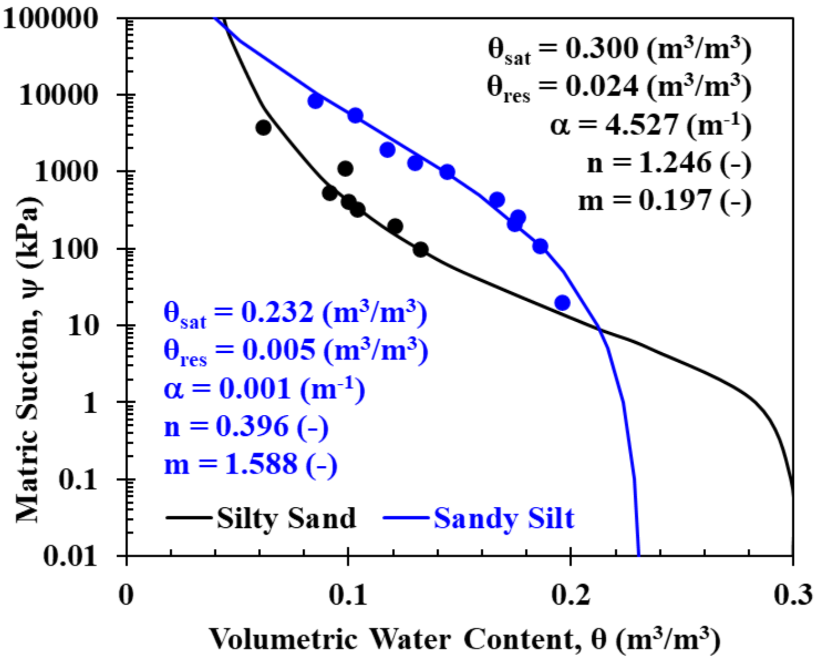

Fig. 3-6. Soil-water retention characteristics of sandy silt and silty sand.

3.2.1 Soil Properties Calibration

Since the heating tests of unsaturated soil involve transient thermal, hydraulic, and mechanical properties, it is important to calibrate certain soil properties to determine their variations and responses to temperature or moisture fluctuations. Therefore, soil thermal conductivity, which could not be captured at all desired location in the soil, was calibrated using the dry density and moisture variations. The calibration was conducted as follows: a mixture of water and silty sand, with moisture levels ranging from 0 to 21% gravimetric water content, was prepared. The soil was initially densely packed into a cylindrical mold with dimensions of 7.8 cm in diameter and 15 cm in height, undergoing compaction in three stages at room temperature. Subsequent to compaction, the density of the soil was determined. A thermal property sensor was inserted into the compacted soil to assess various thermal characteristics. Subsequently, small soil samples from the vicinity of the measured area were collected and subjected to oven-drying to determine the actual moisture content. These investigations aimed to establish correlations between water content, dry density, and thermal conductivity, providing insights into the influence of moisture on these properties.

Fig. 3-7 shows the compaction curve in relation to various moisture contents and their corresponding thermal conductivity. A regression analysis was conducted, considering thermal conductivity as the dependent variable and volumetric water content and dry density as independent variables. Eqs. (3-1) and (3-2) were derived for sandy silt and silty sand, respectively, and the comparison of the measured and predicted λ is shown in Fig. 3-8.

$$\lambda = -2.860 + 2.893\theta_w + 2.405\rho_d \tag{1}$$

$$\lambda = -4.359 + 3.360\theta_w + 3.023\rho_d \tag{2}$$

where λ: thermal conductivity [W/mK]; θ_w: volumetric water content [m^3/m^3]; and ρ_d: dry density [g/cm^3].

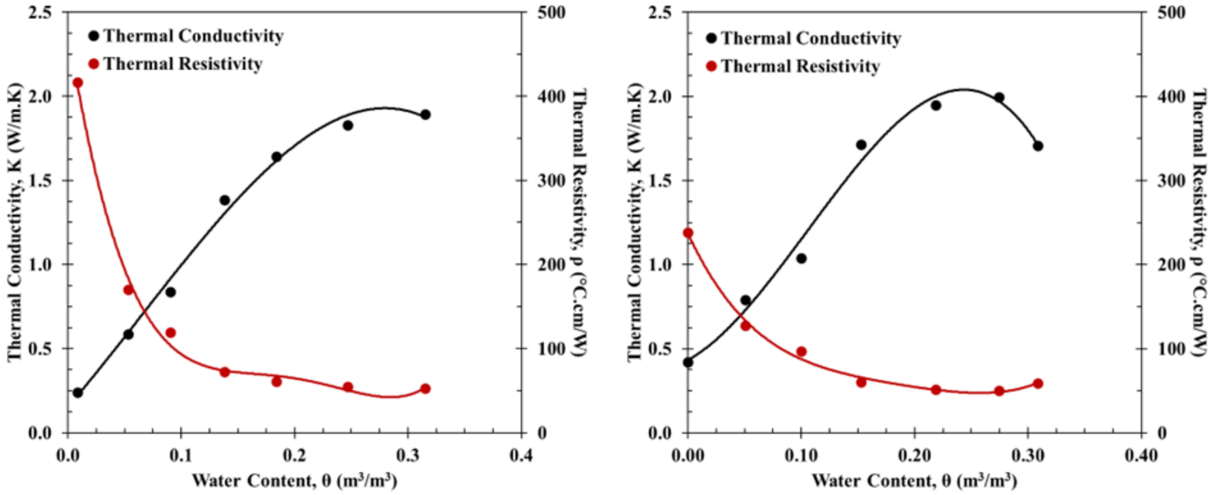

(a) (b)

Fig. 3-7. Thermal conductivity and density of (a) sandy silt and (b) silty sand.

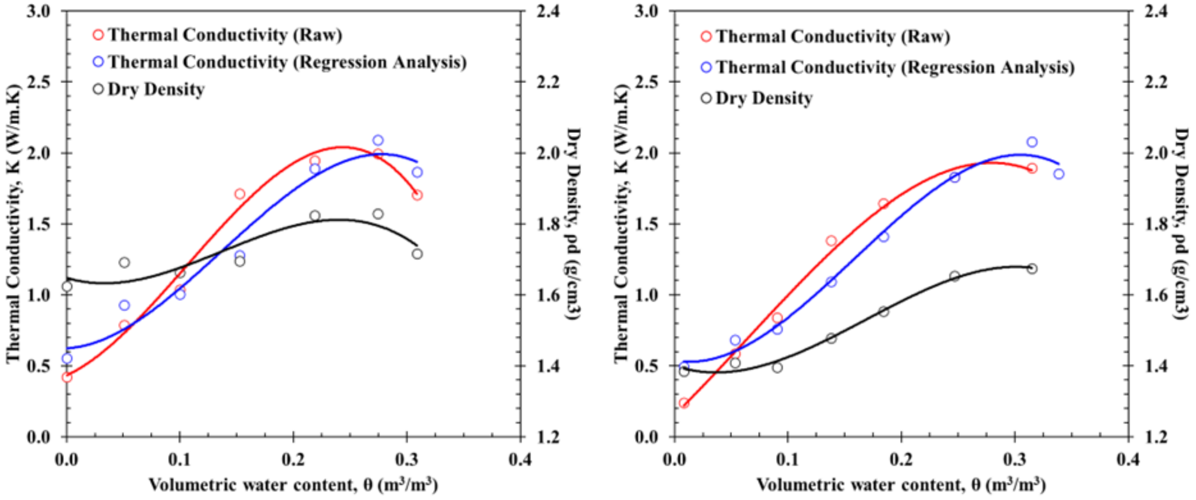

(a) (b)

Fig. 3-8. Thermal conductivity and density of (a) sandy silt and (b) silty sand.

3.2.2 Modified Soil Cell Device

A testing device, illustrated in Fig. 3-9, was modified from previous soil testing studies: the cell comprises an inner and an outer cell, 20.32 cm in height and 1.27 cm in thickness. The inside diameter of the inner cell has an inside diameter of 8.89 mm, and the outer cell has an inside diameter of 20.95 cm. Two heat exchanger plates, each 2.54 cm thick with a diameter of 29.21 cm, were placed at the top and bottom of the soil cells, and they feature an inner 6.5 mm x 6.5 mm spiral channel (Fig. 3-10), where warm and cool water was circulated from the temperature-controlled circulator (Model SD07R-20-A11B, PolyScience). A 0.238 cm thick copper plate with a diameter of 29.21 cm was placed at between the heat exchanger plates and the soil cells to uniformly distribute the water heat from warm water to the soil compacted in the soil cell. To connect the outer column to the heat exchanger plates, two ring plates and O-rings were employed. The heat exchangers incorporate threaded holes to maintain a sealed cell. The columns, heat exchanger plates, and rings are constructed from clear cast acrylic by Nationwide Plastics Inc.

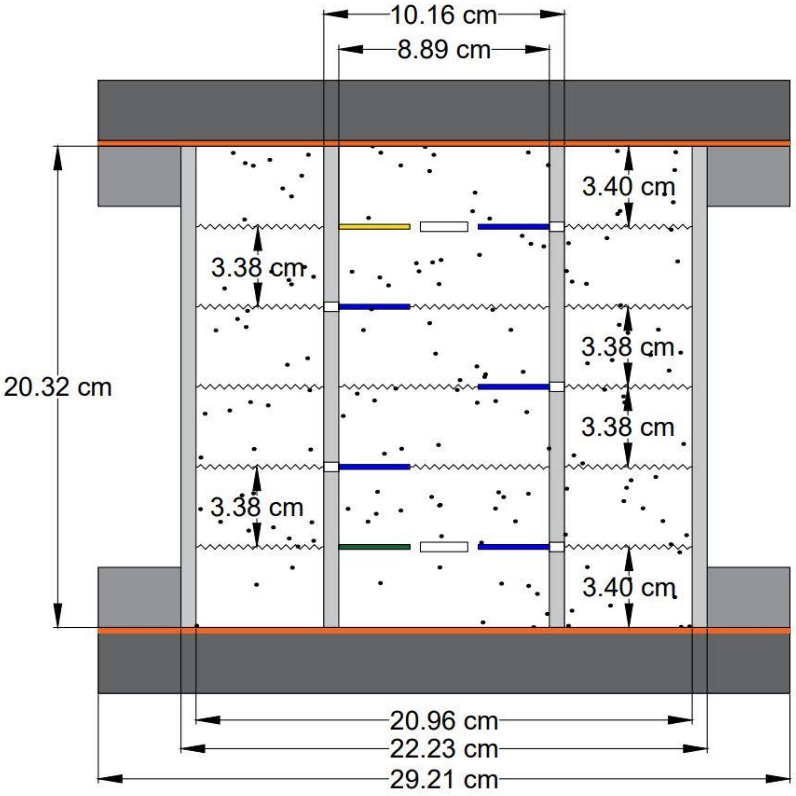

Fig. 3-9. Modified soil cell.

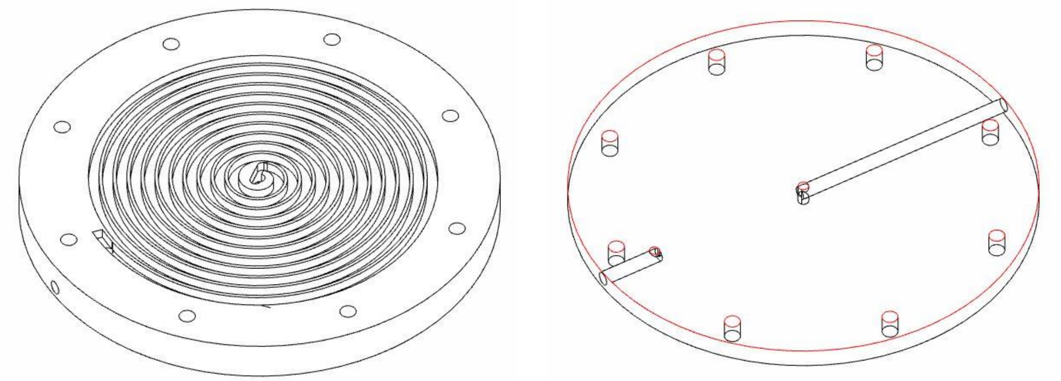

Fig. 3-10. Heat exchanger featuring a spiral channel for water circulation.

3.3 Numerical Procedures

3.3.1 Uncoupled Processes

To study the coupling of THM processes, it is critical to study each process individually. In this case, each of the three fields (thermal, hydraulic, and mechanical) is analyzed independently from the others. First, the thermal field is defined by Fourier's law of heat conduction ($q = -\lambda \nabla T$, Eq. 3-3) and the first law of thermodynamics (energy conservation) (Eq. 3-3). Fourier's law describes the proportionality of the thermal conductivity and negative thermal gradient ($-\nabla T$) to heat flux in a system. A convective term (CvT) was added to Eq. 3-3 to consider heat convection. The energy conservation states that the sum of the changes in internal energy ($C\frac{\partial T}{\partial t}$) and heat flux ($\nabla \cdot q$) is equal to the heat storage (Q). This means that the energy in the system cannot be created or destroyed.

$$q_h = -\lambda \nabla T + CvT \tag{3}$$

$$C\frac{\partial T}{\partial t} + \nabla \cdot q_h = Q \tag{4}$$

where q_h: heat flux (W/m^2); λ: thermal conductivity (W/m·K); T: temperature (K); ρ: density (kg/m^3); C: volumetric heat capacity (J/m^3·K); v: fluid velocity (m/s); t: time (s); Q: heat source or sink (W/m^3).

Next, the hydraulic field is defined by Darcy's law (derived from Stoke's equations) (Eq. 3-5) and the mass conservation law (Eq. 3-6). Eq. 3-6 specifies that the amount of fluid flow remains the same with time.

$$q_f = q_w + q_g + q_v \tag{5}$$

$$\rho \frac{\partial \theta}{\partial t} + \nabla \cdot \left(\rho q_f\right) = \mp R_{gw} \tag{6}$$

where q$_f$: fluid flux (m/s); q$_{w,g,v}$: liquid water/air/vapor velocity (m/s); ρ: fluid density (kg/m^3); θ: volumetric fluid content (m^3/m^3); R$_{gw}$: phase change rate (kg/m^3·s).

Lastly, the mechanical field is governed by Navier's equation. The stress in the system is defined by the momentum equation (Eq. 7) and the equation for strain-displacement is described by Eq. 8.

$$\nabla \cdot \sigma + F = 0 \tag{7}$$

$$\varepsilon = \frac{1}{2}[\nabla u + (\nabla u)^T] \tag{8}$$

where σ: stress tensor (Pa); F: body force vector (Pa/m); ε: strain tensor (-); u: deformation vector (mm).

3.3.2 Heat Transfer

The energy flow within a porous medium is mathematically represented by the following energy conservation equation Eq. (3-9). In this equation, several factors are considered, including the heat conduction within the solid soil particles, the heat convection involving the pore fluid (liquid water and air), and the phase change to water vapor. The left-hand side of the equation accounts for variation in heat and the transfer of heat within the soil through conduction and convection in different mediums such as liquid water (w), air (g), and water vapor (v). On the right-hand side, the terms represent the variations and movement of latent heat associated with water vapor.

$$C_{eq}\frac{\partial T}{\partial t} + \nabla \cdot \left(-\lambda_{eq}\nabla T\right) + C_{eq}\left(q_w\nabla T + q_g\nabla T + q_v\nabla T\right)$$

$$= -L_w\rho_w\nabla q_g - L_w\rho_w\frac{\partial \theta_g}{\partial t} - L_w\rho_w\nabla q_v - L_w\rho_w\frac{\partial \theta_v}{\partial t} \tag{9}$$

$$q_w = -K_{wh}\nabla(h+Z) - K_{wt}\nabla T \tag{10}$$

$$q_g = -K_{gh}\nabla(h) - K_{gt}\nabla T \tag{11}$$

$$q_v = -K_{vh}\nabla(h) - K_{vt}\nabla T \tag{12}$$

The equivalent volumetric heat capacity and thermal conductivity, as well as the latent heat of water vaporization, are given by the following equations.

$$C_{eq} = C_s\,\theta_s + C_w\,\theta_w + C_g\,\theta_g + C_v\,\theta_v \tag{13}$$

$$\lambda_{eq} = \lambda_s\,\theta_s + \lambda_w\,\theta_w + \lambda_g\,\theta_g + \lambda_v\,\theta_v \tag{14}$$

$$L_w = 2.501 \text{ x } 10^6 - 2369.2\,T \tag{15}$$

where C_{eq}: equivalent volumetric heat capacity ($J/m^3 \cdot K$); λ_{eq}: equivalent thermal conductivity ($W/m \cdot K$); L_w: latent heat of water vaporization (J/kg); $\rho_{w,g,v}$: liquid water/air/vapor density (kg/m^3); $\theta_{s,w,g,v}$: volumetric liquid water/air/vapor content (m^3/m^3); h: water head (m); K_{wh}: hydraulic conductivity of liquid water related to water head (m/s); K_{wt}: hydraulic conductivity of liquid water related to temperature (m/s); K_{gh}: hydraulic conductivity of air related to water head (m/s); K_{gt}: hydraulic conductivity of air related to temperature (m/s); K_{vh}: hydraulic conductivity of vapor related to water head (m/s); K_{vt}: hydraulic conductivity of vapor related to temperature (m/s); $C_{s,w,g,v}$: solids/liquid water/air/vapor volumetric heat capacity ($J/m^3 \cdot K$); $\lambda_{s,w,g,v}$: solids/liquid water/air/vapor thermal conductivity (W/m·K).

3.3.3 Fluid Flow

The mass flow describing the movement of pore liquid water, pore air, and water vapor is given by the following mass conservation equation. Richard's equation is used to quantify the pore fluid flow, where the movement is governed by the gradients in water head potential and temperature, and is proportional to hydraulic conductivity. The combined expression of water vapor movement involves both the isothermal flux component and a temperature-driven flux component, as proposed by (Philip and de Vries 1957). The final equation taking into account elastic strain due to fluid flow is described by Eq. 3-18.

$$\frac{\partial \theta}{\partial t} = -\nabla \cdot \ (q_w + q_g + q_v) \qquad (16)$$

$$\theta = \theta_w - \frac{\rho_g}{\rho_w}\theta_g - \frac{\rho_v}{\rho_w}\theta_v \qquad (17)$$

$$\frac{\partial \theta_w}{\partial t} + \nabla \cdot \ (q_w + q_g + q_v) = -\frac{\rho_g}{\rho_w}\frac{\partial \theta_g}{\partial t} - \frac{\rho_v}{\rho_w}\frac{\partial \theta_v}{\partial t} - \frac{\rho_{eq}}{\rho_w}\frac{\partial \varepsilon_{hp}}{\partial t} \qquad (18)$$

These equations involve the incorporation of the mass fraction of water vapor, denoted as w_v [-], and given by Eq. (3-19). Additionally, the phase diagram was utilized to determine the volumetric content of both water vapor and air.

$$w_v = \frac{\rho_v}{\rho_g} \qquad (19)$$

$$\theta_v = \frac{\theta_g}{w_v} \qquad (20)$$

$$\theta_g = w_v \frac{n - \theta_w}{(1 + w_v)} \qquad (21)$$

3.3.4 Stress and Deformation

Temperature fluctuations induce alterations in material volume, giving rise to thermal strains.

When a material lacks the ability to freely deform in response to volume variations, it experiences thermal stresses, influenced by factors such as thermal expansion capacity, modulus of elasticity, and constraint level. Consideration unsaturated soil as an elastic material, the momentum conservation equation can be described by the constitutive equation given by Eq. (3-22), which can then be extended to Eq. (3-23) to account for strains caused by heat transfer and fluid flow.

$$\sigma = C : \varepsilon \tag{22}$$

$$\sigma = D\varepsilon_{el} + \sigma_0 \tag{23}$$

where C: fourth-order tensor of material stiffness (Pa); D: stiffness matrix (Pa); ε_{el}: elastic strain (-); and σ_0: initial stress vector (Pa).

$$\varepsilon_{el} = \varepsilon - \varepsilon_{th} - \varepsilon_{hp} - \varepsilon_{tr} - \varepsilon_0 \tag{24}$$

where ε_{th}: strain caused by thermal expansion (-); ε_{hp}: strain caused by matric potential (-); ε_{tr}: strain caused by phase change of water (-); ε_0: initial strain (-). This study only considers the strains caused by thermal expansion and matric potential.

$$\varepsilon_{th} = [\alpha(T\text{-}T_{ref}), \alpha(T\text{-}T_{ref}), 0]^{T} \tag{25}$$

$$\varepsilon_{hp} = [h/\beta, h/\beta, 0]^{T} \tag{26}$$

where α: thermal expansion coefficient (1/K); T and T_{ref}: temperature at time t and reference temperature (K); and β: poro-elastic expansion coefficient (Pa).

3.3.5 Other Constitutive Equations

In order to address the equations governing heat transfer and fluid flow, it is crucial to establish certain constitutive relationships, namely, the water head potential and hydraulic conductivity. The relationship between water head and liquid water is defined by the soil-water characteristic curve (SWCC) based on van Genuchten's model. Furthermore, Mualem (1976) suggested the extension of this equation to calculate hydraulic conductivity. Consequently, we can express the water head potential and hydraulic conductivity as follows.

$$h = \frac{-\left(S_e^{-1/m} - 1\right)^{1/n}}{\alpha} \tag{27}$$

$$S_e = \frac{\theta_w - \theta_{res}}{\theta_{sat} - \theta_{res}} \tag{28}$$

$$K_{wh/gh} = K_s S_e^l \left(1 - \left(1 - S_e^{1/m}\right)^m\right)^2 \tag{29}$$

$$K_{wt/gt} = K_{wh/gt} \left(h G_{wT} \frac{1}{\gamma_0} \frac{d\gamma}{dT}\right) \tag{30}$$

$$\gamma_0 = 75.6 - 0.1425T - 2.38 \text{ x10-4} T^{2} \tag{31}$$

$$K_{vh} = \frac{D_a}{\rho_w} \rho_{vs} H_r \frac{Mg}{RT}$$

$$= \frac{2.12 \text{ x } 10\text{-}5 \ (\mathrm{T}/273.15)2 \ \frac{\theta_v^{\frac{10}{3}}}{\theta_{sat}^2}}{\rho_w} \left(\frac{\exp\left(31.37 - \frac{6014.79}{\mathrm{T}} - 7.92 \text{ x } 10^{-3}\mathrm{T}\right)}{10^3\mathrm{T}}\right) \exp\left(\frac{hM_g}{RT}\right) \frac{Mg}{RT} \tag{32}$$

$$K_{vt} = \frac{D_a}{\rho_w} \eta H_r \frac{d\rho_{vs}}{dT}$$

$$= \frac{2.12 \text{ x } 10^{-5} \ (\mathrm{T}/273.15)^2 \ \frac{\theta_v^{\frac{10}{3}}}{\theta_{sat}^2}}{\rho_w} \left(9.5 + 3\frac{\theta_v}{\theta_{sat}} - 8.5\, exp\left\{-\left[\left(1 + \frac{2.6}{\sqrt{fc}}\right)\frac{\theta_w}{\theta_{sat}}\right]^4\right\}\right)$$

$$\text{x } \exp\left(\frac{hM_g}{RT}\right) \frac{d\left(\frac{\exp\left(31.37 - \frac{6014.79}{\mathrm{T}} - 7.92 \text{ x } 10^{-3}\mathrm{T}\right)}{10^3\mathrm{T}}\right)}{dT} \tag{33}$$

$$\mathrm{D} = \begin{bmatrix} 2G + \lambda_e & \lambda_e & 0 \\ \lambda_e & 2G + \lambda_e & 0 \\ 0 & o & G \end{bmatrix} \tag{34}$$

$$\mathrm{G} = \frac{E}{2(1+\nu)} \tag{35}$$

$$\lambda_e = \frac{E\nu}{(1+\nu)(1-2\nu)} \tag{36}$$

$$F = -\rho_w g\beta(T-T_{ref}) \tag{37}$$

where S_e: effective saturation (-); a, m, n: van Genuchten parameters (-); θ_{res}: residual volumetric water content (m^3/m^3); θ_{sat}: saturated volumetric water content (m^3/m^3); K_s: saturated hydraulic conductivity (m/s); G_{wT}: gain factor (= ~7 for coarse soil); γ_0: surface tension at 25°C (N/m); γ: surface tension (N/m); D_a: vapor diffusivity (m^2/s); ρ_{vs}: vapor density (kg/m^3); H_r: relative humidity (-); M: molecular weight of water (kg/mol); g: gravitational acceleration (m/s^2); R: universal gas constant (J/mol·K); η: enhancement factor (-); f_c: clay fraction (-); G: shear modulus (Pa); λ_e: elastic modulus (Pa), E: Young's modulus (Pa); ν: Poisson's ratio (-).

3.3.6 Mathematical Formulation Implementation

In this study, the energy conservation and mass conservation equations were solved simultaneously using COMSOL Multiphysics, version 5.3, incorporating the corresponding constitutive equations. To accomplish this, the partial differential equations (PDEs) interface of the "Mathematics" physics was employed, specifically the coefficient form PDE, as defined in Eq. (38). Eqs (9), (18), and (23) respectively that represent the heat transfer, fluid flow, and stress and deformation, were rearranged to align with the coefficient form PDE equation, and the associated constants are presented herein.

$$e_a \frac{\partial^2 u}{\partial t^2} + d_a \frac{\partial \mathrm{u}}{\partial t} + \nabla \cdot (-c\nabla u - \alpha u + \gamma) + \beta \cdot \nabla \mathrm{u} + \mathrm{au} = f \tag{38}$$

where e_a: mass coefficient; u is the dependent variable (T for heat transfer and θ_w); d_a: damping coefficient; c = diffusion coefficient; a = conservative flux convection coefficient; γ: conservative flux source: β: convection coefficient; a = absorption coefficient; f: source term.

3.3.7 Soil Input Parameters

Thermal properties, moisture, stress, and deformation fluctuations in sandy silt and silty sand were predicted using simulations conducted in COMSOL Muliphysics. The purpose of this study was to assess the coupling of the thermo-hydro-mechanical processes of the two soil specimens. The model was simulated in a 2D axisymmetric space (Fig. 3-11), with the focus solely on the inner cell, as the soil specimen in the outer cell only serves as a soil buffer to limit ambient temperature interference. The top heat exchanger was subjected to 60°C, while the bottom heat exchanger was kept at 20°C. The initial temperature was set to 20°C. Two different initial moisture contents were analyzed (w = 6 and 10% or θ_w = 0.096 and 0.192 m^3/m^3, since the investigated dry density, ρ_d, was 1.6 g/cm^3). Soil displacement was limited to the limits of the soil cell wall, prohibiting movement away from the cell. The soil and other materials input parameters are summarized in Table 3-3.

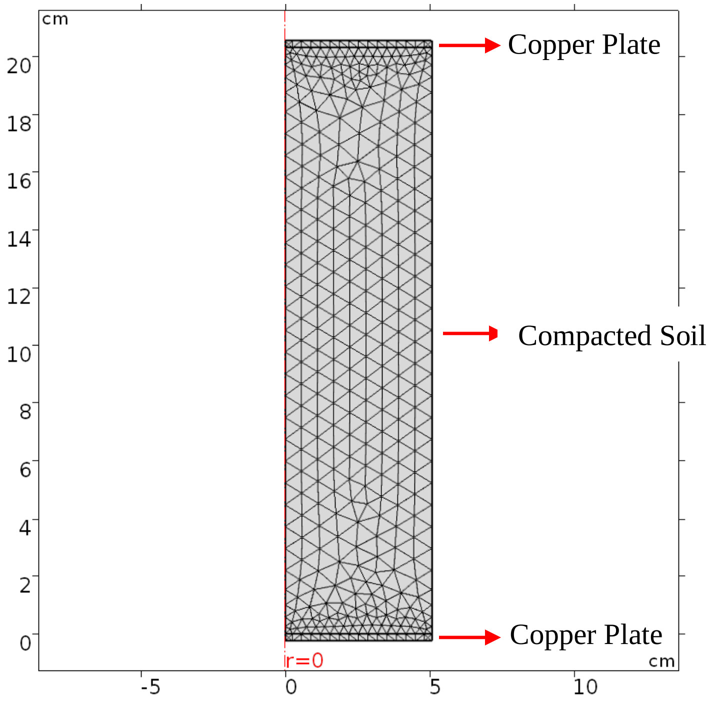

Fig. 3-11. COMSOL Model.

Table 3-3. Materials Input Parameters.

Parameter	Value	Units	Description
C_g	1000	J/(kg·K)	Specific heat capacity of air
C_s	950	J/(kg·K)	Specific heat capacity of sandy silt
C_s	850	J/(kg·K)	Specific heat capacity of silty sand
C_v	1000	J/(kg·K)	Specific heat capacity of vapor
C_w	4200	J/(kg·K)	Specific heat capacity of water
f_c	0.2	-	Clay fraction of sandy silt
f_c	0.07	-	Clay fraction of silty sand
g	-9.81	m/s^2	Acceleration
G_{wT}	3	-	Gain factor for sandy silt
G_{wT}	5	-	Gain factor for silty sand
Ks_g	3.20E-05	m/s	Hydraulic conductivity of air
Ks_w	3.20E-04	m/s	Hydraulic conductivity of water
M	18.01528	g/mol	Molecular weight of water
R	8.31432	J/mol·K	Universal gas constant
λ_g	0.025	W/m·K	Thermal conductivity of gas
λ_p	0.48	W/m·K	Thermal conductivity of pipe
λ_t	0.13	W/m·K	Thermal conductivity of tube
λ_v	0.025	W/m·K	Thermal conductivity of vapor
λ_w	0.6	W/m·K	Thermal Conductivity of water
nu_p	0.3		Poisson's Ratio
H	7653[Pa]	Pa	Poroelastic Expansion Coefficient
E	1e5[MPa]	Mpa	Young's Modulus
Beta	8e-7 [1/K]	1/K	Thermal Expansion Coefficient
ρ_g	1.2	kg/m^3	Density of gas
ρ_v	1000	kg/m^3	Density of water

3.4 Results and Discussions

3.4.1 Thermal Behavior in Unsaturated Soil

Steady-state conditions were reached in the temperatures of unsaturated soils approximately 2 days after initiation, with soils containing lower initial moisture content requiring a longer time for stabilization. This delay suggests that water movement and moisture redistribution within low-moisture soil, influenced by thermal behavior, occurred at a slower rate, resulting in a more gradual establishment of moisture flux compared to soils with higher initial moisture levels. By the end of the 2-day heating period, it is anticipated that the soil has achieved its thermal storage capacity. Figs. 3-12 and 3-13 depict the experimental temperature evolution over time, while Fig. 3-14 and 3-15 illustrate the steady-state temperature conditions after a 96-hour heating period.

Temperature profiles within the soil exhibit a concave shape, indicating moisture redistribution. Discrepancies between experimental measurements and numerically predicted temperatures are noticeable, particularly towards the warmer end, with the silty sand at a 6% moisture level showing more pronounced deviations. This discrepancy may arise from variations in material properties such as thermal conductivity (estimated through regression analysis before the heat testing), thermal diffusivity, soil density, or potential relocation of temperature sensors during soil compaction. Addressing this issue requires thorough investigations into material properties and ensuring test repeatability.

Additionally, heat loss occurred at the interfaces between the heat exchangers and compacted soil, primarily due to thermal contact resistance between copper plates and soil. Fig. 3-16 provides an overall temperature profile for the two soil specimens. Corrections to these discrepancies can be achieved through comprehensive investigations into material properties and ensuring the repeatability of tests.

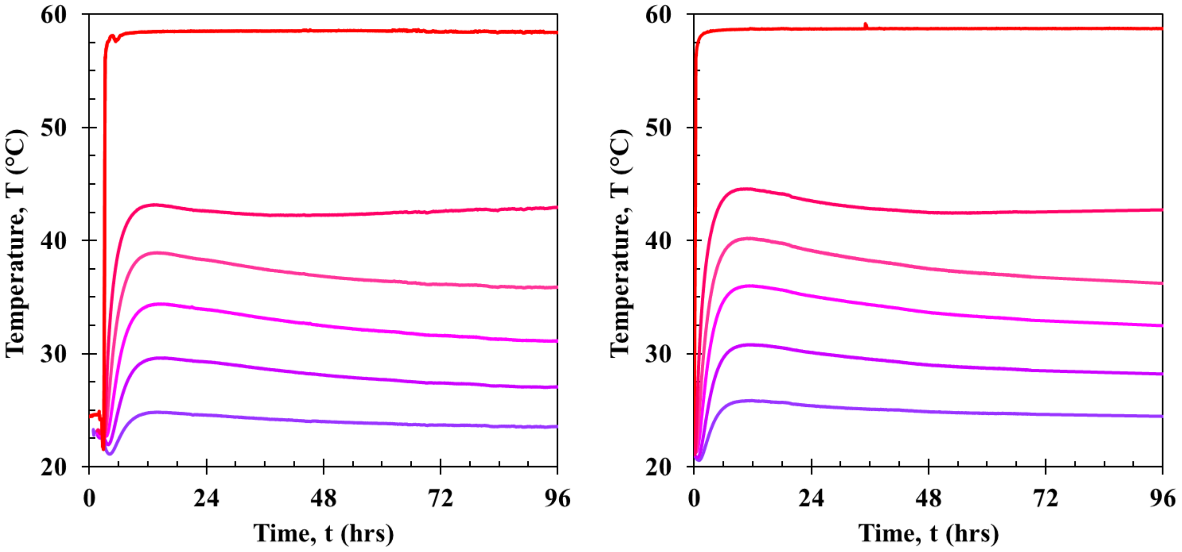

(a)

(b)

Fig. 3-12. Evolution of temperature for soil with w = 6% (a) sandy silt, (b) silty sand.

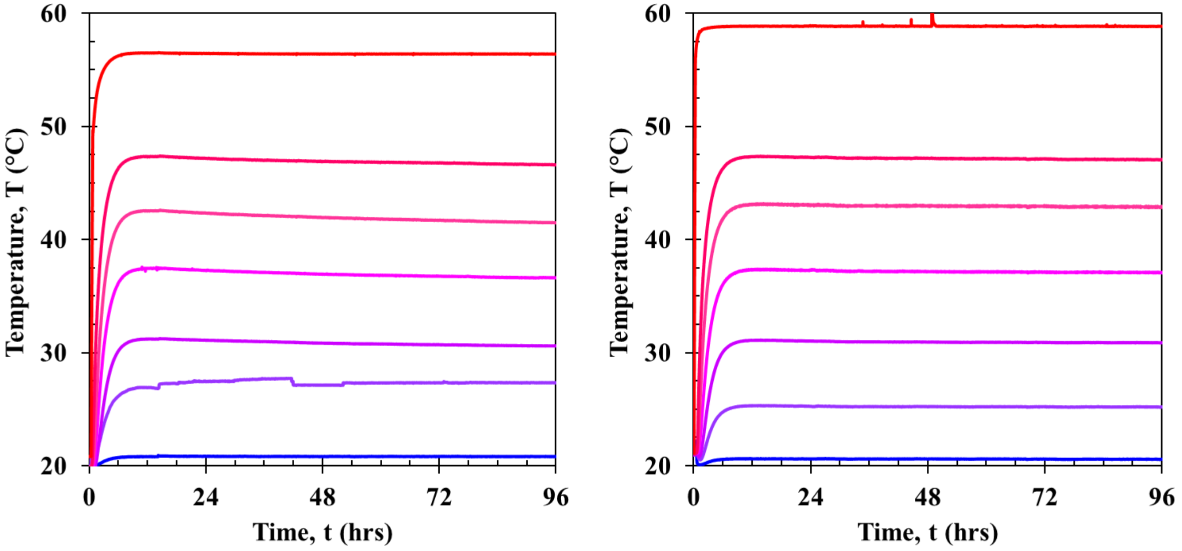

(a)

(b)

Fig. 3-13. Evolution of temperature for soil with w = 12% (a) sandy silt, (b) silty sand.

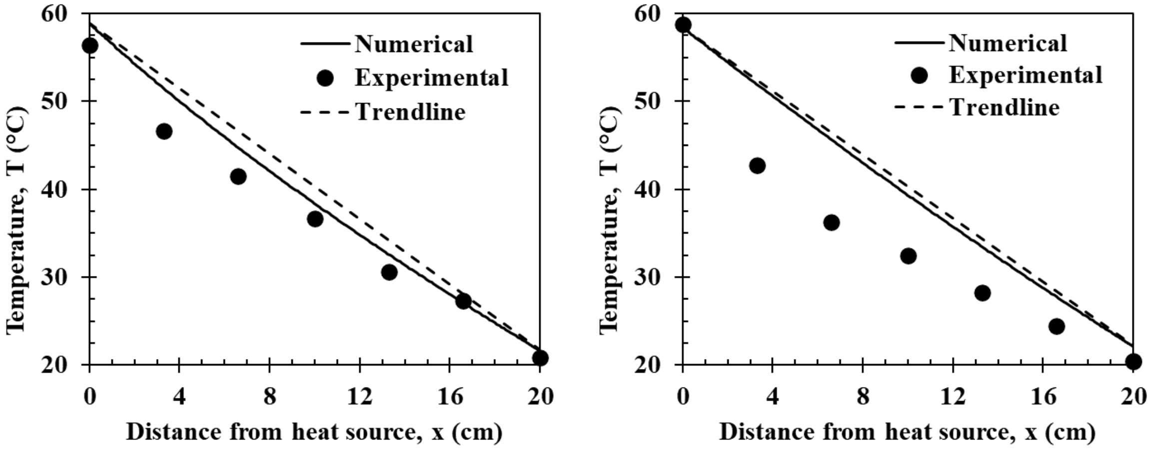

(a) (b)

Fig. 3-14. Steady-state temperature for soil with w = 6% (a) sandy silt, (b) silty sand.

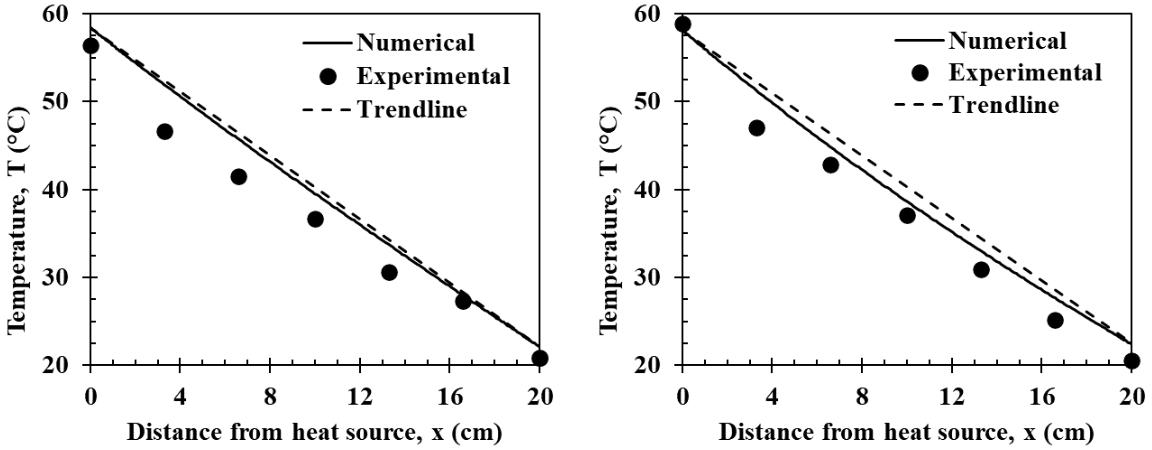

(a) (b)

Fig. 3-15. Steady-state temperature for soil with w = 12% (a) sandy silt, (b) silty sand.

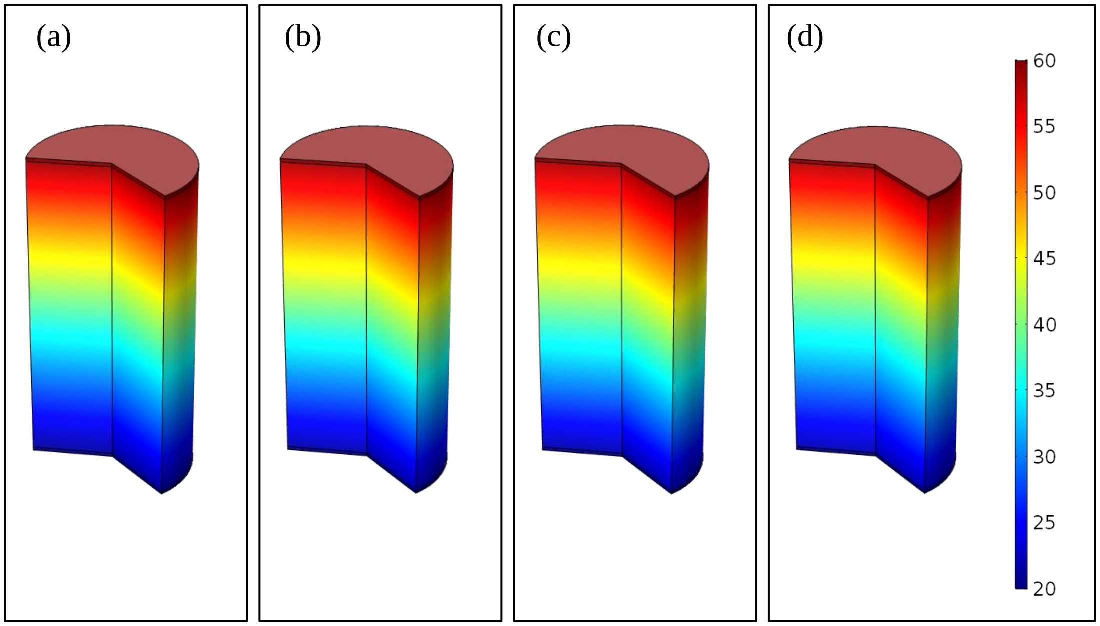

Fig. 3-16. Temperature profile of (a) sandy silt, w = 6%; (b) silty sand, w = 6%; (c) sandy silt, w = 12%; (d) silty sand, w=12%.

3.4.2 Hydraulic Behavior in Unsaturated Soil

Figs. 3-17 and 3-18 illustrate the numerical measurements of liquid water, air, and water vapor volumes at various distances following a 96-hour heating period. Theoretical analysis, as presented by Gurr et al. (1952), indicates that under the influence of thermal and hydraulic head gradients, equilibrium is less likely to be reached, particularly with high water contents. Consequently, a continuous circulation of water within the system is anticipated in such cases.

In general, the air content remains consistently low across all scenarios and gradually diminishes with increasing distance from the heat source. Similarly, the water vapor content is initially high but significantly decreases as one moves away from the heat source. Notably, the silty sand exhibits higher vapor content, attributed to its larger pore size that accommodates both water vapor and air.

The liquid water content decreases with soil heating, a trend evident in Figs. 3-17 and 3-

18. The moisture profile varies between sandy silt and silty sand. It is crucial to consider all three components—liquid water, air, and water vapor—in the hydraulic field to comprehensively capture the interactions between heat transfer, fluid flow, and other associated mechanisms.

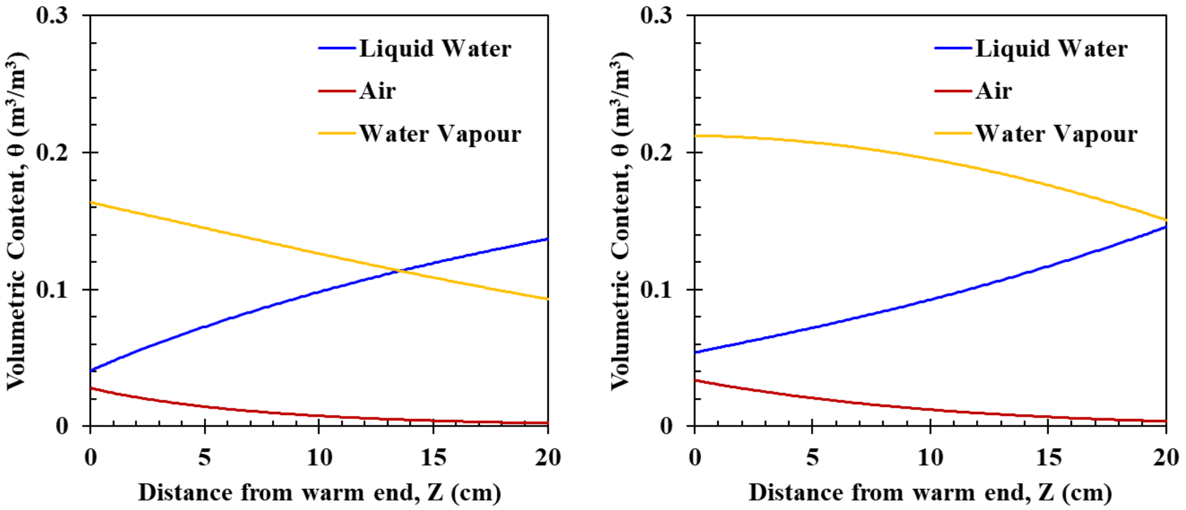

(a) (b)

Fig. 3-17. Volumetric content of soil with initial moisture content of w = 6% (a) sandy silt, (b) silty sand.

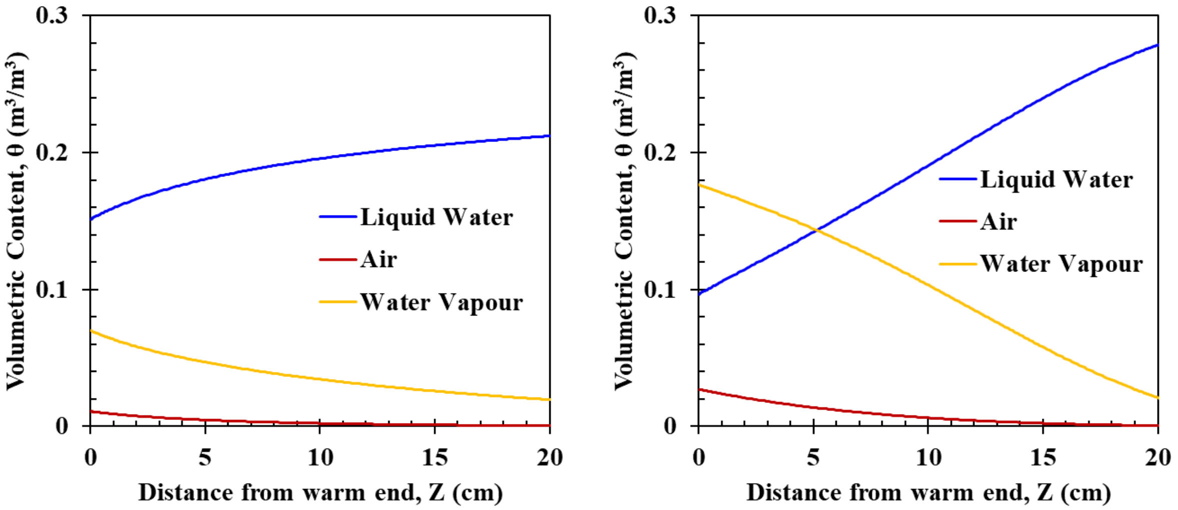

(a) (b)

Fig. 3-18. Volumetric content of soil with initial moisture content of w = 12% (a) sandy silt, (b) silty sand.

The comparison between numerical and experimental findings for the volumetric liquid water content of sandy silt and silty sand is illustrated in Figs. 3-19 and 3-20. Since the experimental measurements are not perfectly consistent throughout the soil specimen (this is because, although the soil is thoroughly mixed prior to compaction, the moisture may be redistributed during or shortly after compaction), only the difference between the initial readings and the final (1hr of the 96-hr heating period) is captured in these figures. Generally, there is a satisfactory agreement between the measured and predicted volumetric water content, except for the silty sand at a 12% gravimetric moisture level, where the experimental readings seem to remain constant. This deviation may be attributed to sensor errors or technical issues in data acquisition. Nevertheless, the overall agreement instills confidence in the accuracy of the numerical modeling. Fig. 3-21 presents a moisture profile derived from numerical simulations, highlighting distinct variations in fluid flow between sandy silt and silty sand. Sandy silt exhibits lower thermal conductivity than silty sand, resulting in a reduced heat-induced moisture flux. Additionally, in accordance with the soil-water characteristic curves (SWCC), silty sand demonstrates more effective moisture retention than sandy silt, leading to a significant difference in moisture content at the two ends of the soil column.

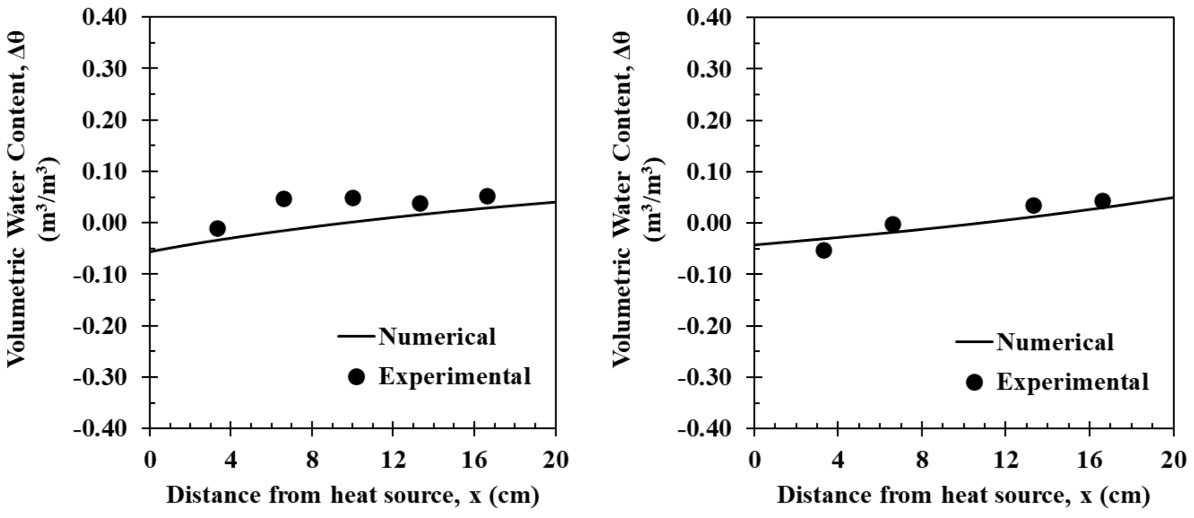

(a) (b)

Fig. 3-19. Comparison of the numerical and experimental volumetric water content of soil with initial moisture content of w = 6% (a) sandy silt, (b) silty sand.

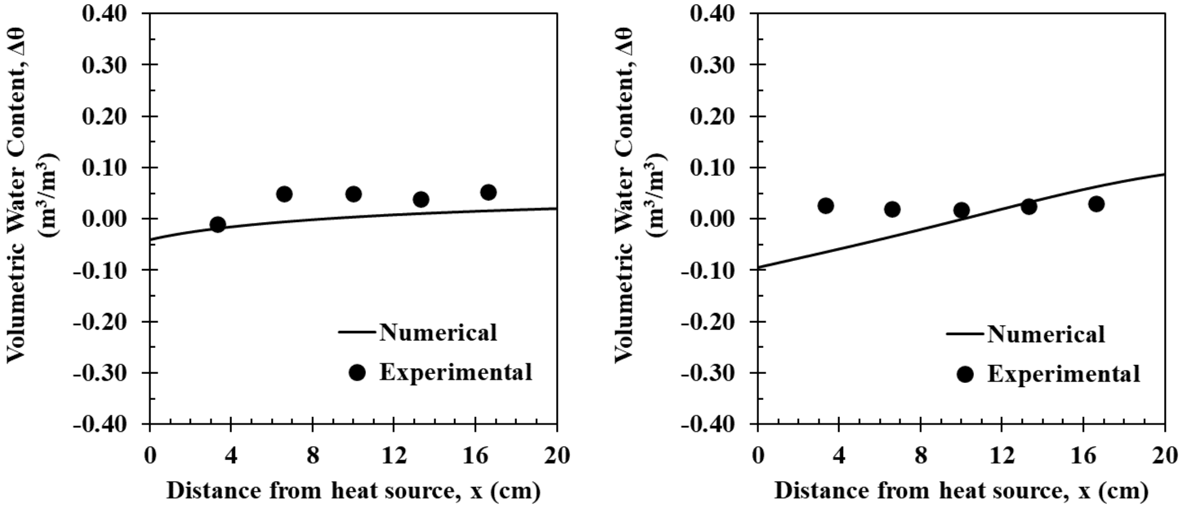

(a) (b)

Fig. 3-20. Comparison of the numerical and experimental volumetric water content of soil with initial moisture content of w = 12% (a) sandy silt, (b) silty sand.

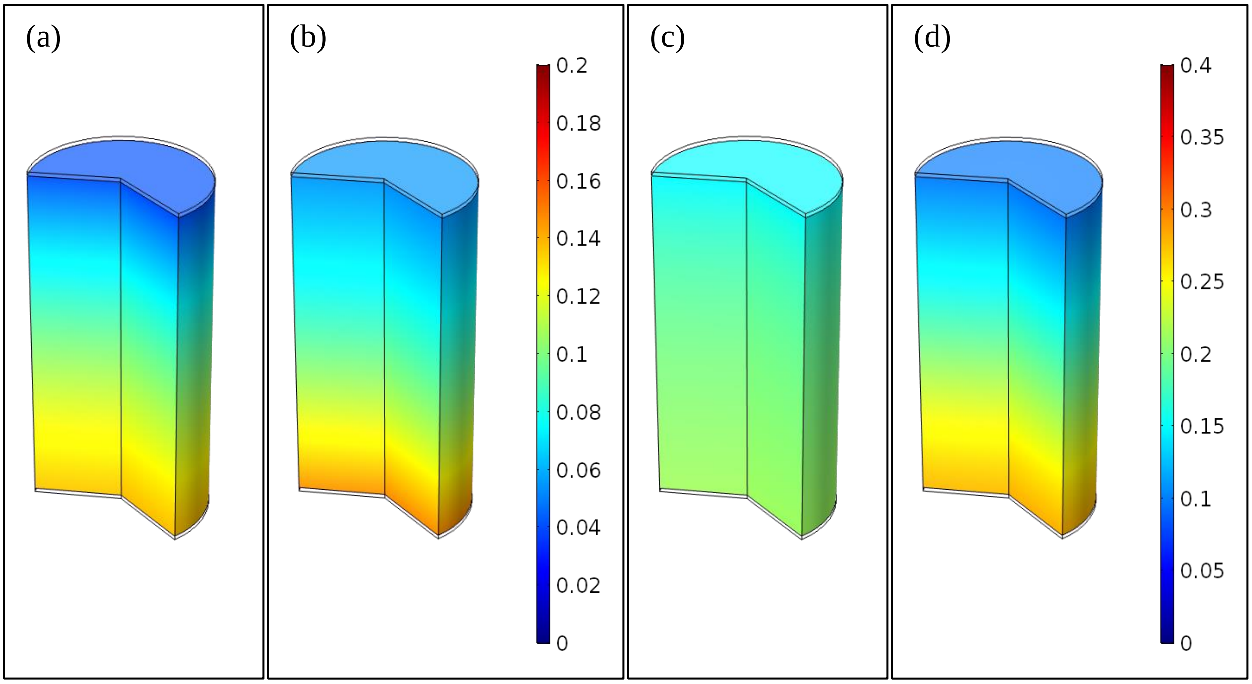

Fig. 3-21. Moisture profile of (a) sandy silt, w = 6%; (b) silty sand, w = 6%; (c) sandy silt, w = 12%; (d) silty sand, w=12%.

3.4.3 Mechanical Behavior in Unsaturated Soil

Changes in soil stress and deformation of sandy silt and silty sand were predicted at different steps of the test. The actual experimental measurements are not included here due to the limitations of sensors in accurately capturing the full extent of thermo-hydro-induced stresses. The soil specimens were confined within the soil cell, preventing any displacement away from it during numerical simulation. This restriction resulted in significant stresses within the soils, as depicted in Fig. 3-22. Notably, the sandy silt exhibited higher stresses compared to silty sand, and soils with elevated moisture levels experienced reduced stresses. This discrepancy is attributed to the distinct thermal expansion coefficients of the two soils; higher coefficients in one soil lead to greater stress magnitudes upon expansion. Furthermore, as soil releases water as vapor, thermal stresses may rise, clarifying why soils with lower initial moisture content displayed higher stresses. A stress profile for the four scenarios is provided to offer a more comprehensive understanding of the mechanical processes in heated moist sandy silt and silty sand.

The soil deformation in unsaturated soil was also evaluated and are shown in Figs. 24 and 3-25. In soils with lower moisture content, both radial and total displacement were found to be significantly greater compared to soils with higher moisture content. This observation was unexpected, as conventionally, soils with higher moisture content are anticipated to display greater deformability under heating conditions. This is because the presence of water typically weakens cohesive forces, resulting in reduced shear strength. Consequently, soils with higher moisture content are generally expected to be more prone to deformation. In terms of radial displacement, a sinusoidal pattern was observed, with soil deformation primarily concentrated in proximity to the inner soil cell wall and near the center. The profiles of deformation, both in the radial direction and the combination of axial and radial directions, are illustrated in Figs. 3-26 and 3-27.

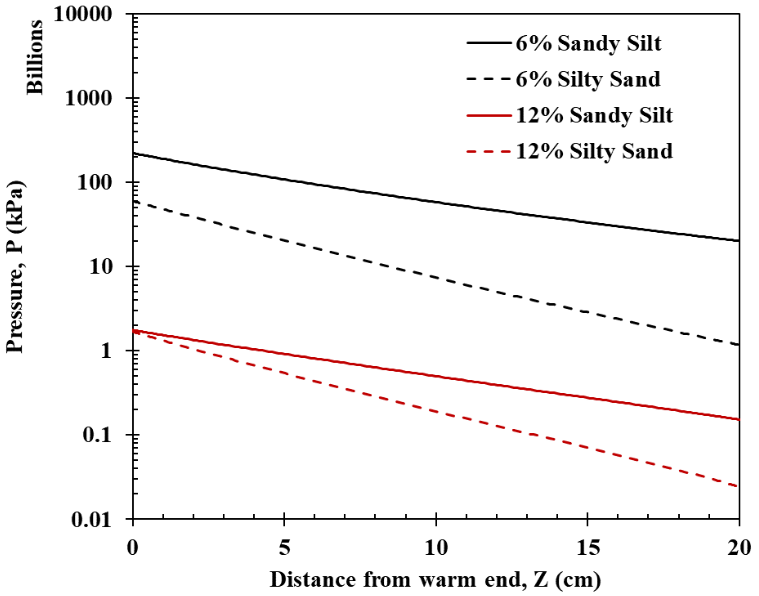

Fig. 3-22. Thermo-hydro-induced stress in sandy silt and silty sand.

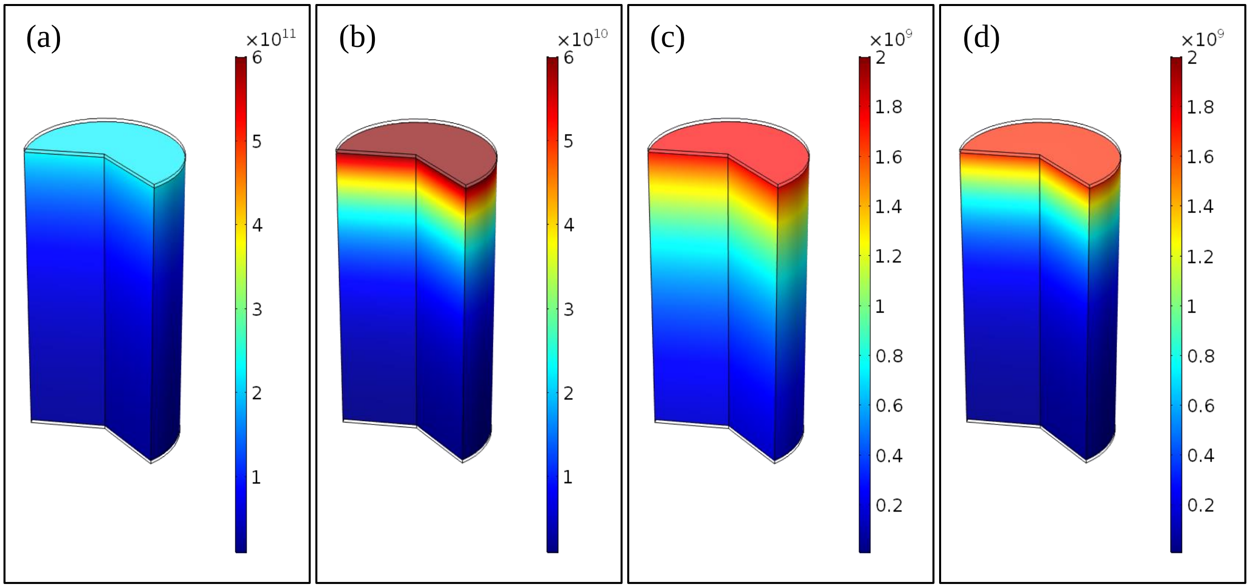

Fig. 3-23. Stress profile of (a) sandy silt, w = 6%; (b) silty sand, w = 6%; (c) sandy silt, w = 12%; (d) silty sand, w=12%.

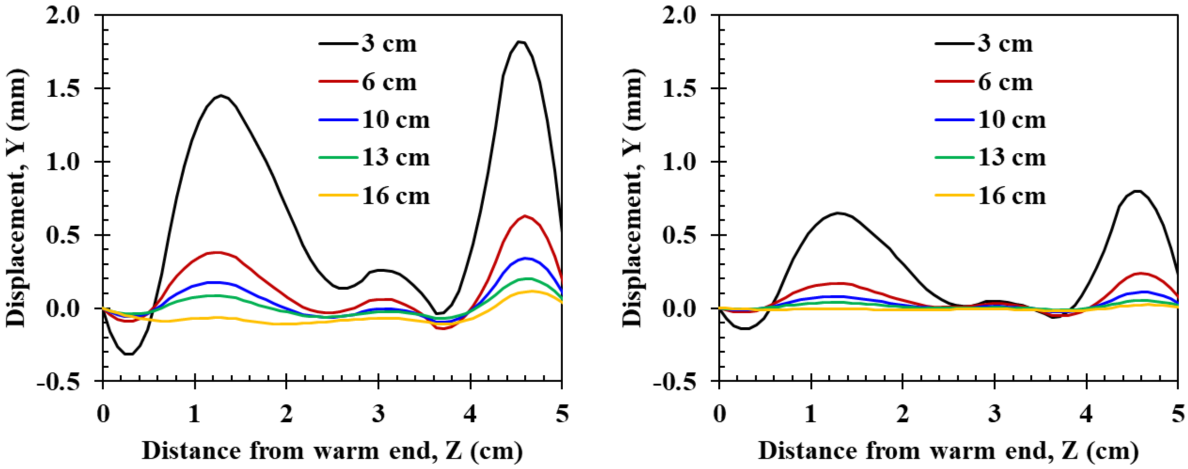

(a) (b)

Fig. 3-24. Radial displacement of soil with initial moisture content of w = 6% (a) sandy silt, (b) silty sand.

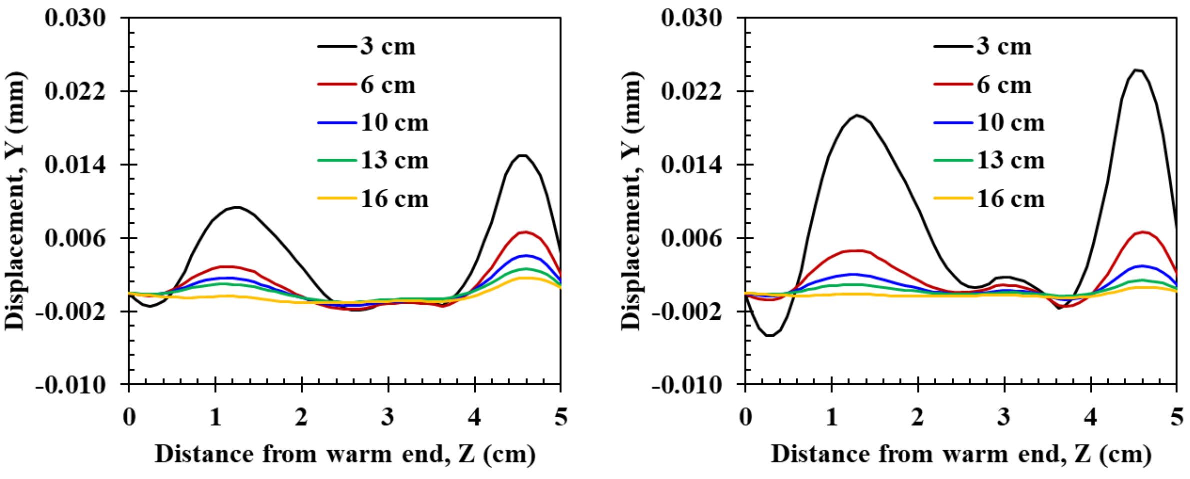

(a)

(b)

Fig. 3-25. Radial displacement of soil with initial moisture content of w = 12% (a) sandy silt, (b) silty sand.

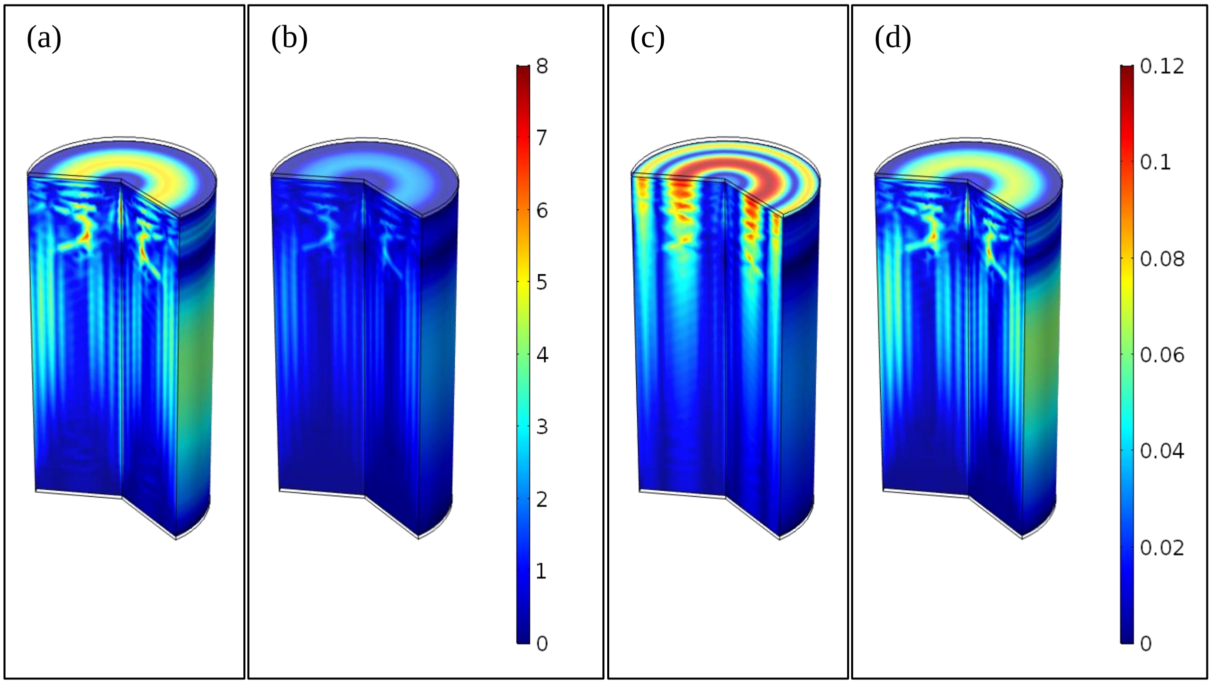

Fig. 3-26. Total displacement profile of (a) sandy silt, w = 6%; (b) silty sand, w = 6%; (c) sandy silt, w = 12%; (d) silty sand, w=12%.

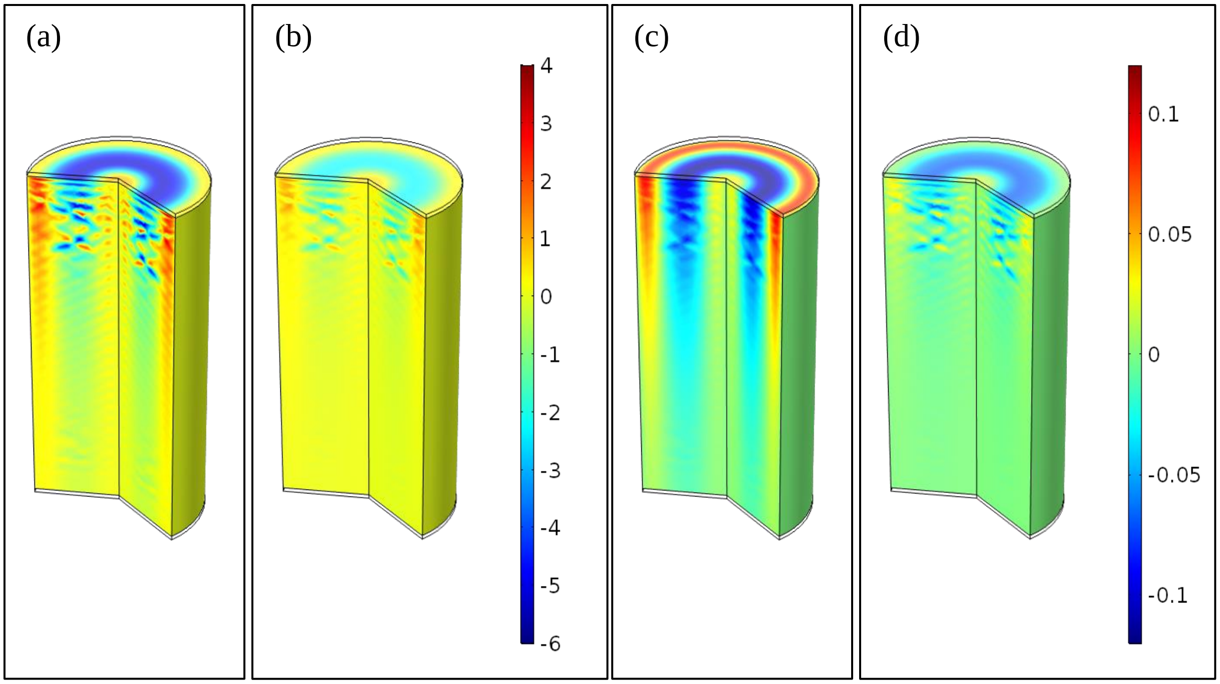

Fig. 3-27. Radial displacement profile of (a) sandy silt, w = 6%; (b) silty sand, w = 6%; (c) sandy silt, w = 12%; (d) silty sand, w=12%.

3.4.4 Other Soil Thermal Properties

Another soil property that is important to explore is the thermal conductivity, and how it is affected by the moisture content. Both the thermal conductivity and volumetric water content of sandy silt and silty soil were experimentally monitored at approximately 3 cm form the heat source. In Fig. 3-28, it is shown that the overall thermal conductivity of the soil decreases in proportion with the volumetric water content as the soil specimen undergo heating. This decrease is caused by the heat-induced-dissipation of pore liquid water, as well as its vaporization, leaving behind pore air and water vapor that have lower thermal conductivity. Although not captured in the present figure, the thermal conductivity changes are caused by the expansion of water vapor and pore air.

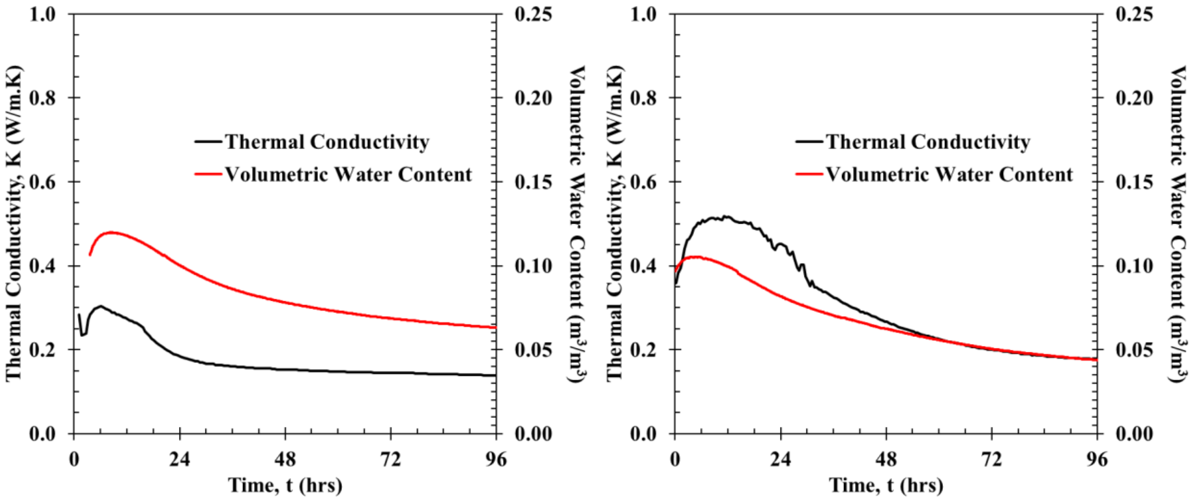

(a) (b)

Fig. 3-28. Thermal and hydraulic properties of soil with w = 6% (a) sandy silt, (b) silty sand.

3.5 Conclusion

This study examined the coupled thermo-hydro-mechanical behavior of soil using an experimental and numerical approach. Sandy silt and silty sand were tested experimentally at 6 and 12% gravimetric moisture level, and a numerical model was developed to predict the mechanisms occurring in the unsaturated soil when subjected to constant heating. The following conclusions were drawn.

- Steady-state temperature conditions were observed after approximately 2 days, with drier soils requiring more time. Water movement in low-moisture soil was slower, affecting moisture flux stabilization. After 2 days, soils likely reached thermal storage capacity, and temperature profiles revealed a concave shape, indicating moisture redistribution. Experimental measurements differed from numerical predictions, possibly due to material property variations. Heat loss at interfaces was attributed to thermal contact resistance.
- Volumetric liquid water, air, and water vapor content were monitored for 96 hours. Air content remained consistently low and decreased with distance from the heat source. Water vapor,

initially high, decreased especially in silty sand due to larger pores. Liquid water content decreased with soil heating, showing variations between sandy silt and silty sand. Experimental and numerical results generally align, except for a discrepancy in silty sand at 12% gravimetric moisture. The numerical model accurately represents moisture profiles, revealing differences in fluid flow between sandy silt and silty sand attributed to variations in thermal conductivity and moisture retention.

- Soil stress and deformation in sandy silt and silty sand were predicted under various conditions, excluding experimental measurements due to sensor accuracy limitations. Confined soil specimens exhibited high stresses, with sandy silt experiencing greater stress than silty sand. Increased moisture levels resulted in lower stresses due to thermal expansion coefficient differences. Unexpectedly, soils with lower moisture content showed significantly larger radial and total displacements. Radial displacement followed a sinusoidal pattern, primarily near the inner soil cell wall and close to the center.
- Experimental results show that as the soil heats up, overall thermal conductivity decreases with increasing water content due to heat-induced dissipation and vaporization of pore liquid water. The changes are attributed to the expansion of water vapor and pore air.
- The results obtained from the stress analysis show significantly high stresses, requiring further future investigation to thoroughly assess the stress response influenced by the interaction of thermal and hydraulic processes.

3.6 References

Alrtimi, A., M. Rouainia, and D. A. C. Manning. 2014. “An improved steady-state apparatus for measuring thermal conductivity of soils.” *Int J Heat Mass Transf*, 72: 630–636.

https://doi.org/10.1016/j.ijheatmasstransfer.2014.01.034.

Börgesson, L., M. Chijimatsu, T. Fujita, T. S. Nguyen, J. Rutqvist, and L. Jing. 2001. *Thermo-hydro-mechanical characterisation of a bentonite-based buffer material by laboratory tests and numerical back analyses*. *International Journal of Rock Mechanics & Mining Sciences*.

Bouyoucos, G. T. 1915. "Effect of Temperature on the Movement of Water vapor and Capillary Moisture in Soils." *J Agric Res*, 5: 141–172.

Cuevas, J., M. V. Villar, A. M. Fernández, P. Gómez, and P. L. Martín. 1997. "Pore waters extracted from compacted bentonite subjected to simultaneous heating and hydration." *Applied Geochemistry*, 12 (4): 473–481. https://doi.org/10.1016/S0883-2927(97)00024-3.

Dang, L. 2017. *Experimental and Numerical Studies of Heat and Moisture Transfer in Soils at Various Conditions*.

Faizal, M., A. Bouazza, and J. S. McCartney. 2021. "Thermohydraulic Responses of Unsaturated Sand around a Model Energy Pile." *Journal of Geotechnical and Geoenvironmental Engineering*, 147 (10): 04021105. American Society of Civil Engineers (ASCE). https://doi.org/10.1061/(asce)gt.1943-5606.0002640.

Gurr, C. G., T. J. Marshall, and J. T. Hutton. 1952. "Movement of Water in Soil due to a Temperature Gradient." *Soil Sci*, 74(5): 335–346.

Hedayati-Dezfooli, M. 2016. *DEVELOPMENT OF AN EXPERIMENTAL APPARATUS FOR STUDYING HIGH-TEMPERATURE HEAT AND MASS TRANSFER IN SOILS*.

Heitman, J. L., F. Battaglia, R. M. Cruse, B. K. Hornbuckle, and T. J. Sauer. 2007a. *Measurement of coupled soil heat and water processes*.

Heitman, J. L., R. Horton, T. Ren, and T. E. Ochsner. 2007b. "An Improved Approach for

Measurement of Coupled Heat and Water Transfer in Soil Cells." *Soil Science Society of America Journal*, 71 (3): 872. https://doi.org/10.2136/sssaj2006.0327.

Jackson, R. D., D. A. Rose, and H. L. Penman. 1965. "Circulation of Water in Soil under a Temperature Gradient." *Nature*, 205: 314–316.

Kuzmak, J. M., and P. J. Sereda. 1957a. "The Mechanism by which Water Moves Through a Porous Material Subjected to a Temperature Gradient, II: Salt Tracer and Streaming Potential to Defect Flow in the Liquid Phase." *Soil Sci*, 84: 419–422.

Kuzmak, J. M., and P. J. Sereda. 1957b. "The Mechanism by Which Water Moves Through a Porous Material Subjected to a Temperature Gradient, I: Introduction of a Vapor Gap into a Saturated System." *Soil Sci*, 84: 291–299.

Maclean, D. J., and P. M. Gwatkin. 1953. "Moisture Movements Occurring in Soil Due to the Existence of a Temperature Gradient." *Road Research Laboratory*.

Moradi, A., K. M. Smits, J. Massey, A. Cihan, and J. McCartney. 2015. "Impact of coupled heat transfer and water flow on soil borehole thermal energy storage (SBTES) systems: Experimental and modeling investigation." *Geothermics*, 57: 56–72. Elsevier Ltd. https://doi.org/10.1016/j.geothermics.2015.05.007.

Nassar, I. N., and R. Horton. 1989. "Water Transport in Unsaturated Non-isothermal Salty Soil: I. Experimental Results." *Soil Science Society of America*, 53: 1323–1329.

Prunty, L. 2003. "Soil water retention and conductivity when vapor flow is important." *Journal of Irrigation and Drainage Engineering*, 129: 201–207.

Prunty, L., and R. Horton. 1994. "Steady-state Temperature Distribution in Non-isothermal, Unsaturated Closed Soil Cells." *Soil Science Society of America*, 58: 1358–1363.

Rawat, A., W. Baille, and S. Tripathy. 2019. "Swelling behavior of compacted bentonite-sand mixture during water infiltration." *Eng Geol*, 257. Elsevier B.V. https://doi.org/10.1016/j.enggeo.2019.05.018.

Saba, S., Y. J. Cui, A. M. Tang, and J. D. Barnichon. 2013. "Investigation of the swelling behaviour of compacted bentonite–sand mixture by mock-up tests." *Canadian Geotechnical Journal*, 51 (12): 1399–1412. Canadian Science Publishing. https://doi.org/10.1139/cgj-2013-0377.

Schanz, T., L. Nguyen-Tuan, and M. Datcheva. 2013. "A column experiment to study the thermo-hydro-mechanical behaviour of expansive soils." *Rock Mech Rock Eng*, 46 (6): 1287–1301. https://doi.org/10.1007/s00603-012-0361-8.

Taylor, S. A., and L. Cavazza. 1954. "The Movement of Soil Moisture in Response to Temperature Gradients." *Soil Science Society of America*, 18: 351–358.

Tripathy, S., H. R. Thomas, and P. Stratos. 2017. "Response of compacted bentonites to thermal and thermo-hydraulic loadings at high temperatures." *Geosciences (Switzerland)*, 7 (3). MDPI AG. https://doi.org/10.3390/geosciences7030053.

Villar, M. V., P. L. Martín, and J. M. Barcala. 2005. "Modification of physical, mechanical and hydraulic properties of bentonite by thermo-hydraulic gradients." *Eng Geol*, 81 (3): 284–297. https://doi.org/10.1016/j.enggeo.2005.06.012.

Wang, T.-H., and L.-J. Su. 2010. "Experimental Study on Moisture Migration in Unsaturated Loess under Effect of Temperature." *Journal of Cold Regions Engineering*, 24 (3): 77–86. https://doi.org/10.1061/ASCECR.1943-5495.0000015.

Zhou, J., J. L. Heitman, R. Horton, T. Ren, T. E. Ochsner, L. Prunty, R. P. Ewing, and T. J. Sauer. 2006. "Method for Maintaining One-Dimensional Temperature Gradients in Unsaturated, Closed Soil Cells." *Soil Science Society of America Journal*, 70 (4): 1303–1309. Wiley. https://doi.org/10.2136/sssaj2005.0336n

CHAPTER 4. GRAVITY EFFECT ON MOISTURE MIGRATION IN UNSATURATED SANDS UNDER CONTROLLED THERMAL GRADIENT: A HEAT CELL STUDY

4.1 Introduction

When testing the coupling of heat and moisture transport in the heat exchange experimental test, it is conventionally recognized that moisture moves away from the heat source and migrates toward a cooler region. Temperature gradient is responsible for this flux, as the fluid density and viscosity change with temperature. However, large pores and high temperatures can impede the interstitial fluid flow and contribute to its retention (Dang 2017; Kaneza et al. 2023). Therefore, a choice of testing soil specimens with smaller pores arises to limit the effect of gravity.

Previous research established three soil heating scenarios, where the researcher imposed a lower and higher temperature at the top and bottom testing cell, respectively, then reversed the direction of the temperature gradient, and replicated the set-up in the horizontal direction (Dang 2017). Another researcher also performed a similar experiment with the direction of the temperature gradient directed upward (lower temperature at the top and higher temperature at the bottom) (Kaneza 2020). The researchers observed a tendency of stagnant flow towards the warm end when the latter is at the bottom, which is intensified by a combination of gravity, high temperature, and large pores.

This paper aims to evaluate more closely the effect of gravity on moisture migration at two different moisture states and one temperature gradient. Initial target gravimetric moisture content of 5 and 10% were selected, and 20 and 60°C were the boundary temperatures. Geotechnical laboratory tests were initially performed to classify the soil and find index properties; then the soil was heated in a soil testing cell, where boundary temperatures were imposed in two different scenarios to monitor the effect of gravity on the migration of pore fluid.

4.2 Materials and methods

4.2.1 Preliminary Tests

A series of preliminary geotechnical tests were performed on Benbrook sand, namely the wet sieve analysis (American Society for Testing and Materials 2000), dry sieve (American Society for Testing and Materials 2017), hydrometer analysis (American Society for Testing and Materials n.d.), Atterberg limits tests (liquid limit, LL, and plastic limit, PL—(American Society for Testing and Materials) and (Texas Department of Transportation 1999)), and specific gravity (G_s) test (American Society for Testing and Materials). The sieve analyses and hydrometer analysis established the particle size curves of the soil. The LL and PL tests were attempted to determine the consistency of the soils and allowed the classification of the soil samples using the Unified Soil Classification and System (USCS) plasticity chart. However, it was found to be non-plastic. Finally, the density of Benbrook sand as compared to the density of water was obtained from the G_s test. The results of the soil index properties, including the percentage of particle sizes and specific gravity are summarized in Table 4-1. Benbrook sand is classified as silty sand (SM) with 33.4% of fine particles. The residual and saturated volumetric moisture content (θ_r and θ_s) of 0.06 and 0.55 m^3/m^3 were estimated, and the van Genuchten empirical parameters of $\alpha = 0.950$, $n = 1.650$, and $m = 0.394$ were determined. Therefore, the matric suction for $w = 5$ and 10% are $\varphi = 1000$ and 110 kPa, respectively.

Table 4-1. Particle size analysis.

D_{60} (mm)	D_{30} (mm)	D_{10} (mm)	C_u (-)	C_c (-)	F_{200} (%)	G_s (-)
0.125	0.073	0.032	3.9	1.3	33.4	2.71

4.2.2 Soil Heating Tests

A series of soil heating tests were performed in a soil heating device, where soil was tested under different moisture content and temperature gradients. This was done to monitor the soil moisture movement in response to changed thermal properties and vice versa. Three time domain reflectometry (TDR) sensors and eight thermocouples (TCs) were used to measure the water content and temperature variations. The testing device, its dimensions, and all its main features are detailed by Kaneza (2020) and the measuring devices are illustrated in Figs. 4-1 and 4-2. Details of the testing procedures are also provided by Kaneza (2020).

Two soil specimens with initial water contents of 5 and 10% were both tested under two different heating scenarios. In the first scenario, 60ºC was imposed at the upper heat exchanger and 20ºC at the lower heat exchanger (T60_B20). In the second scenario, the temperature gradient was reversed, and 20ºC was imposed at the upper heat exchanger and 60ºC at the lower heat exchanger (T20_B60). This allowed the influence of gravity on the coupled heat and moisture transport to be evaluated.

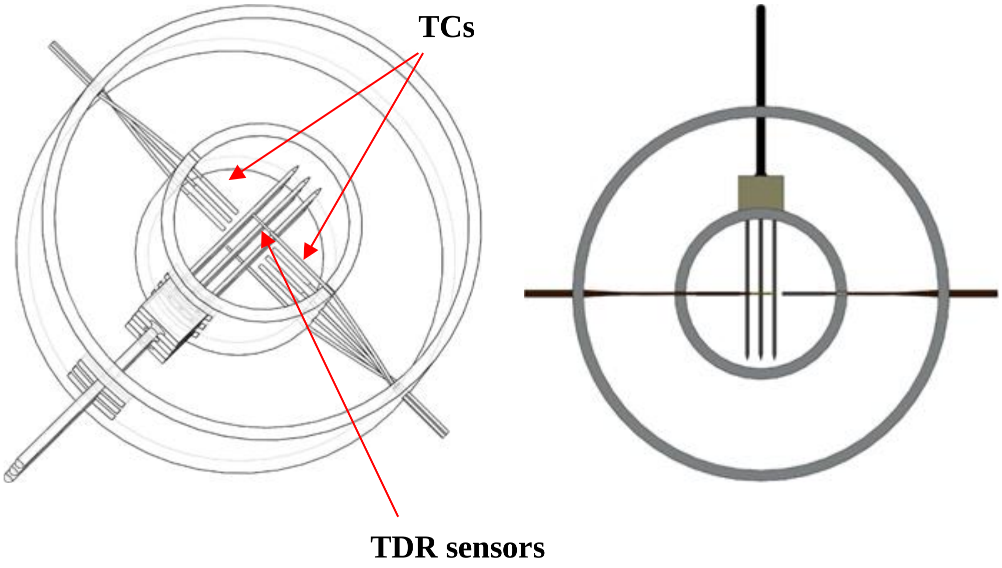

Fig. 4-1. Placement of TDR sensors and TCs.

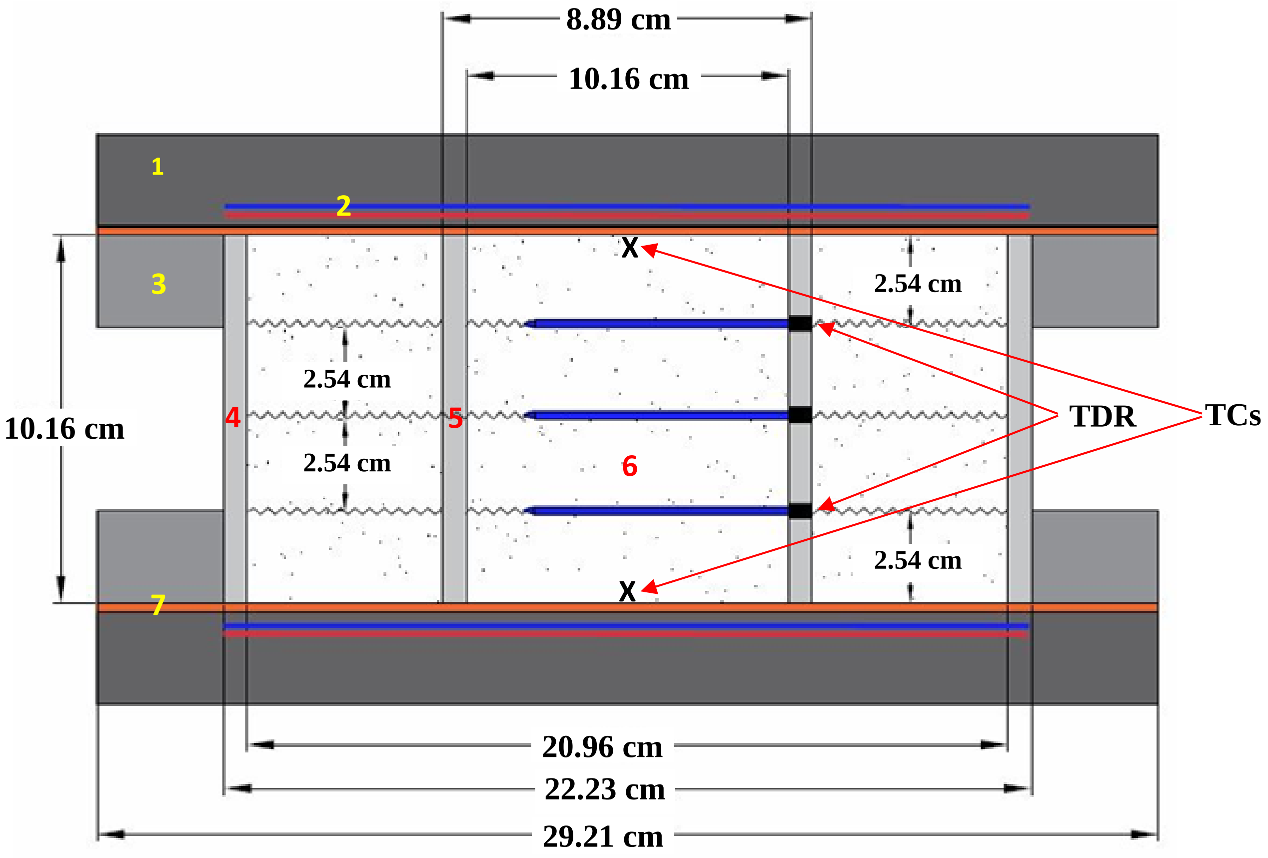

Fig. 4-2. Heating test configuration.

1: Heat exchanger plate; 2: spiral channel; 3: supporting ring; 4: outer column wall; 5: inner column wall; 6: soil specimen; 7: copper plate. (Adapted from Kaneza (2020)).

4.3 Results and Discussions

4.3.1 Temperature Variations with Time

The temperature variations with time for w_{Target} = 5% are shown in Fig. 4-3, where (a) and (b) represent the T60_B20 and T20_B60 cases, respectively. The temperatures at the two ends do not exactly correspond to the temperatures imposed on the boundaries. Temperatures at the warm end are slightly less than 60°C and temperatures at the cool end are slightly higher than the imposed 20°C. This can be attributed by the imperfect thermal contact between the copper plates of the heat exchangers and the soil specimen. Temperatures at 2.5, 5.0, 7.5 cm for w_{Target} = 5% show that temperature equilibrium is reached after 24 hrs of heating, while equilibrium is reached in less than 12 hrs for w_{Target} = 10%, although not shown here. Besides, the temperatures for w_{Target} = 5% display a significantly high peak, which gradually decreases before the soil reaches thermal equilibrium. It is also noticed that the T20_B60 case produces higher temperatures than the T60_B20 case at the same locations. These discrepancies will be discussed later.

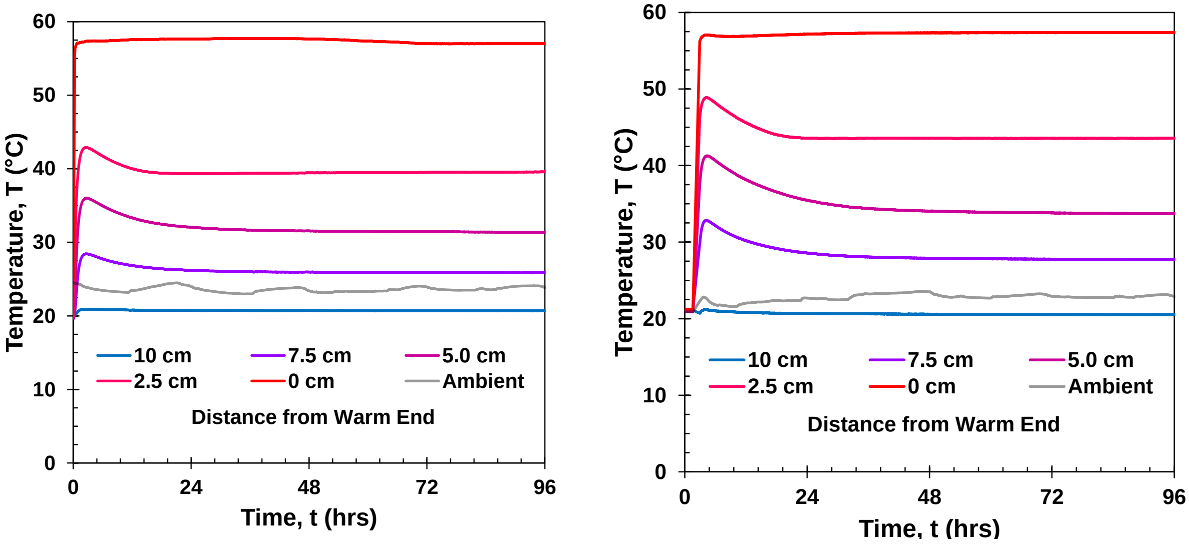

(a)

(b)

Fig. 4-3. Temperature variations with time for w_{Target} = 5% (a) T60_B20 and (b) T20_B60.

4.3.2 Moisture Distribution with Time

The moisture variations are shown in Figs. 4-4 and 4-5, where Figs. 4-4(a) and 4-5(a) represent the moisture distribution for T60_B20, while Figs. 4-4(b) and 4-5(b) represent T20_B60, when w_{Target} = 5 and 10%, respectively. All four graphs illustrate the migration of pore water from the heat source towards the cooler region. The migration is a result of the changes in fluid density and viscosity caused by thermal gradients. The figures show that the measured water content at 7.5 cm from the warm end (which is 2.5 cm from the cool end) gradually increases with time and the water content at 2.5 cm near the warm end decreases with time. When w_{Target} = 10%, the pore water slightly increases from its initial content at the center of the soil cell for the T60_B20 case, but it slightly decreases for the T20_B60 case. Conversely, when w_{Target} = 5%, the water content at 5.0 cm is relatively stable for both cases, indicating that soil equally gains and loses moisture.

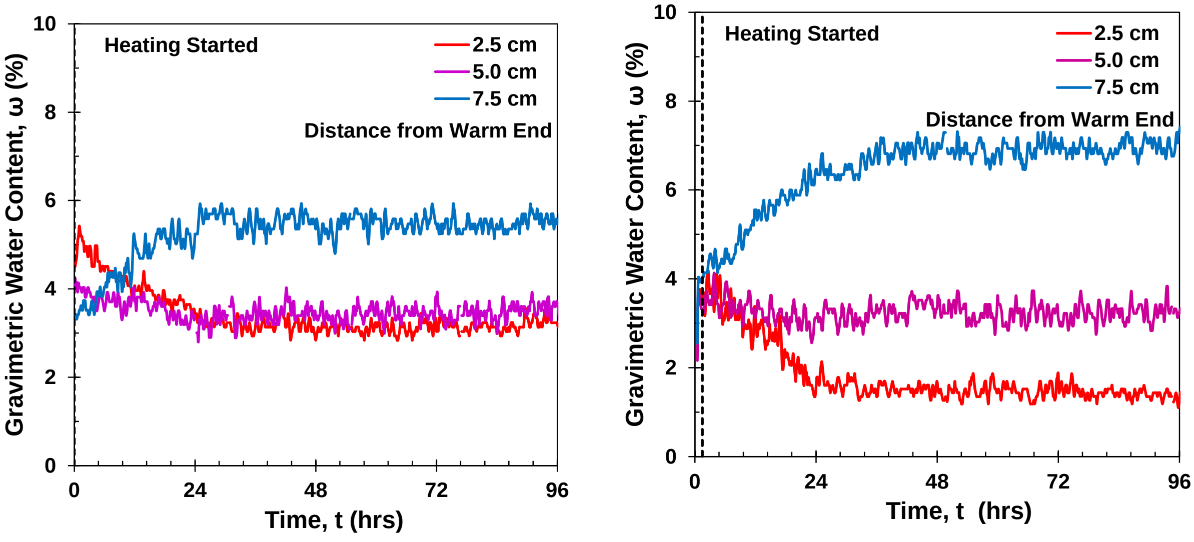

(a) (b)

Fig. 4-4. Moisture variations with time for w_{Target} = 5% (a) T60_B20; and (b) T20_B60.

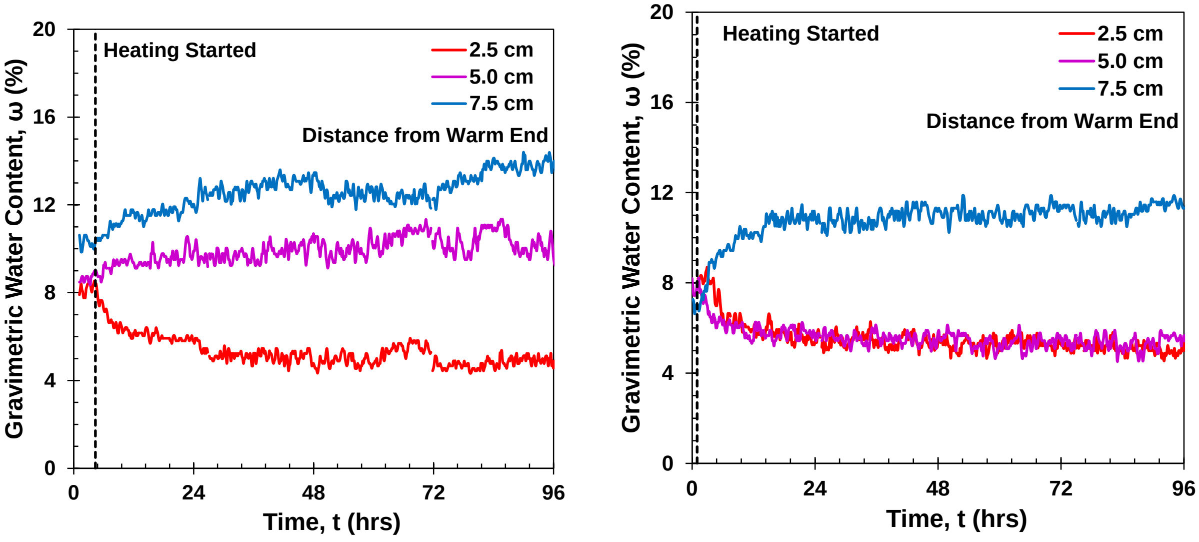

(a) (b)

Fig. 4-5. Moisture variations with time for w_{Target} = 10% (a) T60_B20; and (b) T20_B60.

4.3.3 Temperature distribution with distance

The temperature profiles for the T60_B20 set-up display concavity, as shown in Figs. 4-6(a) and 5-7(a), where the two slopes represent the changes in temperature caused by moisture migration. The thermal conductivity of water surpasses that of air by a magnitude of about 20. This explains the distinct temperature changes resulting from the decrease in thermal conductivity when soil dries and its water content volume decreases while its air content volume increases. The steepest slope near the warm end indicates a decrease in temperature caused by a reduction in thermal conductivity, as pore water moves away from the warm end. The slope near the cool end is less steep and indicates a recovery in thermal conductivity, as water moves towards this end. The soil specimen with the least amount of pore water (w_{Target} = 5%) displayed a deeper concavity. This may be explained by the resulting larger volume of air, as water migrates away from the warm end. Although the temperature-dependent thermal conductivity has not been determined experimentally, the dependency of the thermal conductivity on moisture content is described by Eq. 4-1.

$$\boldsymbol{k = 6.16\theta_w + 0.38\mathrm{e}^{-(3.61\theta_w)^{14.09}}} \tag{4-1}$$

Constants that are based on empirical data are utilized the equation. The original equation is established by McInnes (1981) and Hansson et al. (2004).

Concavity is also known to increase with temperature gradient and mean temperature of the two boundaries (Heitman et al. 2007). The shape of the concavity may also be explained by the difference in the dry density. For the T20_B60 set-up, the temperature gradient is reversed and so is the resulting temperature profile, which shifts to a convex shape: Figs. 4-6(b) and 4-7(b). As shown in these figures, the temperature profile is convex when the soil specimen reaches its maximum temperatures; after 96h of continuous heating, the temperature profile for w_{Target} = 5%

shifts back to a concave shape, while that of w_{Target} = 10% remains convex.

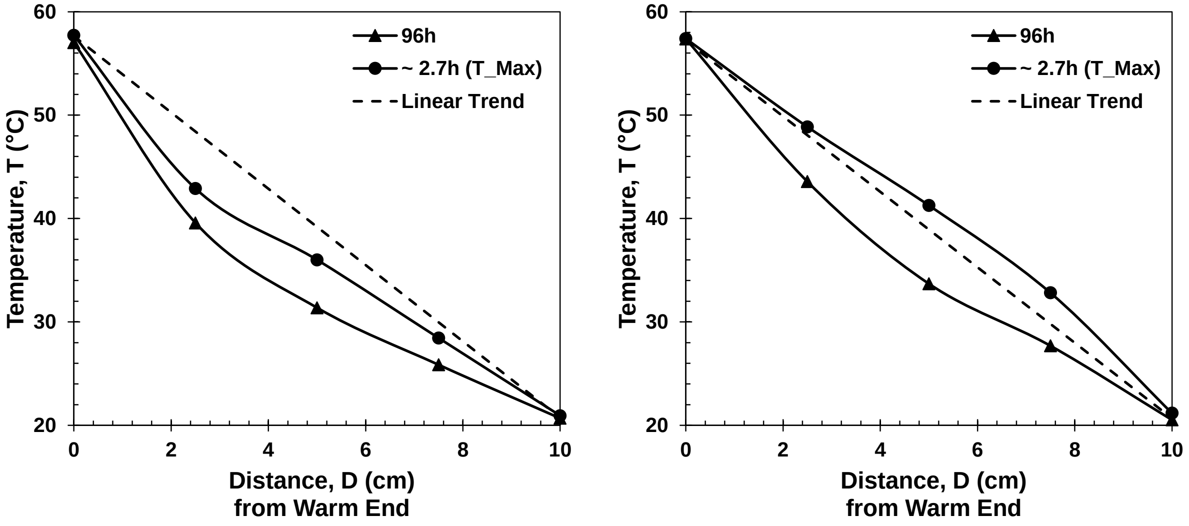

(a) (b)

Fig. 4-6. Temperature variations with distance for w_{Target} = 5% (a) T60_B20; and (b) T20_B60.

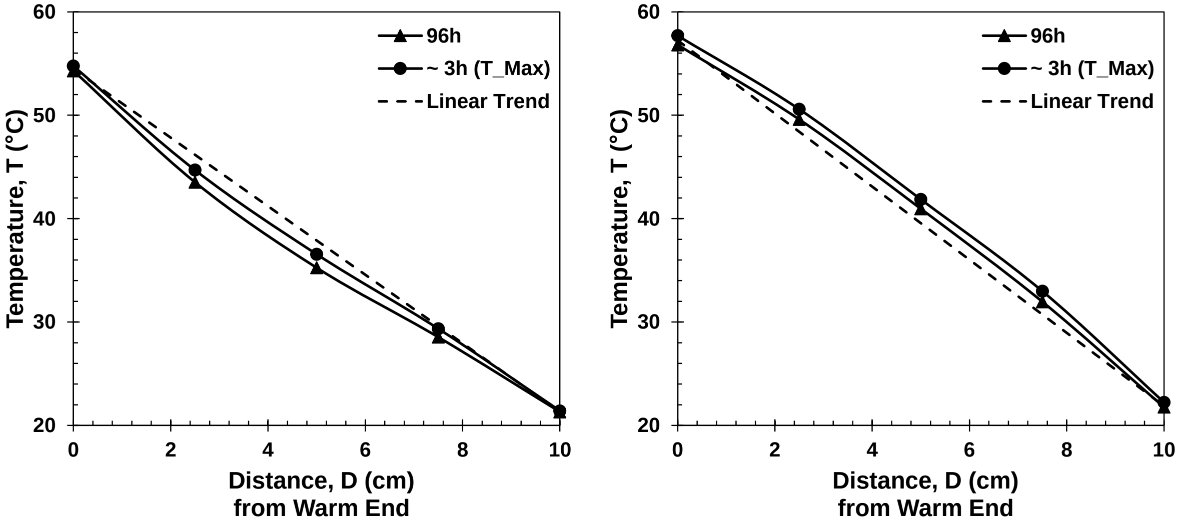

(a) (b)

Fig. 4-7. Temperature variations with distance for w_{Target} = 10% (a) T60_B20; and (b) T20_B60.

This convexity indicates that temperature increases near the warm end, and this results from an increase in thermal conductivity caused by the increase of pore water around this region. In this scenario, the warm end is at the bottom of the cell, and it is believed that pore water is easily pulled down by gravity, since the pore water has a lower density and the surface tension and viscosity are reduced in this region, because of the higher imposed temperature (60º, versus 20ºC in the other scenario). Therefore, a portion of pore water is pulled down and another migrates away from the warm end. This effect lessens as the distance from the warm end increases — towards the cool end. For w_{Target} = 5%, Figs. 4-3(b) and 4-6(b) show that this phenomenon occurred until the maximum temperatures were reached, then pore water started to migrate "freely" without the influence of gravity until temperature variations were constant. This resulted in the typical concave shape. In contrast, for w_{Target} = 10%, although one portion of pore water is pulled down and the other migrates away from the warm end, it is observed that this phenomenon does not lessen with distance. This is possibly due to a higher initial moisture content and therefore a lower surface tension and matric suction, which makes it easier for gravity to pull down the pore water. This effect persists until temperature equilibrium is achieved. Consequently, the resulting temperature distribution is a convex shape.

4.3.4 Moisture Distribution with Distance

The moisture migration is portrayed in Figs. 4-8 and 4-9. They show the measured initial and final pore water content after 96h of heating; additionally, these show a rise in water content near the cool end and a drop near the warm end. These differences are illustrated in Fig. 4-10 and Tables 4-2 and 4-3. The degree of saturation from the warn end is also summarized in Table 4-4. When w_{Target} = 5%, the loss in moisture content near the warm end and center are greater for the T20_B60 case; whereas, the loss is similar at the warm end but significanty greater at the center for the same case when w_{Target} = 10%. It was observed that the T20_B60 scenario generated a higher pore fluid transport as compared to the T60_B20 scenario due to gravity.

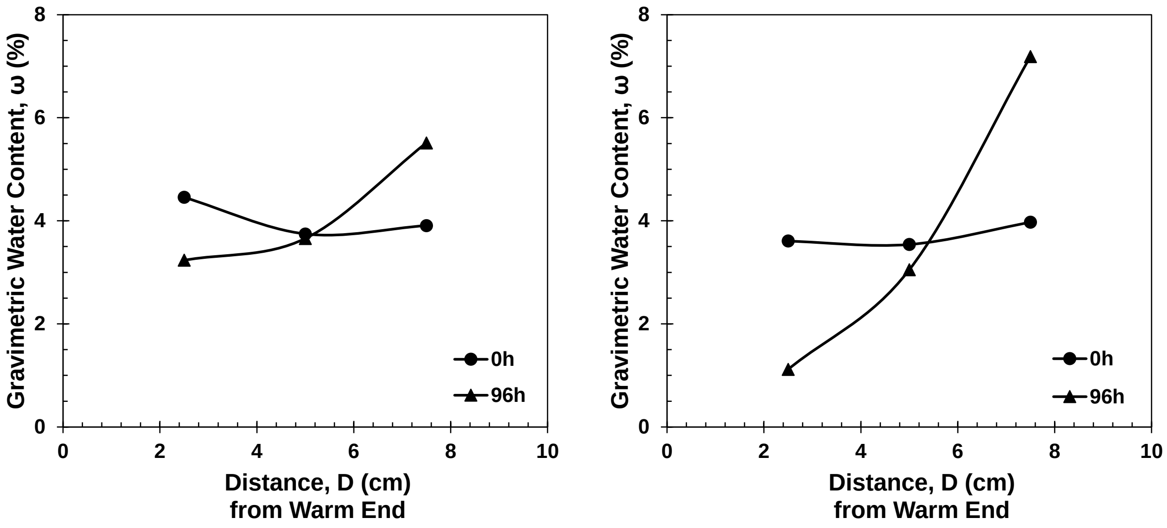

(a) (b)

Fig. 4-8. Moisture variations with distance for w$_{\text{Target}}$ = 5% (a) T60_B20; and (b) T20_B60.

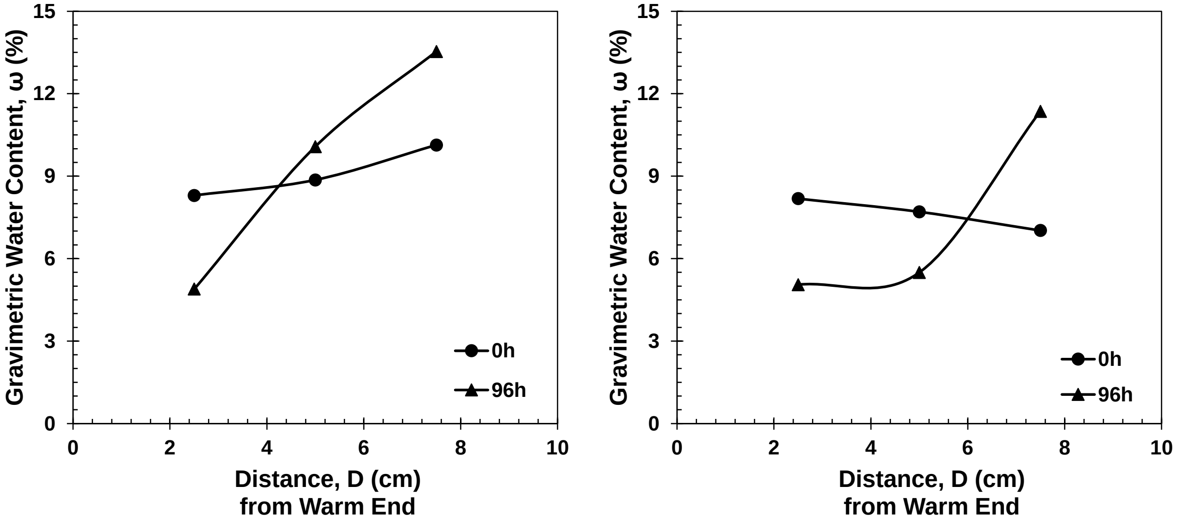

(a) (b)

Fig. 4-9. Moisture variations with distance for w$_{\text{Target}}$ = 10% (a) T60_B20; and (b) T20_B60.

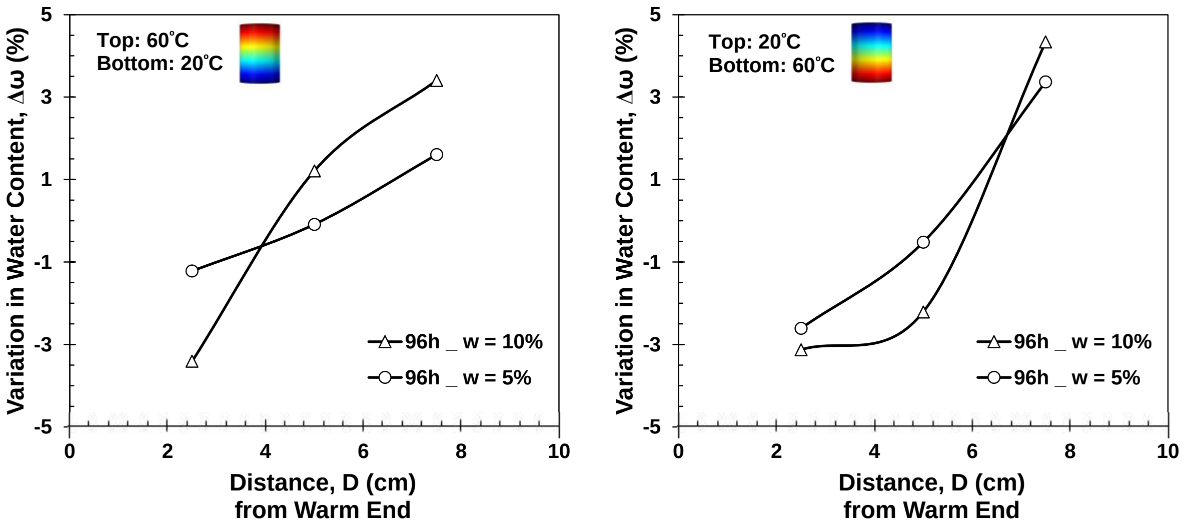

(a) (b)

Fig. 4-10. Changes in initial moisture with distance for (a) T60_B20; and (b) T20_B60.

Table 4-2. Initial and final moisture contents for w_{Target} = 5%.

	2.5 cm		5.0 cm		7.5 cm	
	(a)*	(b)*	(a)	(b)	(a)	(b)
0h	4.46	3.61	3.74	3.54	3.91	3.97
96h	3.24	1.12	3.66	3.05	5.51	7.19
Δω (%)	-1.22	-2.49	-0.09	-0.49	1.60	3.21

Notes: (a)*: T60_B20; (b)*: T20_B60.

Table 4-3. Initial and final moisture contents for w_{Target} = 10%.

	2.5 cm		5.0 cm		7.5 cm	
	(a)	(b)	(a)	(b)	(a)	(b)
0h	8.30	8.18	8.86	7.70	10.13	7.02
96h	4.89	5.05	10.07	5.49	13.53	11.36
Δω (%)	-3.41	-3.13	1.21	-2.21	3.40	4.34

Table 4-4. Initial and final degree of saturation.

	2.5 cm		5.0 cm		7.5 cm	
			w = 5%			
	(a)	(b)	(a)	(b)	(a)	(b)
0h	15.2	14.7	14.6	14.3	16.6	16.1
96h	12.1	4.5	14.3	12.3	21.4	29.1
			w = 10%			
0h	32.2	31.7	34.1	30.0	39.1	27.4
96h	19.0	19.6	38.8	21.4	52.3	44.3

4.3.5 Coupled Heat Transport and Moisture Migration

This section presents an evaluation and a comparison of heat and moisture transport for w_{Target} = 5 and 10% for two different scenarios. Generally, it was observed that moisture moves in the opposite direction of heat (Figs. 4-11 and 5-12). Interestingly, Figs. 4-11(a) and (b) show correspondence in the shapes of temperature and moisture variations at different locations for w_{Target} = 5%. Near the warm end, the temperature profile exhibits a steeper slope and the moisture profile exhibit a flatter slope and vice versa near the cool end. The inflection point of the concavity is spotted within 3.0 and 5.0 cm near the warm region, and it occurs at a temperature of around 35ºC. In a similar manner, the slopes of the temperature and moisture profiles are consistent for w_{Target} = 10%. The concave shape of the temperature profile produced a convex shape of the moisture and vice versa, and the inflection point locations are within 3.0 and 5.0 cm from the warm end, although they occur at different temperatures for the temperature and moisture.

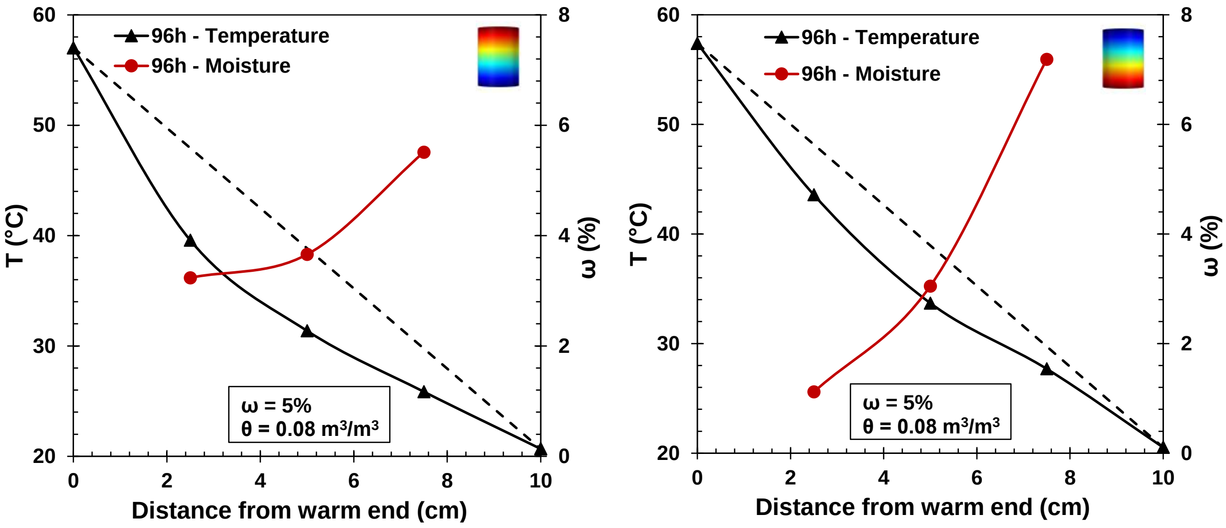

(a) (b)

Fig. 4-11. Temperature and moisture with distance for w_{Target} = 5% (a) T60_B20; and (b) T20_B60.

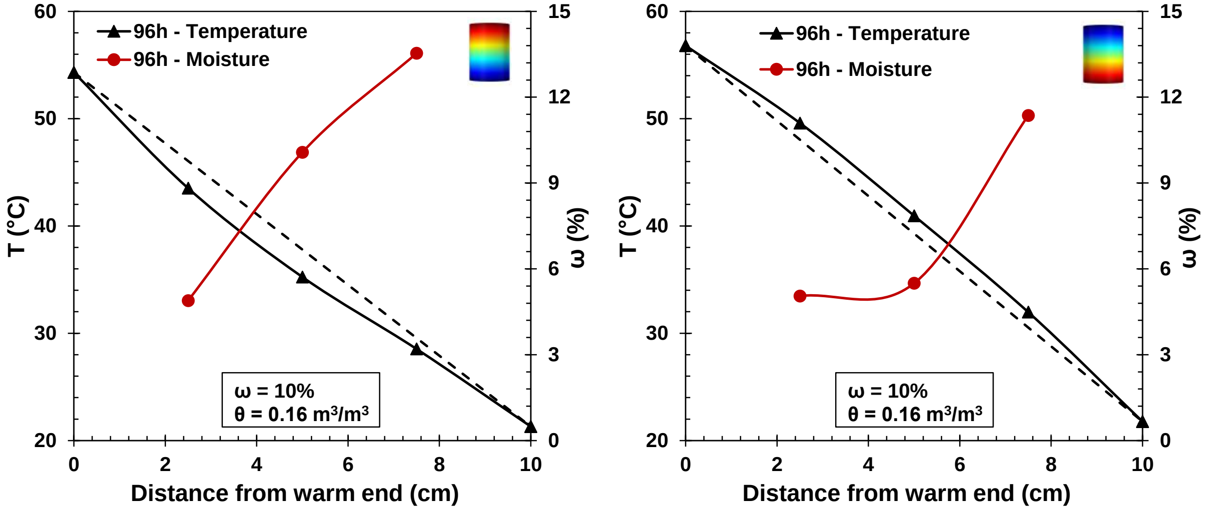

(a) (b)

Fig. 4-12. Temperature and moisture variations with distance for w_{Target} = 10% (a) T60_B20; and (b) T20_B60.

4.4 Conclusion

A series of heating tests were performed on Benbrook sand to evaluate the moisture migration with heat transport and the effect of gravity on the migration of the pore fluid. Sand columns were prepared and tested at 5 and 10% initial gravimetric moisture contents (matric suction of 1000 and 110 kPa, respectively). The following summarize the key findings from this experimental effort:

- The unsaturated sand with w_{Target} = 10% reached thermal equilibrium within 12 hrs, while it took more than 24 hrs with w_{Target} = 5%. At the location of the sensors, the temperatures were higher in the case of T20_B60. This is the case where gravity hinders moisture migration towards the cool end, which means that the retained moisture will ease heat conduction in comparison to a drier specimen, thus resulting in higher temperatures.
- The concavity and convexity of the temperature profile is dominated by the thermal conductivity and initial moisture content, but gravity appears to play a critical role in the forming of the shape. The temperature profile is concave for the T60_B20 set-up and convex for the T20_B60 set-up; however, it was observed that as moisture is redistributed, the shape of the temperature profile tends to revert to a concave shape.
- Changes in fluid density and viscosity caused moisture migration from the heat source to the cool region. At the center of the cell, the moisture content either increases or decreases depending on the direction of the thermal gradient. This was observed for w_{Target} = 10%, but the moisture content for w_{Target} = 5% seems stable at this location. Although the moisture migrates in the opposite direction of the heat source, the gain and drop in moisture content at the cool and warm regions are not relatively the same for scenarios T60_B20 and T20_B60: a lower amount of moisture migrated away from the heat source for the T20_B60 scenario, confirming gravity effect on moisture movement. Although vapor transport was not considered, it can exceed 10% of total mass flux in unsaturated sand.

4.5 References

American Society for Testing and Materials. 2000. Standard Test Methods for Amount of Material in Soils Finer Than the No. 200 (75-µm) Sieve.

American Society for Testing and Materials. 2017. Standard Test Methods for Particle-Size Distribution (Gradation) of Soils Using Sieve Analysis.

American Society for Testing and Materials. n.d. Standard Test Method for Particle-Size Distribution (Gradation) of Fine-Grained Soils Using the Sedimentation (Hydrometer) Analysis 1.

American Society for Testing and Materials. n.d. “Designation: D4318 − 17´117´1 Standard Test Methods for Liquid Limit, Plastic Limit, and Plasticity Index of Soils 1.” https://doi.org/10.1520/D4318-17E01.

American Society for Testing and Materials. n.d. “Standard Test Methods for Specific Gravity of Soil Solids by Water Pycnometer 1.” https://doi.org/10.1520/D0854-14.

Dang, L. 2017. Experimental and Numerical Studies of Heat and Moisture Transfer in Soils at Various Conditions.

Hansson, K., J. Šimůnek, M. Mizoguchi, L. Lundin, and M. Th. van Genuchten. 2004. “Water Flow and Heat Transport in Frozen Soil: Numerical Solution and Freeze–Thaw Applications.” Vadose Zone Journal, 3 (2): 693–704. https://doi.org/10.2136/vzj2004.0693.

Heitman, J. L., R. Horton, T. Ren, and T. E. Ochsner. 2007. “An Improved Approach for Measurement of Coupled Heat and Water Transfer in Soil Cells.” Soil Science Society of America Journal, 71 (3): 872. https://doi.org/10.2136/sssaj2006.0327.

Kaneza, N. 2020. An Experimental Study of Coupled Thermo-Hydro Behavior in Unsaturated

Soil.

Kaneza, N., X. Yu, and X. Wang. 2023. “Moisture Migration in Unsaturated Sands under Controlled Thermal Gradient: A Heat Cell Study.” International Journal of Geomechanics.

McInnes, K. J. 1981. “Thermal conductivities of soils from dryland wheat regions of Eastern Washington.” M. S. Thesis, Washington State University.

Texas Department of Transportation. 1999. Test Procedure for Determining Plastic Limit of Soils.

CHAPTER 5. HEAT AND MOISTURE FLOW IN SILTY SAND NEAR THE INTERFACE OF SOIL AND HEAT-EXCHANGER PIPE: THE IMPACT OF THERMAL CONTACT RESISTANCE AND SOIL DENSITY

5.1 Introduction

The integration of geothermal heat exchangers (GHEs) systems in foundations has become increasingly popular to enhance the operational efficiency of heating and cooling buildings during winter and summer, as an alternative to traditional heating, ventilation, and air conditioning (HVAC) systems (Brandl 2006; Laloui et al. 2006; Loveridge et al. 2020; McCartney et al. 2019). GHEs are an essential part of the vertical closed-circuit ground source heat pump systems (GSHPS), and their primary function is to facilitate heat exchange between a borehole pipe and subsurface soil. The pipes function as conduits for a circulating fluid responsible for distributing temperature to the adjacent soil, and the thermal process occurring at the interface between the heated pipe and the soil, as well as within the soi, is influenced by both the thermal and hydraulic properties of the soil, as well as the thermal properties of the pipe.

The heated pipe transfers thermal energy to the soil, resulting in a temperature gradient inside the soil which alters the hydraulic properties of the soil, influencing moisture redistribution in unsaturated soil. The flow of pore water inside the soil is caused by thermal gradients and is closely linked to heat transfer; this coupled thermal and hydraulic behavior constitutes a critical aspect in geotechnics (Heitman et al. 2007; Dang 2017; Kaneza et al. 2023). Several research studies have presented models to measure how temperature impacts variables such as matric suction, degree of saturation, and a range of mechanical properties (van Genuchten 1980; Mualem 1976; Thota et al. 2021).

Inadequate contact between the pipe and soil can also lead to heat loss at the pipe-soil interface, which is attributed to the thermal contact resistance between two materials. Thermal contact resistance (R) measures how well heat is transferred from one material to the other, when two materials are in contact. The value of R is high if there is significant resistance to heat transfer, and it is low when heat transfer is more direct, and heat is negligibly lost. Although the value of R is sometimes neglected, assumed, or incorrectly estimated, a precise assessment of this parameter is important for the design of ground heat exchangers like energy geo-structures; heat is extracted and released through the exchangers from and to the surrounding geo-material, where the temperature is relatively constant throughout all seasons, in order to cool buildings in the summer and warm them during winter. Heat exchange occurs along the external surface of the heat exchanger, and heat is lost due to thermal contact resistance. Generally, the internal temperature of the heat exchanger is assumed to be almost steady (Beier et al. 2011; Tilley et al. 2017), but the temperature of the external surface in contact with the geo-material is dependent upon the thermal contact resistance at pipe-borehole interface.

Although most research focuses on this particular thermal resistance and various methods were proposed to derive it, as reviewed by Lamarche et al. (2010), this parameter does not represent that at the soil-borehole interface. On the other hand, a total thermal resistance that comprehends the thermal resistance of soil and that inside the pipe/borehole can be calculated using the line source theory (LST) and cylindrical source theory (CST), but these approaches are not representative of the heat loss occurring when two materials come into contact.

The value of R can be influenced by thermal and hydraulic properties, such as the magnitude of the temperature at the interface, thermal conductivity of the solid soil particles and the pipe, and type of pore fluid of the soil (Yovanovich 1999). Other factors include surface roughness, contact pressure, and surface hardness. Assunção et al. (2014) observed considerable changes in heat flux and temperature loss when R increases at the pipe-soil interface. The temperature loss is even more significant when R surpasses 0.04 m^2K/W. Although the importance of thermal contact resistance is recognized in the design of heat exchange, its value has been ignored, assumed without supporting details, or accounted for by considering a gap between the pipe and soil (Al-Temeemi and Harris 2003; Bourne-Webb et al. 2020; Cecinato et al. 2016; Thomas and Rees 1998). Therefore, Bourne-Webb et al. (2020) proposed a test methodology where the value of the geo-contact thermal resistance (geo-CTR) can be determined directly at the pipe-soil interface. The geo-CTR at the interface of concrete and dry soil was estimated, but this methodology can also be applied to heat exchange at the contact of pipe and dry and moist soils.

This paper presents an experimental study to estimate the thermal contact resistance of a single vertical ground heat exchanger in a laboratory setting. Performing tests on a small scale in a laboratory provides a relatively easy way to conduct the study in a well-controlled condition. A high-density polyethylene (HDPE) pipe was installed in a soil cell filled with dry and unsaturated soil, and the pipe was connected to a warm water bath circulator to simulate the heating of a ground heat exchanger in the field. The pipe carried warm water from top to bottom, and internal and external temperature variations of the pipe were monitored. Simultaneously, heat transfer and moisture flux within the soil were observed at different locations around the heated pipe. This research offers a thorough examination of thermal contact resistance using both experimental and numerical methods across various scenarios involving moisture levels and compaction.

5.2 Experimental Methodology

5.2.1 Soil Index Properties

Soil particle size analysis was conducted to determine the selected soil sample, and the soil was classified as silty sand (SM) in accordance with the Unified Classification System (USCS). The particle size analysis determined the following information: D_{60} = 0.186 mm; D_{50} = 0.153 mm; D_{30} = 0.064 mm; D_{10} = 0.005 mm; c_u = 35.1; and c_c = 4.1, as shown in Fig. 5-1(a). The soil sample is non-plastic, and the specific gravity is 2.66. The soil-water retention characteristics of the silty sand was also assessed. Soil specimens for the SWCC test were compacted at 95% of dry unit weight ($\gamma_{d,max}$) and optimum moisture content (w_{opt}) obtained from the standard Proctor test results. Soil matric suction was measured using the pressure plate method for low suction and filter paper method for high suction. The relationship resulting from the two methods was further examined by constructing a best-fitting curve using the van Genuchten (1980) model, as shown in Fig. 5-1(b). Finally, the residual and saturated volumetric moisture content (θ_r and θ_s) were estimated, and the van Genuchten empirical parameters (α, n, and m) were calculated.

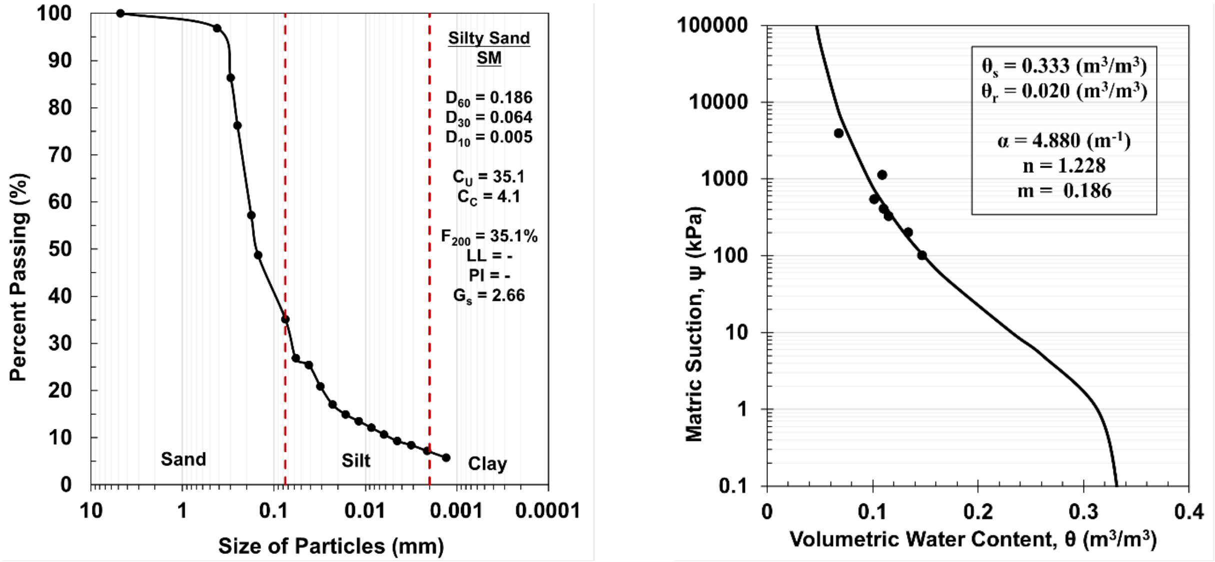

(a) (b)

Fig. 5-1. Soil (a) particle size distribution curve and (b) water retention curve.

5.2.2 Calibration of Soil Moisture Sensors and Evaluation of Thermal Conductivity

This section discusses the procedure for calibrating sensors used to measure moisture content and thermal properties. A silty sand sample was mixed with water at various moisture levels, ranging from 0 to 21% gravimetric water content. Initially, the soil was densely packed into a cylindrical mold measuring 7.8 cm in diameter and 15 cm in height, compacted in three stages at room temperature. Following the compaction, the density of the compacted soil was determined, then five different moisture sensors were sequentially inserted into the mold at different locations, ensuring no overlap with the previous insertion point. After obtaining moisture readings, a thermal property sensor was introduced into the mold to assess various thermal characteristics. Finally, small soil samples from the vicinity of the measured area were collected and dried in the oven to determine the actual moisture content. These investigations were conducted to establish correlations between water content and both dry density and thermal conductivity, providing insight into how moisture affects these properties (Fig. 5-2).

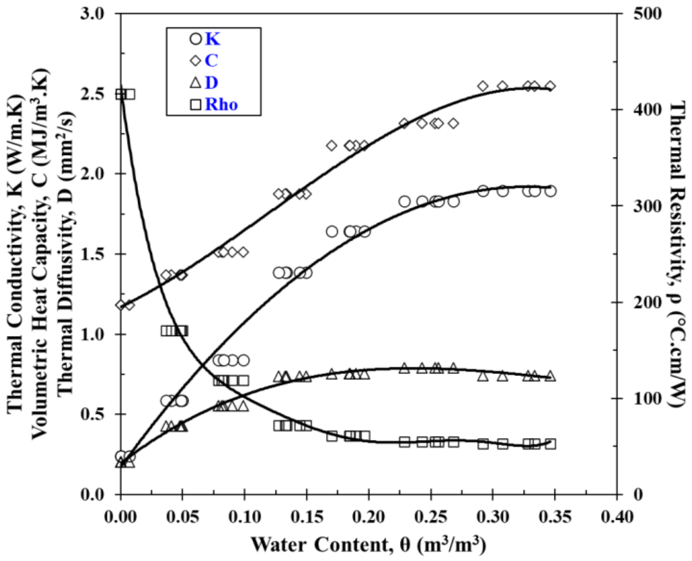

Fig. 5-2. Thermal conductivity and density for various moisture contents.

Fig. 5-3 shows the compaction curve in relation to various moisture contents and their corresponding thermal conductivity. As the level of moisture increases, the thermal conductivity goes up as the pore space becomes filled with water, which has a higher thermal conductivity compared to air. Initially, the dry density increases, but once it surpasses the optimum moisture content, the density declines rapidly. A regression analysis was conducted, considering thermal conductivity as the dependent variable and volumetric water content and dry density as independent variables. Eq. (1) was derived, and the comparison of the measured and predicted λ is shown in Fig. 5-3. Furthermore, an evaluation of sensor performance was conducted by comparing the measured and actual moisture content. Fig. 5-4 demonstrates a strong agreement between measured and actual values, although slight deviations become noticeable as moisture increases.

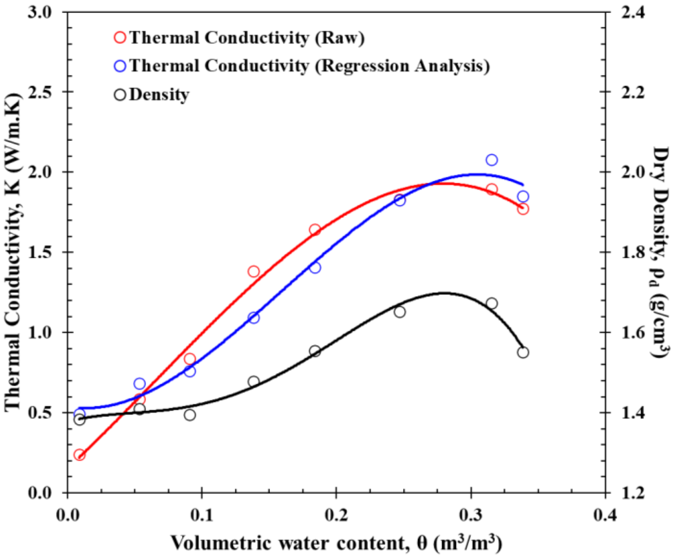

Fig. 5-3. Thermal conductivity and density for various moisture contents.

$$\lambda = -2.860 + 2.893\theta_w + 2.405\rho_d \tag{1}$$

where λ: thermal conductivity [W/mK]; θ_w: volumetric water content [m^3/m^3]; and ρ_d: dry density [g/cm^3].

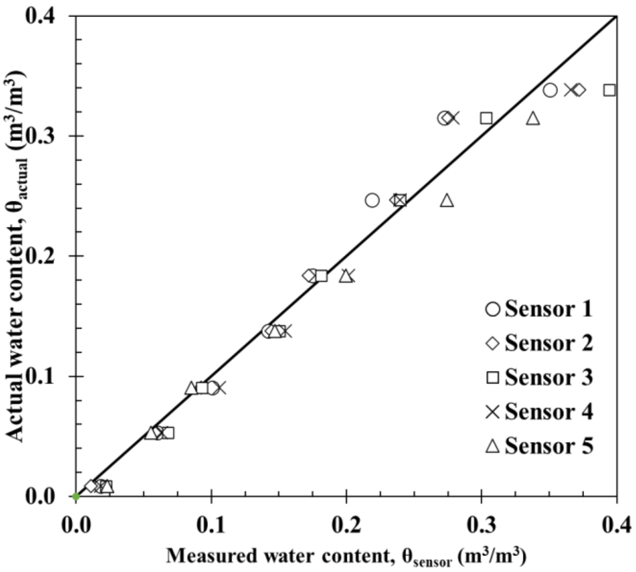

Fig. 5-4. Comparison between the measured and actual moisture contents.

5.2.3 Testing Device Configuration

A soil column device was designed to simulate field tests conducted for geothermal energy heating. A 25.4-cm inner diameter plastic column was attached to a perforated polyvinyl chloride (PVC) plate, and a 2.54-cm inner diameter high-density polyethylene (HDPE) pipe was installed at the center of the soil cell to operate as a ground heat exchanger, as shown in Fig. 5-5. A 3.51-cm x 2.85-cm heat flux sensor (HFS-4) from Omega Engineering, Inc. was attached at mid-height of the pipe to measure the heat transfer at the soil-pipe interface, where the HFS-DAQ recorded both the heat flux and temperature. Five type-T thermocouples and five ECH20 EC-5 moisture sensors were vertically inserted on opposite sides of the pipe at distances of approximately 1, 3, 5, 7, and 9 cm from the center. Temperature variations were measured with the Picolog Recorder, while the moisture content was measured by the ZL6 Data Logger. An additional type-T thermocouple was placed inside the pipe to measure the temperature of the water circulating in the pipe. A dual-needle sensor measuring the thermal conductivity was also placed at 1 cm from the pipe.

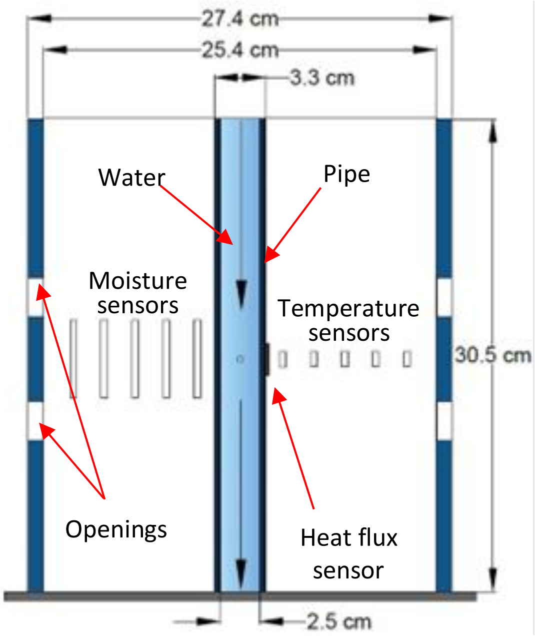

Fig. 5-5. Soil testing column with instrumentation.

The soil specimens were compacted in the soil testing column in 6 layers, and the target gravimetric moisture contents (w_{Target}) were 0, 3, 6, 9, and 12. The dry density (ρ_d) of approximately 1.25 g/cm^3 (loose) and 1.50 g/cm^3 (dense) were also targeted for the testing. During the compaction of the soil, the pipe was covered, so as not to accidentally pour soil particles into the pipe. Fig. 5-6 shows three stages of the soil cell compaction; the left image indicates the empty soil cell, the middle image presents the halfway compacted soil cell with installed measuring devices, and the right image shows the fully compacted soil column.

Fig. 5-6. Top view of the soil column at different stages of compaction.

Following the compaction and installation of the sensors, a plastic plate was placed at the top and bottom of the soil cell, and the plastic plate incorporated a 2.54-cm thick geofoam for thermal insulation. A temperature-controlled circulator (Model SD07R-20-A11B, PolyScience) was connected to the pipe, where water was distributed from the top to the bottom of the soil column. Then the temperature of the water bath circulator was set to 60°C. For a period of 2 and 4 days (dry and moist soil, respectively), the temperature and heat flux readings were taken at a 1-min interval, whereas the moisture readings were taken at a 5-min interval, and the thermal conductivity at 30-min interval. The dataloggers provided the temperature in °C, volumetric moisture content in m^3/m^3, and heat flux in W/m^2.

5.3 Numerical Approach

5.3.1 Coupled Thermo-Hydro Equations

In this investigation, the energy and mass conservation equations were solved simultaneously using COMSOL Multiphysics version 5.3. The resulting equations for the thermal and hydraulic fields are described as follows. Eq. (2) delineates the dynamics of energy transfer within a porous medium, accounting for heat conduction in solid soil particles, heat convection in pore fluids (including liquid water and air), and the phase change of water vapor. Eq. (3) describes the movement of pore liquids, air, and water vapor, employing Richard's equation, which depends on factors such as water head potential, temperature gradients, and hydraulic conductivity. Further details on how to implement these equations in COMSOL Multiphysics are given in Chapter 3.

$$C_{eq}\frac{\partial T}{\partial t} + \nabla \cdot \left(-\lambda_{eq}\nabla T\right) + C_{eq}\left(q_w\nabla T + q_g\nabla T + q_v\nabla T\right) = -L_w\rho_w\nabla q_g - L_w\rho_w\frac{\partial \theta_g}{\partial t} - L_w\rho_w\nabla q_v - L_w\rho_w\frac{\partial \theta_v}{\partial t} \tag{2}$$

$$\frac{\partial \theta_w}{\partial t} + \nabla \times \left(q_w + q_g + q_v\right) = -\frac{\rho_g}{\rho_w}\frac{\partial \theta_g}{\partial t} - \frac{\rho_v}{\rho_w}\frac{\partial \theta_v}{\partial t} \tag{3}$$

5.3.2 Geometry and Soil Properties

Simulations were conducted to predict temperature and volumetric water content distributions within a silty sand surrounding a heated pipe in a column testing apparatus to evaluate the geo-contact thermal resistance at the interface between the soil and the pipe. The soil column had a length of 30.5 cm and an inner diameter of 25.4 cm, with a 2.5-cm inner diameter pipe positioned at its center. The analysis was conducted in a 2D axisymmetric spatial dimension, as illustrated in Fig. 5-7. The model geometry incorporated four distinct materials: water circulating within the pipe, the pipe wall, the compacted soil, and the wall of the column or tube. A uniform temperature of 60ºC was applied radially to the water, while the surface of the column wall was held at a constant temperature to represent the ambient conditions. The top and bottom boundaries were adiabatic, simulating insulation as in the experimental setup, thus allowing heat dissipation solely in the radial direction. A constant thermal conductance, as determined experimentally, was applied at the soil-pipe interface. No mass flux was applied at any of the boundaries.

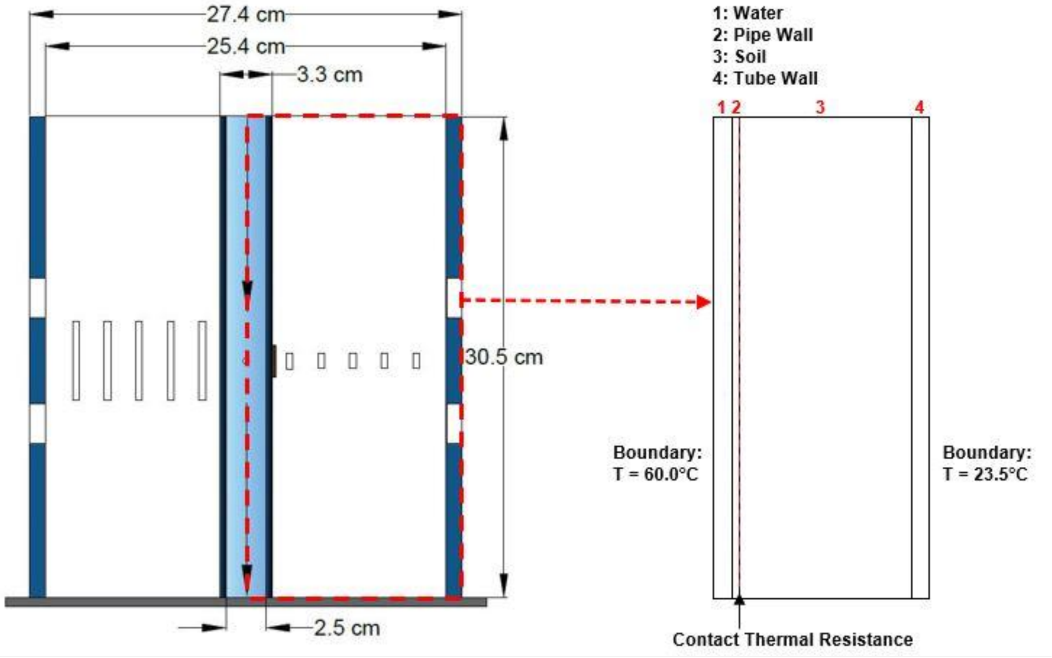

Fig. 5-7. Model geometry.

The porosity of the soil and soil parameters used in this study are summarized in Table 5-1 and 5-2, respectively.

Table 5-1. Porosity of the loose and dense soils.

	0%	**3%**	**6%**	**9%**	**12%**
			Porosity		
Loose	0.530	0.527	0.525	0.527	0.526
Dense	0.437	0.460	0.457	0.470	0.444

Table 5-2. Soil input parameters.

Parameter	**Value**	**Units**	**Description**
C_g	1000	J/(kg·K)	Specific heat capacity of air
C_p	2000	J/(kg·K)	Specific heat capacity of pipe
C_s	850	J/(kg·K)	Specific heat capacity of soil solids
C_t	880	J/(kg·K)	Specific heat capacity of tube
C_v	1000	J/(kg·K)	Specific heat capacity of vapor
C_w	4200	J/(kg·K)	Specific heat capacity of water
f_c	0.07	-	Clay fraction
g	-9.81	m/s^2	Acceleration
G_{wT}	5	-	Gain factor
Ks_g	3.2E-05	m/s	Hydraulic conductivity of air
Ks_w	3.2E-04	m/s	Hydraulic conductivity of water
M	18.01528	g/mol	Molecular weight of water
R	8.31432	J/mol·K	Universal gas constant
λ_g	0.025	W/m·K	Thermal conductivity of gas
λ_p	0.48	W/m·K	Thermal conductivity of pipe
λ_s	0.398	W/m·K	Thermal conductivity of soil solids
λ_t	0.13	W/m·K	Thermal conductivity of tube
λ_v	0.025	W/m·K	Thermal conductivity of vapor
λ_w	0.6	W/m·K	Thermal Conductivity of water
ρ_g	1.2	kg/m^3	Density of gas
ρ_p	950	kg/m^3	Density of pipe
ρ_t	1410	kg/m^3	Density of tube
ρ_v	1000	kg/m^3	Density of water

5.4 Results and Discussions

5.4.1 Temperature Distribution

After subjecting the water bath circulator to a temperature of 60°C, water quickly attaining a stable temperature within 1 hour, while the external surface of the pipe required a slightly longer duration to reach equilibrium, and the soil reached its steady-state temperature even later. Figs. 5-8(a) and (b) illustrate the temperature distribution of the water, pipe surface, and soil after 48 hours of experimental heating, respectively, for both the loose and dense conditions of dry soil. The temperature distributions for moist soils are not presented here for conciseness. The subscripts "w," "p," "s," and single digits denote water, external pipe surface, soil at the pipe-soil interface (or at 0 cm), and distances ranging from 1 to 9 cm from the heat source, respectively. It is evident that in the case of dense soil, the temperatures at the external pipe surface (T_p) and soil at the interface (T_s) are nearly identical, indicating a high thermal conductivity and minimal thermal contact resistance. This enhanced thermal conductivity in dense soil is further demonstrated by the measured temperatures at the specified locations being higher than those in the loose soil. This increased thermal conductivity is attributed to the higher density, resulting from smaller pore voids and greater contact between solid soil particles. T_p was calculated using Fourier's Law of heat conduction given by Eqs. (4 and 5).

$$q = -k\frac{\Delta T}{\Delta x} = -k\frac{T_p - T_w}{\Delta x} \tag{4}$$

where q: the heat flux measured at the pipe-soil interface (W/m^2); k: thermal conductivity of the pipe (= 0.48 W/·K); and Δx: thickness of the pipe (=0.004 m). T_w represents the temperature of the circulating water, which is also regarded as the temperature of the internal pipe surface.

By rearranging Eq. (4), the temperature of the external pipe can be obtained by Eq. (5).

$$T_p = T_w - q\frac{\Delta x}{k} \tag{5}$$

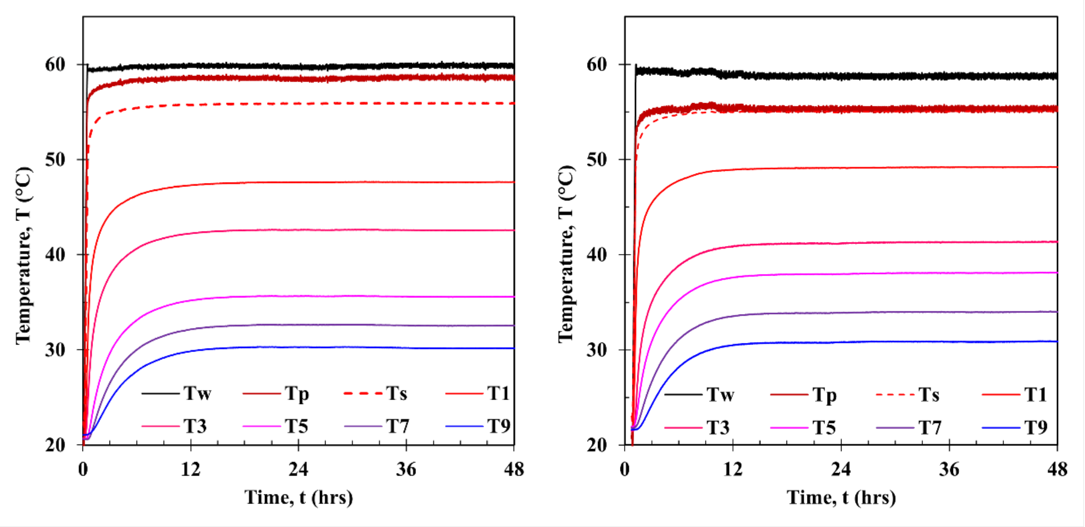

(a) (b)

Fig. 5-8. Experimental temperature variations for (a) 0% loose and (b) 0% dense.

Fig. 5-9 presents the thermal profiles of the loosely and densely packed silty sand using numerical analysis. In terms of the color scale representing temperature variations, distinctions between the distributions of dry soil are not readily discernible. However, as shown in Fig. 5-10, the differences become more pronounced when visualizing the temperature gradient in moist soil. Herein, the authors exclusively presented the moist soil samples with a targeted gravimetric water content of 9% to limit the number of figures in this manuscript. Loose moist soils exhibit reduced dissipation of heat emanating from the heat source, whereas dense soils display a more evenly distributed profile throughout the soil column, due to their higher thermal conductivity.

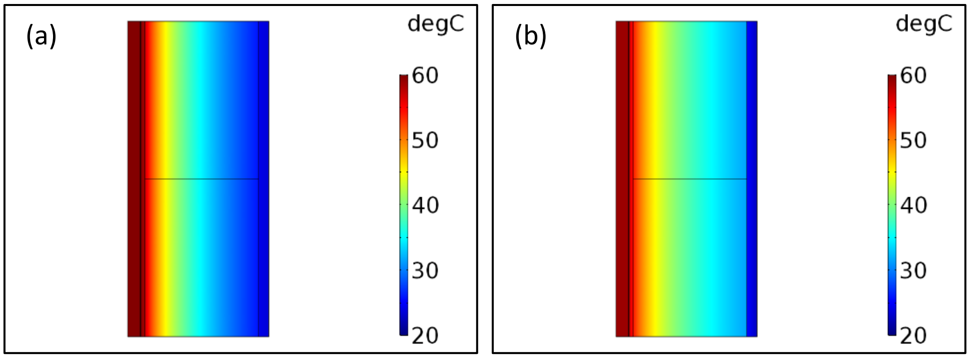

Fig. 5-9. Numerical temperature variations for (a) 0% loose and (b) 0% dense.

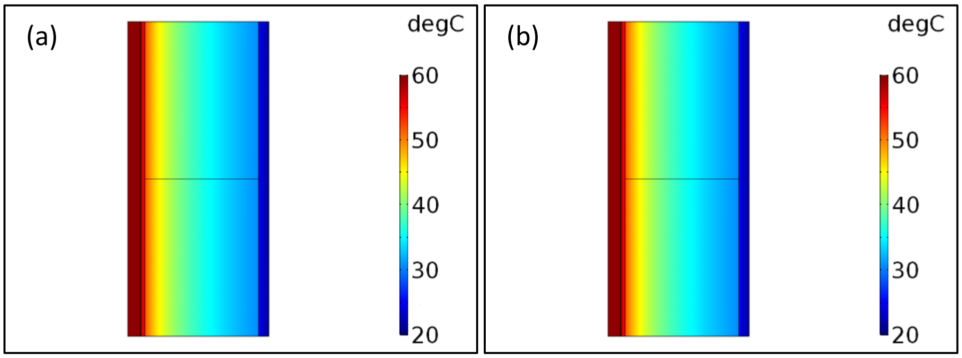

Fig. 5-10. Numerical temperature variations for (a) 9% loose and (b) 9% dense.

5.4.2 Moisture Distribution

This study investigated the impact of varying moisture levels (ranging from 3 to 12%) on thermal contact resistance. Over a 96-hour heating period, moisture distribution patterns were examined. Generally, moisture migrated away from the heat source towards the column's wall, with higher initial moisture content leading to greater moisture flux. Fig. 5-11 illustrates the initial state of moist soil before heating and after 96 hours of heating. It demonstrates that the uniformly distributed moisture of compacted soil (left) subsequently exhibited drying around the pipe, indicating moisture movement away from the heated pipe (right).

Fig. 5-11. Initial and final moisture distribution state.

The moisture sensors used in the experiments only detected alterations in liquid water changes, and Fig. 5-12 displays the moisture distributions within initially 9% moist loose and dense soil samples during the heating process. Near to the heat source, there was a significant reduction in pore water content, while other locations exhibited minimal changes, and the moisture migration stabilized after 48 hours of heating. The moisture sensors overestimated the measured volumetric water content of the dense soils, probably due to the densely-packed state of the latter. This was observed across all the initial moisture contents, and the reason may be because the sensors and cables were tightly embedded in the soil which may have created some disturbances.

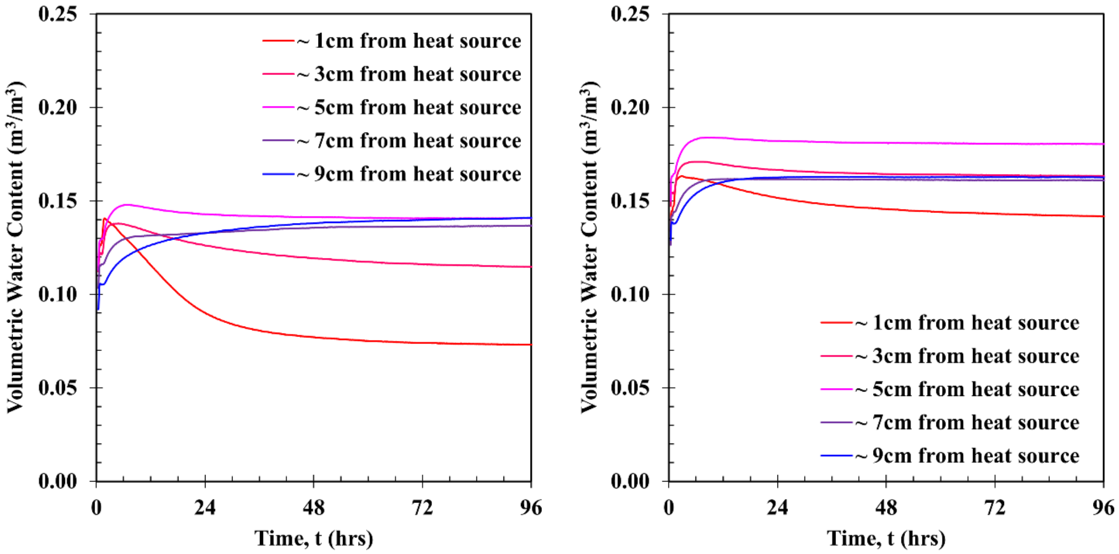

(a) (b)

Fig. 5-12. Experimental moisture variations for (a) 9% loose and (b) 9% dense.

The COMSOL Multiphysics software was employed to compute the volumetric pore fluid content. Figs. 5-13 and 5-14 depict the variation in volumetric content across the radial direction. It is important to note that when the initial moisture content is lower, as shown in Figs. 5-13(a) and (b), the pore space within the silty sand is predominantly occupied by air, and this gas phase undergoes substantial changes with fluctuations in temperature. In the proximity of the heat source where temperatures are elevated, the liquid phase transforms into the gas phase, whereas at a greater distance from the heat source, liquid migrating away from the heat source converts into water vapor, resulting in a significant increase in volume of vapor. Conversely, for higher initial moisture content, the proportion of air present within the soil is small, while the presence of water vapor is greater; therefore, temperature fluctuations have a more significant impact on liquid water movement under these circumstances.

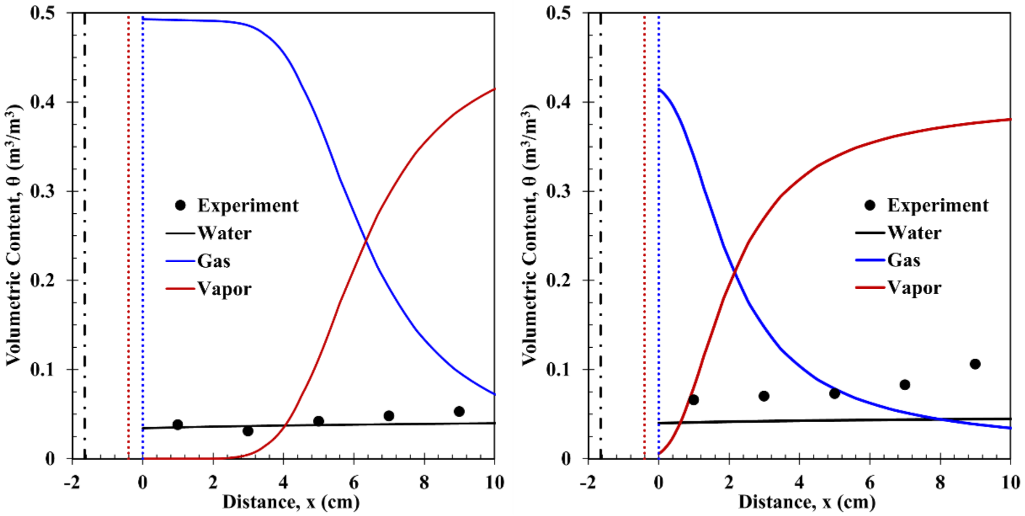

(a) (b)

Fig. 5-13. Volumetric content of the pore fluid (a) 3% loose and (b) 3% dense.

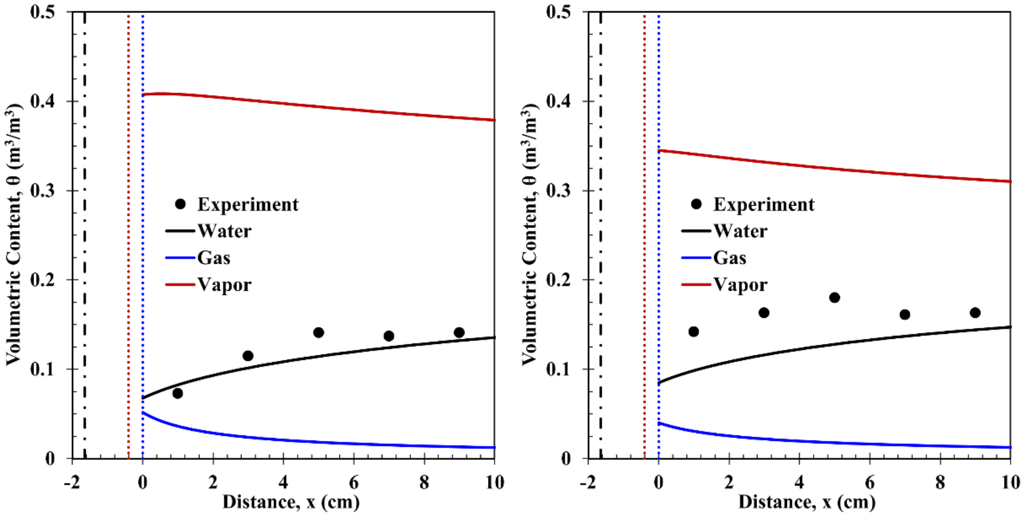

(a) (b)

Fig. 5-14. Volumetric content of the pore fluid (a) 9% loose and (b) 9% dense.

The thermal properties of the silty sand were impacted by the variations in the soil's volumetric water content, as demonstrated in Fig. 5-15. The volumetric water content and thermal conductivity measured at 1 cm from the pipe showed that thermal conductivity decreased proportionally with the volumetric water content. This reduction in thermal conductivity subsequently affected the temperature at the interface between the pipe and the soil, as will be discussed in the following section.

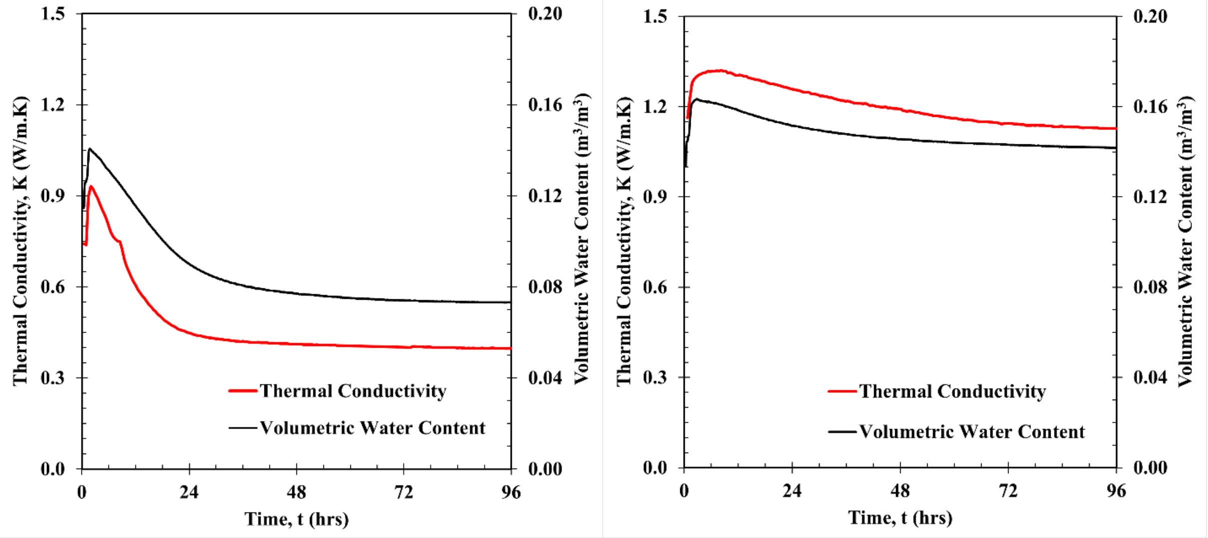

(a) (b)

Fig. 5-15. Thermal and hydraulic properties at 1 cm from the pipe (a) 9% loose and (b) 9% dense.

The moisture fluctuations obtained through numerical modeling of moist soil (with a moisture content of 9%) indicate that denser soil allows for greater moisture movement, as illustrated by the color gradient in Fig. 5-16 and confirmed by experimental data. This phenomenon can be attributed to the increased capillary action in soils with smaller pores, which is characteristic of densely compacted soil. The units of the volumetric water content shown in Fig. 5-16 is m^3/m^3.

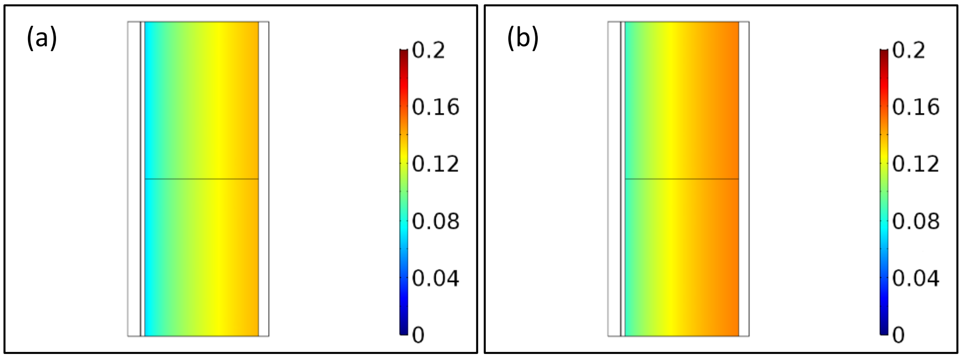

Fig. 5-16. Thermal and hydraulic properties at 1 cm from the pipe (a) 9% loose and (b) 9% dense.

5.4.3 Geo-Contact Thermal Resistance

The thermal contact resistance occurring at the interface connecting the pipe and the surrounding soil is a result of the temperature difference and heat flux at this particular location, and it can be determined using Eq. (6). Specifically, ΔT represents the temperature difference that arises from imperfect contact between the external surface of the pipe and the soil located at a distance of 0 cm from the pipe.

$$R = \frac{\Delta T}{q} \tag{6}$$

where R: thermal contact resistance (m^2K/W); ΔT: temperature difference (K); and q: heat flux measured at the pipe-soil interface (W/m^2).

Fig. 5-17 and Table 5-3 provide a summary of heat flux, temperature difference, and thermal contact resistance values for the loose and dense soils. Dense soils consistently exhibited higher heat flux than loose soils in all moisture scenarios, due to enhanced contact between the pipe surface and soil particles. In loose soils, the heat flux and temperature difference increased with rising moisture content, while the thermal contact resistance decreased (Fig. 5-17(a)). This suggests that the thermal contact resistance of loose silty soils can be determined based on moisture content. In contrast, there was no clear trend observed for the densely packed soils (Fig. 5-17(a)), likely due to non-uniform dry density. Despite targeting a density of approximately 1.50 g/cm^3, achieving this density proved challenging, and the obtained values (Table 6-3) represent the maximum densities attainable for the specified moisture content in the soil column. Consistency in densely-packed soil densities would likely yield more accurate assessments, similar to those for loose soils.

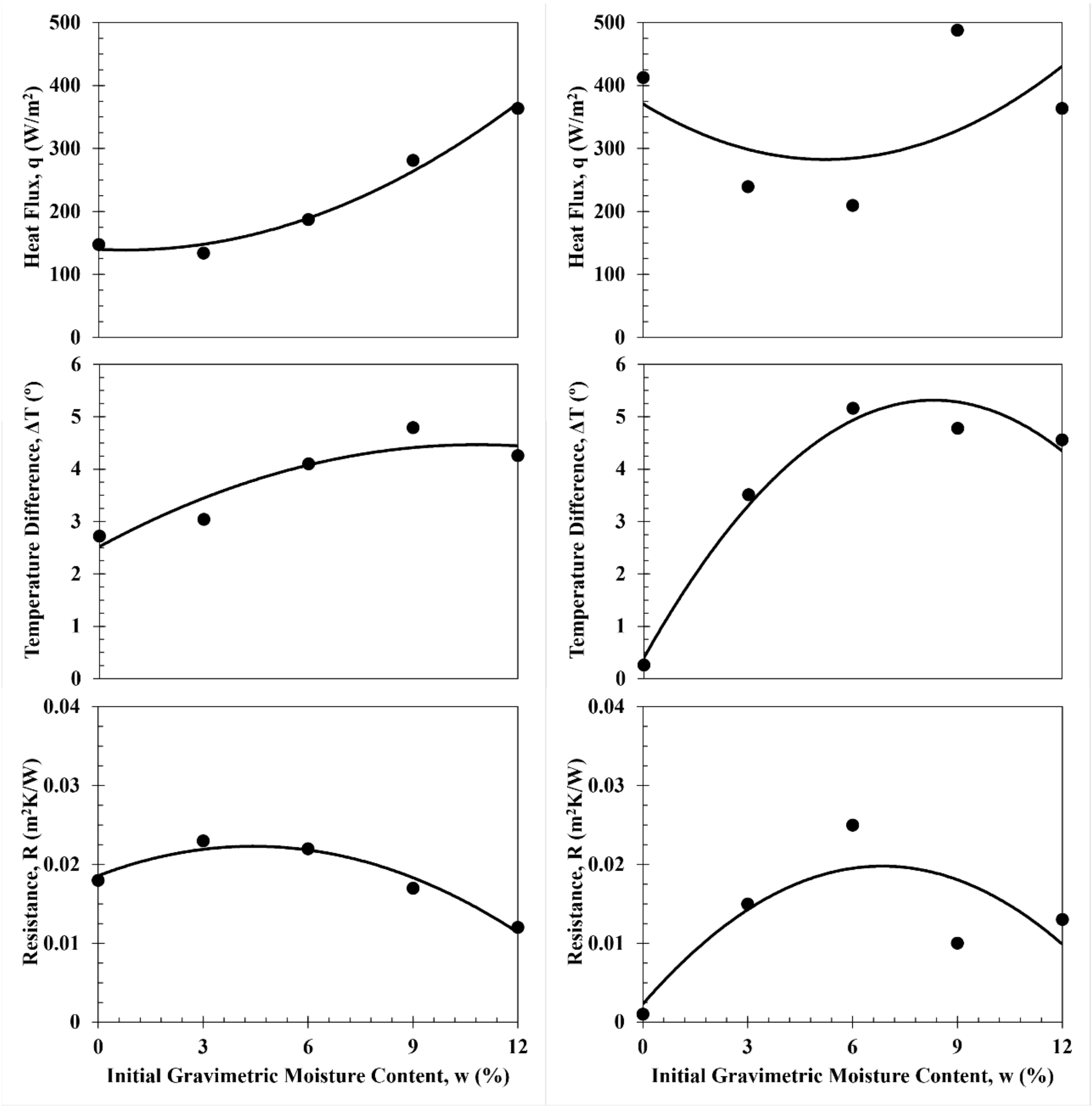

(a) (b)

Fig. 5-17. Thermal properties in function of moisture content (a) loose and (b) dense.

Table 5-3. Measured heat flux and calculated thermal contact resistance.

	0%	**3%**	**6%**	**9%**	**12%**
			Loose		
ρ_d (g/cm^3)	1.25	1.26	1.26	1.26	1.26
Q (W/m^2)	147.4	133.8	187.0	281.1	363.6
ΔT (°)	2.72	3.04	4.10	4.79	4.25
R (m^{2}K/W)	0.018	0.023	0.022	0.017	0.012
			Dense		

ρ_d (g/cm^3)	1.50	1.44	1.44	1.41	1.48
Q (W/m^2)	412.4	239.4	209.5	487.6	363.6
ΔT (º)	0.26	3.51	5.16	4.78	4.56
R (m^{2}K/W)	0.001	0.015	0.025	0.010	0.013

Following experimental evaluation of thermal contact resistance, the reciprocal parameter known as thermal conductance (h [W/m^{2}K]) was subsequently integrated into the pipe-soil interface of the numerical model using the Thermal Contact functionality within the Heat Transfer Module of COMSOL Multiphysics. This step enabled further assessment of the computed thermal contact resistance. Thereafter, the numerical modelling generated temperature variations throughout the soil column, and the resulting temperature profiles were then compared with the experimental data. Table 6-4 provides a summary of temperature differences at the pipe-soil interface for both experimental and numerical values. This location serves as a focal point for our analysis because it is where the thermal contact resistance is applied. The discrepancies between the measured and predicted temperature differences remain relatively small and consistent across various moisture scenarios, with the exception of soil mixed at 12% moisture content, which exhibits the largest difference of 1.97°C. This suggests that the calculation of thermal contact resistance in the present study is generally reliable, and any discrepancies may be attributed to the thermal contact resistance of the heat flux sensor itself.

Figs. 5-18 and 5-19 indicate that the temperatures observed through both experimental observations and numerical simulations at specific soil locations demonstrate a certain level of consistency. This consistency is particularly pronounced in dry soil conditions but slightly decreased in moist soil. This phenomenon is the result of additional factors exerting an influence in moist soils, where heat transfer is influenced not solely by heat conduction within the solid soil particles but also by heat convection within the fluid-filled pores. Furthermore, as discussed earlier, fluctuations in liquid water content can lead to changes in thermal conductivity; thus, variations in thermal conductivity, as described by Eq. (3-8), can result in temperature variations.

Table 5-4. Temperature difference at the pipe-soil interface.

	0%	**3%**	**6%**	**9%**	**12%**
			Loose		
Experimental	2.72	3.04	4.10	4.79	4.25
Numerical	1.38	2.53	3.03	2.99	2.28
Difference	1.34	0.51	1.07	1.80	1.97
			Dense		
Experimental	0.26	3.51	5.21	4.78	4.56
Numerical	0.19	3.58	6.40	2.85	4.15
Difference	0.08	-0.08	-1.23	1.94	0.41

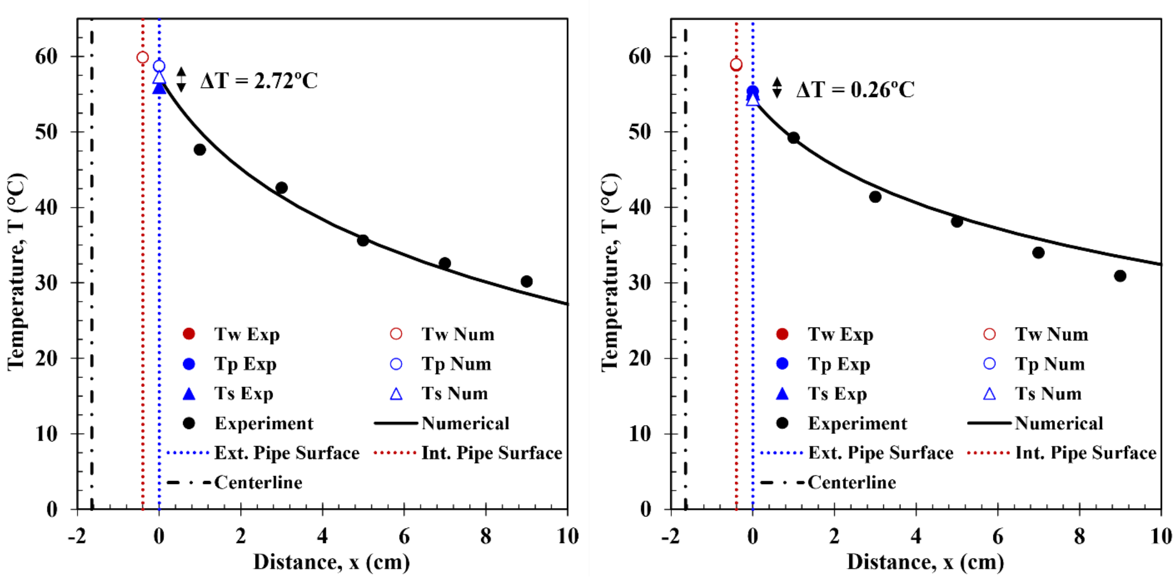

(a) (b)

Fig. 5-18. Experimental and numerical temperature profiles (a) 0% loose and (b) 0% dense.

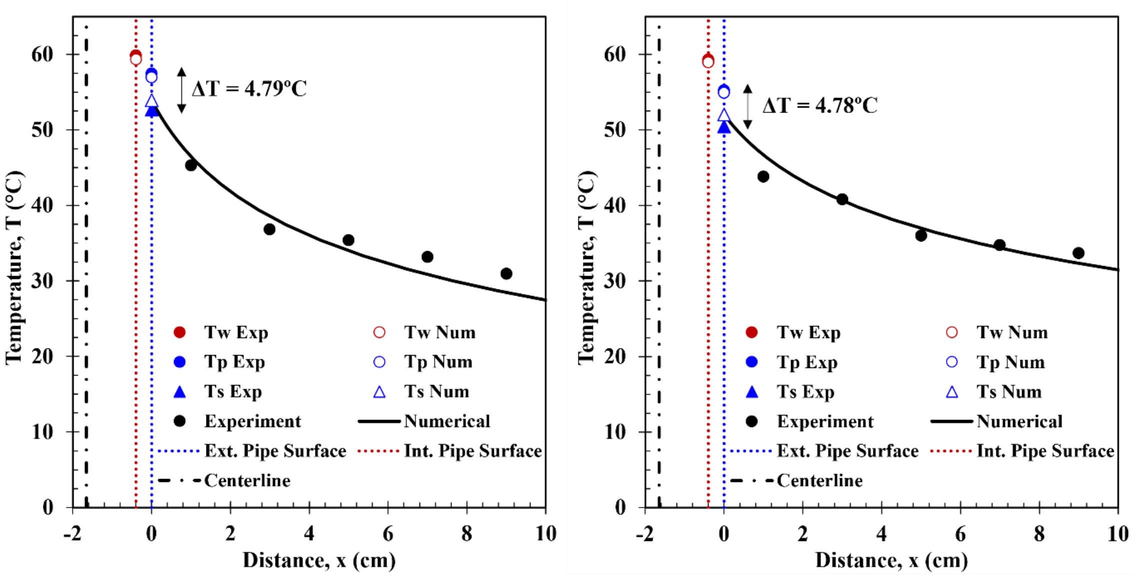

(a) (b)

Fig. 5-19. Experimental and numerical temperature profiles (a) 9% loose and (b) 9% dense.

5.5 Conclusion

This study conducted a comprehensive investigation of the thermal contact resistance occurring at the interface between a heated pipe and the surrounding soil to evaluate how moisture levels and soil density impact this critical parameter. The following key observations can be summarized:

- Dense soil exhibited a significantly higher thermal conductivity compared to loose soil, primarily due to its increased solid particle contact. This was evident in the nearly identical temperatures at the external pipe surface and soil interface in dry soil, as well as the more uniform temperature distribution in moist dense soils compared to their loose counterparts.
- Dense soils consistently displayed higher heat flux compared to loose soils across various moisture levels, primarily attributable to more pipe-soil particle contact. Higher thermal conductivity lead to minimal thermal contact resistance.

- Moisture was found to migrate away from the heat source toward the soil column's wall, with higher initial moisture content resulting in greater moisture flux. Moisture levels in the soil played a significant role in thermal behavior. Thermal conductivity decreased proportionally with volumetric water content, affecting temperature profiles at the pipe-soil interface.
- Thermal contact resistance was evaluated experimentally and compared with numerical simulations. The inverse parameter, thermal conductance, was applied to the numerical model, and resulting temperature profiles were consistent with experimental data in dry soil conditions. Slight discrepancies were noted in moist soil conditions, possibly due to additional factors affecting heat transfer.
- Thermal contact resistance proportionally increased with moisture in loose soils, whereas densely-packed soils, characterized by non-uniform dry density, do not exhibit a clear trend. Consistency in density is vital for precise assessments, as seen in loose soils.

5.6 References

Al-Temeemi, A. A., and D. J. Harris. 2003. “The effect of earth-contact on heat transfer through a wall in Kuwait.” *Energy Build,* 35 (4): 399–404. Elsevier. https://doi.org/10.1016/S0378-7788(02)00114-7.

Beier, R. A., M. D. Smith, and J. D. Spitler. 2011. “Reference data sets for vertical borehole ground heat exchanger models and thermal response test analysis.” *Geothermics,* 40 (1): 79–85. Pergamon. https://doi.org/10.1016/J.GEOTHERMICS.2010.12.007.

Bourne-Webb, P. J., J. D. de Sousa Figueira, and T. M. Bodas Freitas. 2020. “On the resistance to heat flow across soil-structure interfaces.” *Energy Build,* 228. Elsevier Ltd. https://doi.org/10.1016/j.enbuild.2020.110488.

Brandl, H. 2006. “Energy foundations and other thermo-active ground structures.” *Geotechnique,* 56(2): 81–122.

Cecinato, F., R. Piglialepre, F. A. Loveridge, and D. Nicholson. 2016. “Numerical analysis of thermal cycling during a multi-stage energy pile thermal response test.” *Energy Geotechnics - Proceedings of the 1st International Conference on Energy Geotechnics, ICEGT 2016*, 593–599. CRC Press/Balkema.

Dang, L. 2017. *Experimental and Numerical Studies of Heat and Moisture Transfer in Soils at Various Conditions*.

van Genuchten, M. T. 1980. “closed-form equation for predicting the hydraulic conductivity of unsaturated soils.” *Soil Sci. Soc. Am. J.*, 44(5): 892–898.

Heitman, J. L., R. Horton, T. Ren, and T. E. Ochsner. 2007. “An Improved Approach for Measurement of Coupled Heat and Water Transfer in Soil Cells.” *Soil Science Society of America Journal*, 71 (3): 872. https://doi.org/10.2136/sssaj2006.0327.

Kaneza, N., X. Yu, and X. Wang. 2023. “Moisture Migration in Unsaturated Sands under Controlled Thermal Gradient: A Heat Cell Study.” *International Journal of Geomechanics*.

Laloui, L., M. Nuth, and L. Vulliet. 2006. “Experimental and numerical investigations of the behavior of a heat exchanger pile.” *International Journal Numerical and Analytical Methods in Geomechanics*, 30: 763–781.

Lamarche, L., S. Kajl, and B. Beauchamp. 2010. “A review of methods to evaluate borehole thermal resistances in geothermal heat-pump systems.” *Geothermics*, 39 (2): 187–200. CNR-Istituto di Geoscienze e Georisorse. https://doi.org/10.1016/j.geothermics.2010.03.003.

Loveridge, F., J. S. McCartney, G. A. Narsilio, and M. Sanchez. 2020. “Energy geostructures: A review of analysis approaches, in situ testing and model scale experiments.” *Geomechanics* *for Energy and the Environment,* 22. Elsevier Ltd. https://doi.org/10.1016/j.gete.2019.100173.

Manuel Freitas Assunção, R., P. John Bourne-Webb, and J. Alberto dos Santos Supervisor. 2014. *Thermal and Thermal-Mechanical Analysis of Thermo-Active Pile Foundations Civil Engineering Examination Committee*.

McCartney, J. S., N. H. Jafari, T. Hueckel, M. Sánchez, and F. Vahedifard. 2019. “Emerging Thermal Issues in Geotechnical Engineering.” 275–317.

Mualem, Y. 1976. “A new model for predicting the hydraulic conductivity of unsaturated porous media.” *Water Resour Res,* 12 (3): 513–522. https://doi.org/10.1029/WR012i003p00513.

Philip, J. R., and D. A. de Vries. 1957. “Moisture movement in porous materials under temperature gradients.” *Transactions of the American Geophysical Union*, 38(2): 222–232.

Thomas, H. R., and S. W. Rees. 1998. “The thermal performance of ground floor slabs—a full scale in-situ experiment.” *Build Environ*, 34 (2): 139–164. Pergamon. https://doi.org/10.1016/S0360-1323(98)00001-8.

Thota, S. K., F. Vahedifard, and J. S. McCartney. 2021. “A Temperature-Dependent Model for Ultimate Bearing Capacity of Energy Piles in Unsaturated Fine-Grained Soils.” *Journal of Geotechnical and Geoenvironmental Engineering,* 147 (11). https://doi.org/10.1061/(ASCE)GT.1943-5606.0002676.

Tilley, B. S., V. C. Yang, J. C. Baiense, and S. Evans. 2017. “Frequency-dependent thermal resistance of vertical U-tube geothermal heat exchangers.” *J Eng Math*, 102 (1): 131–150. Springer Netherlands. https://doi.org/10.1007/s10665-016-9881-7.

Yovanovich, M. 1999. *Thermal Interface (Joint) Conductance and Resistance*.

CHAPTER 6. HEATING TEST OF A SILTY SAND IN A SHORT CYLINDER WITH A VERTICAL HYDRONIC GROUTED HEATING PIPE

6.1 Introduction

Ground heat exchangers (GHEs) are integral components of vertical closed-circuit ground source heat pump systems (GSHPS). The primary function of GHEs is to facilitate the transfer of heat between a circulating fluid within a pipe or loop and the surrounding ground. These heat exchangers can be either directly buried in the soil or enveloped in grout to enhance heat conduction and stability. They offer an environmentally friendly and energy-efficient solution for heating and cooling buildings, with the potential to reduce harmful CO_2 emissions (Omer 2008). Nevertheless, their installation can be costly, raising the importance of ensuring their optimal performance for cost-effectiveness and sustainability.

The performance assessment of GHEs can be carried out through analytical methods, comprised in three categories: the infinite line source model (ILSM), infinite cylindrical source model (ICSM), and finite line source model (FLSM) (Christodoulides et al. 2016; Lamarche and Beauchamp 2007; Man et al. 2010). These models assume different ground characteristics: ILSM and ICSM treat the ground as infinite, while FLSM considers it semi-infinite. In these models, the borehole of the heat exchanger is approximated as an infinite line or cylindrical source or a finite source, depending on the specific model. However, these analytical approaches tend to overlook critical components of GHEs, such as the pipe, the fluid inside the pipe, and the grout that envelop the pipe, which can lead to potential misinterpretations of the overall GHEs performance.

In addition to analytical methods, numerical simulations have been proposed to address the limitations of analytical solutions, as reviewed by (Bidarmaghz 2014). Nevertheless, these numerical simulations often assume dry ground surrounding the GHEs and consider heat conduction as the sole mode of heat transfer. Notably, they tend to neglect the thermal contact resistance, which is distinct from the thermal resistance associated with GHE components (Al-Khoury 2011; Kreith et al. 2010; Lamarche et al. 2010; Loveridge 2012; Loveridge and Powrie 2014); rather, the thermal contact resistance refers to the hindrance of heat flow at material interfaces. In the case of GHEs enveloped by grout, heat loss occurs at the pipe-grout and grout-ground interfaces. Unfortunately, this thermal contact resistance is frequently overlooked, omitted, or erroneously assumed in many researchers (Bourne-Webb et al. 2020; Cecinato et al. 2016). To address these limitations, Bourne-Webb et al. (2020) proposed a testing methodology for determining the value of the geo-contact thermal resistance (geo-CTR) directly at the interface of two materials. The estimation of geo-CTR at the concrete-soil interface has been explored, but this methodology can also be applied to assess heat exchange at the pipe-grout and pipe-moist soil interfaces, as demonstrated by Kaneza and Xinbao (2024).

This paper overviews an experimental study aimed at estimating the thermal contact resistance of a single vertical ground heat exchanger in a controlled laboratory setting. The study involved the installation of a high-density polyethylene (HDPE) pipe within a soil testing device, with the soil containing 9% gravimetric water content. The pipe was connected to a warm water bath circulator to replicate the conditions of a ground heat exchanger in the field. Temperature variations within the pipe were monitored internally and externally, while heat transfer and moisture flux within the soil were observed at various locations around the heated pipe. The presence and absence of grout were evaluated to understand its contribution to heat exchange, and the thermal conductivity of the grout was varied to assess heat transport. Furthermore, the thermal contact resistance between the grout and the soil was examined. This research provides a comprehensive examination of thermal contact resistance, employing both experimental and numerical methods to explore a range of thermal properties scenarios.

6.2 Experimental Approach

6.2.1 Materials and Soil Properties

The soil used in this study was classified as silty sand (SM), consisting of 35% of fine content, and D_{60} = 0.186 mm; D_{30} = 0.064 mm; D_{10} = 0.005 mm; c_u = 35.1; and c_c = 4.1 were obtained from the particle size analysis. The soil has a specific gravity of 2.66 and is non-plastic. The soil water retention characteristics according to the van Genuchten (1980) model are θ_{sat} = 0.333 m^3/m^3; θ_{res} = 0.020 m^3/m^3; a = 4.880 (m^{-1}); n = 1.228 (-); and m = 0.186 (-). The grout used consisted of 85% bentonite and 15% graphite, and compaction was performed to determine the maximum thermal conductivity (λ), and its corresponding dry density (ρ_d) and moisture content (w). Fig. 6-1 shows that the maximum thermal conductivity (λ = 1.5 W/m×K) was obtained when ρ_d = 1.0 g/cm^3 and w = 36%. The grout is very water-absorbent, with roughly 85% bentonite, which gives it a higher optimal moisture content. When water is added to the grout, its density drops, demonstrating that the densest state occurs when it is dry. The volume of soil expands due to the larger molecular size of water, as compared to air, caused a decrease in density. Additionally, the higher thermal conductivity of water, compared to air, resulted in an increased thermal conductivity of the grout. The soil specimen was compacted in six layers with w = 9% and the dry density targeted was around 1.26 g/cm^3. This density represents the loosest state of the dry soil.

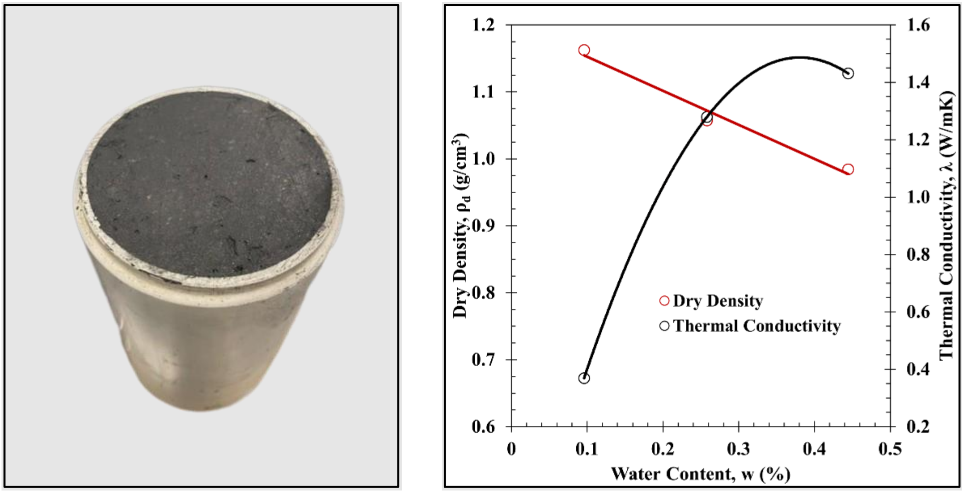

(a) (b)

Fig. 6-1. (a) Grout in a compaction mold and (b) compaction and thermal conductivity curves.

6.2.2 Testing Procedure

The soil column setup consisted of a plastic column with a 25.4-cm inner diameter attached to a perforated PVC plate. Inside the soil cell, there was a 2.54-cm inner diameter HDPE pipe serving as a ground heat exchanger, with a heat flux sensor (HFS-4, Omega Engineering, Inc.) at its midpoint to monitor heat flux at the pipe-grout interface. A total of five type-T thermocouples and five ECH20 EC-5 moisture sensors were inserted at approximately 1, 3, 5, 7, and 9 cm from the pipe center to collect data at various points around the pipe. Temperature data was recorded using the Picolog Recorder, and moisture content was measured with the ZL6 Data Logger. Inside the pipe, an additional type-T thermocouple monitored the water temperature. A dual-needle sensor positioned about 1 cm away from the pipe was used to assess thermal conductivity. This configuration is illustrated by Fig. 6-2, and it includes the model geometry of the testing device, which will be discussed in the *Numerical Analysis* section.

After installing sensors within the soil cell, a 2.54-cm thick geofoam-insulated plastic plate was positioned at both the top and bottom. Water was circulated through the soil column via a temperature-controlled circulator (PolyScience Model SD07R-20-A11B) set to 60°C. For a period of four days, temperature and heat flux measurements were taken every minute, while moisture data was recorded every 5 minutes, and thermal conductivity every 30 minutes.

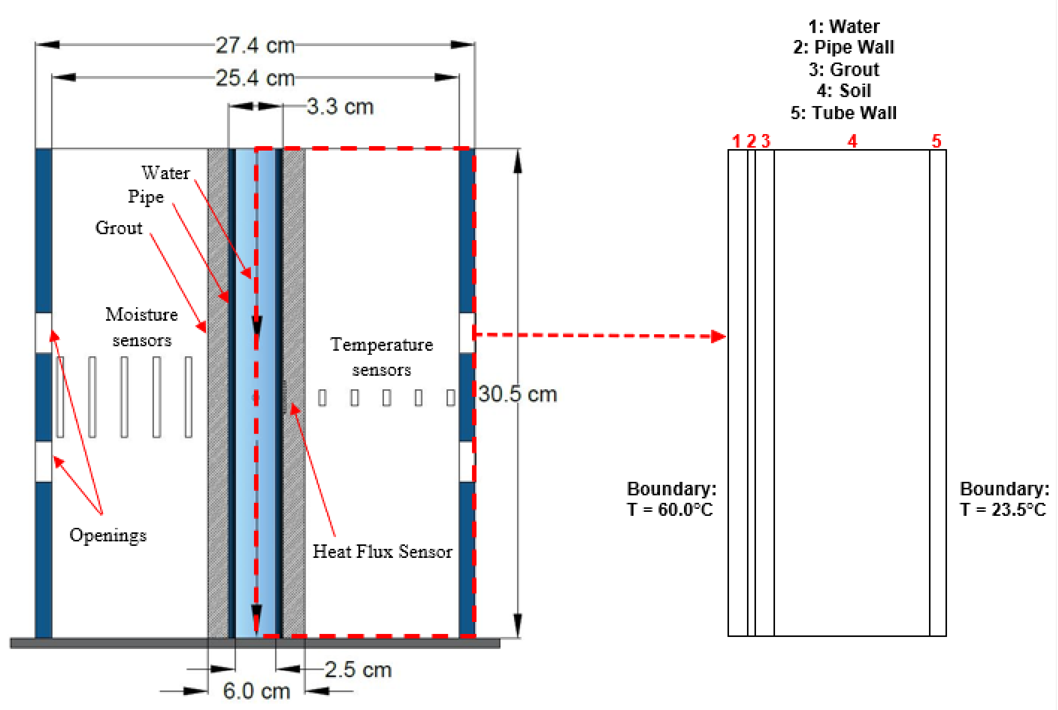

Fig. 6-2. Column testing device set-up and model geometry.

6.3 Numerical Analysis

6.3.1 Mathematical Framework

In this study, COMSOL Multiphysics version 5.3 was used to solve the energy and mass conservation equations (Eq. 1 and Eq. 2). Eq. (1) delineates energy transfer within a porous medium, accounting for heat conduction in solid soil particles, heat convection in pore fluids (liquid water and air), and water vapor phase change. Eq. (2) characterizes the movement of pore liquids, air, and water vapor, using Richard's equation, dependent on factors such as water head potential, temperature gradients, and hydraulic conductivity. Key parameters necessary for solving heat transfer and fluid flow equations include water head potential and hydraulic conductivity.

These parameters are determined based on the soil-water characteristic curve (SWCC), following van Genuchten (1980) model extended by Mualem (1976). Further details of this computational process can be found in the Chapter 3.

$$C_{eq}\frac{\partial T}{\partial t} + \nabla \cdot \left(-\lambda_{eq}\nabla T\right) + C_{eq}\left(q_w \nabla T + q_g \nabla T + q_v \nabla T\right)$$

$$= -L_w \rho_w \nabla q_g - L_w \rho_w \frac{\partial \theta_g}{\partial t} - L_w \rho_w \nabla q_v - L_w \rho_w \frac{\partial \theta_v}{\partial t} \quad (1)$$

$$\frac{\partial \theta_w}{\partial t} + \nabla \times \left(q_w + q_g + q_v\right) = -\frac{\rho_g}{\rho_w}\frac{\partial \theta_g}{\partial t} - \frac{\rho_v}{\rho_w}\frac{\partial \theta_v}{\partial t} \quad (2)$$

where C_{eq}: equivalent volumetric heat capacity (J/m^3·K); T: temperature (K); t: time (s); λ_{eq}: equivalent thermal conductivity (W/m·K); $q_{w,g,v}$: liquid water/air/vapor velocity (m/s); L_w: latent heat of water vaporization (J/kg); $\rho_{w,g,v}$: liquid water/air/vapor density (kg/m^3); and $\theta_{s,w,g,v}$: volumetric liquid water/air/vapor content (m^3/m^3).

6.3.2 Numerical Simulation

Numerical simulations were conducted to predict temperature and moisture distributions in a silty sand surrounding a heated pipe within the column testing setup and to evaluate the impact of grout placement on soil temperature distribution. The analysis was carried out in a 2D axisymmetric space, incorporating five materials in the following order: circulating water, pipe, grout, compacted soil, and column wall (as depicted in Fig. 6-2). Material parameters can be found in Table 6-1. A constant temperature of 60ºC was imposed on the water, while the column wall was held at a steady temperature to mimic ambient conditions. Insulated top and bottom boundaries restricted heat dissipation only radially, with no mass flux at any boundary. The thermal conductance acquired from experiments was applied at the interface between the pipe and the grout.

The soil's thermal conductivity was determined through calibration Kaneza and Yu (2024), while that of the grout was predicted using the model of Sakashita and Kumada (1998). The porosity of soil was 0.527, and that of the grout was 0.723, resulting from a dry density of 0.488 g/cm^3. The low density was due to challenges achieving the target density during compaction, mainly caused by the grout's poor workability under the given moisture content of 36%. In the simulation, the maximum thermal conductivity mentioned earlier (n = 0.550) was used for comparison. Moreover, a simulation of the heat exchange was conducted without using any grout.

Table 6-1. Material properties for simulation.

Parameter	**Value**	**Units**	**Description**
C_g	1000	J/(kg×K)	Specific heat capacity of air
C_p	2000	J/(kg×K)	Specific heat capacity of pipe
C_s	850	J/(kg×K)	Specific heat capacity of soil solids
C_t	880	J/(kg×K)	Specific heat capacity of tube
C_v	1000	J/(kg×K)	Specific heat capacity of vapor
C_w	4200	J/(kg×K)	Specific heat capacity of water
λ_g	0.025	W/m×K	Thermal conductivity of gas
λ_p	0.48	W/m×K	Thermal conductivity of pipe
λ_t	0.13	W/m×K	Thermal conductivity of tube
λ_v	0.025	W/m×K	Thermal conductivity of vapor
λ_w	0.6	W/m×K	Thermal Conductivity of water
ρ_g	1.2	kg/m^3	Density of gas
ρ_p	950	kg/m^3	Density of pipe
ρ_t	1410	kg/m^3	Density of tube
ρ_v	1000	kg/m^3	Density of water

6.4 Results and Discussions

This study investigated temperature variations within the system through experimental and numerical approaches. The experimental method involved heating a soil sample with 9% water content at its center using a heated pipe, and it was conducted both with and without grout surrounding the pipe. In parallel, numerical simulations were carried out for these two scenarios, along with a scenario where the grout's maximum thermal conductivity was considered, and a scenario where there is no thermal contact resistance between the grout and soil. The thermal contact resistance was calculated using the method of Kaneza and Yu (2023). These additional simulations were performed to further assess the impact of the grout and its thermal properties.

Fig. 6-3 illustrates the temperature distribution resulting from a 96-hour heating numerical simulation for all four scenarios. Fig. 6-3(a) offers a broader spectrum of colors, reflecting enhanced heat dissipation and a more evenly spread temperature pattern. Conversely, Fig. 6-3(b) and (c) reveal a marked discrepancy at the external surface of the grout, indicating a disruption caused by thermal contact resistance between the grout and the soil, and leading to a reduction in temperature at this interface. Fig. 6-3(d) demonstrates that the elimination of this thermal contact resistance resolves the disruption but exhibits a shift in the temperature profile shape due to differing properties of the grout and soil.

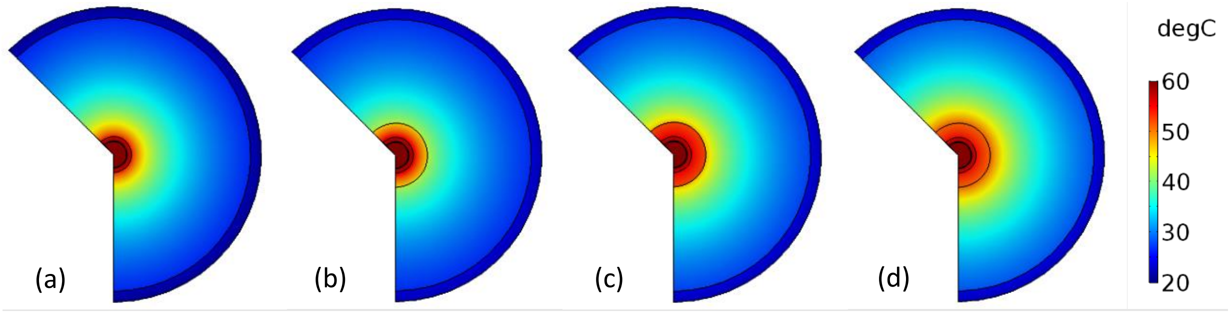

Fig. 6-3. (a) No grout; (b) with grout, lower density; (c) with grout, maximum density; (d) with grout with maximum density, without thermal resistance between grout and soil.

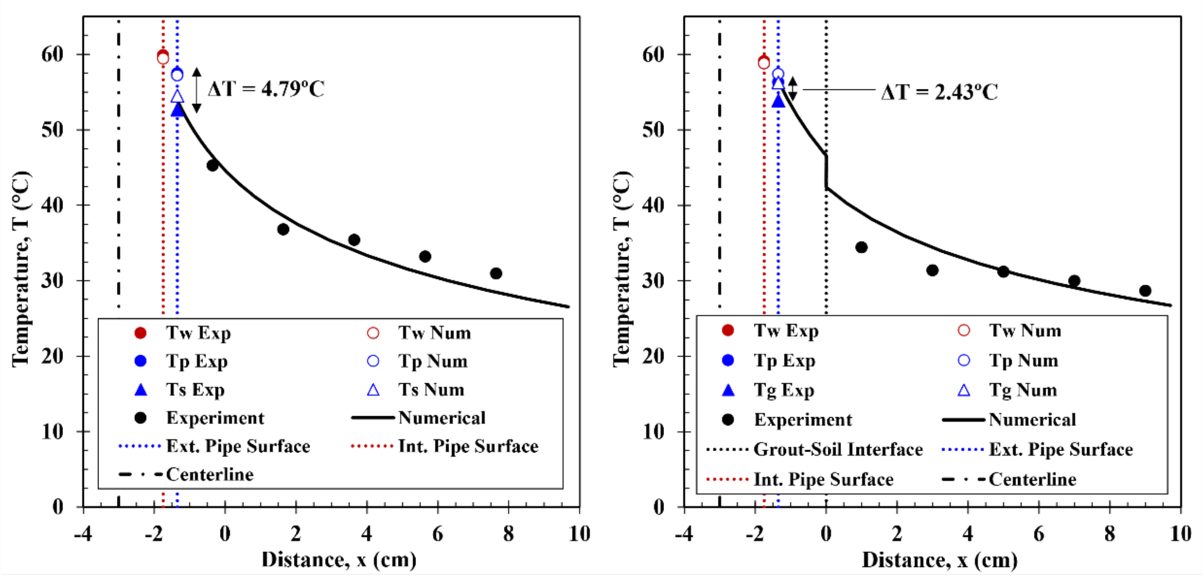

(a) (b)

Fig. 6-4. Temperature distribution of soil (a) without grout; (b) with grout from experiment.

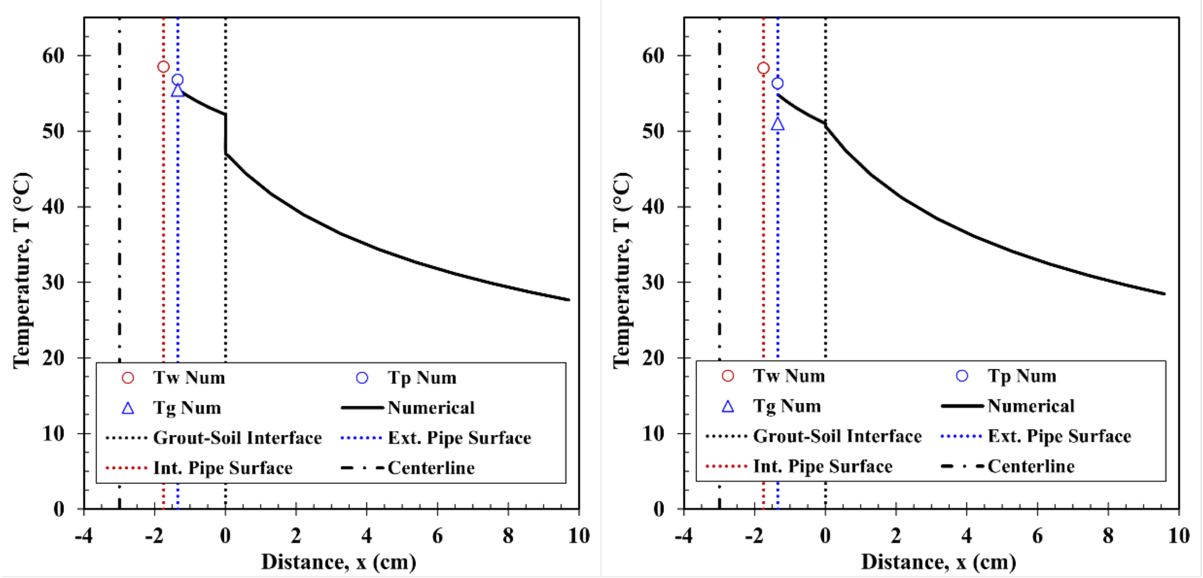

(a) (b)

Fig. 6-5. Temperature distribution of soil and grout at maximum thermal conductivity(a) with thermal contact resistance between grout and soil; (b) without thermal contact resistance between grout and soil.

Figs. 6-4 and 6-5 provide a comprehensive illustration of the temperature distribution, presenting a comparative analysis of experimental and numerical results on the same graph. The grout's maximum thermal conductivity (λ = 1.5 W/m·K) was obtained from the preliminary experimental compaction analysis; this thermal conductivity corresponded to w = 36% and ρ_d = 1.0 g/cm^3, as illustrated in Fig. 6-1. However, in the actual heating test, it was challenging to achieve the 1.0 g/cm^3 dry density during the compaction of the grout mixed with w = 36%, in the 1.35 cm annular space of the soil column. Consequently, a lower thermal conductivity resulted, and two scenarios were developed: scenario 1 (depicted in Fig. 6-4), based on the actual test results, and scenario 2 (depicted in Fig. 6-5), using the maximum thermal conductivity. It's important to note that scenario 2 was not compared to experimental results due to the non-identical thermal conductivity of the grout. When examining the impact of thermal grout, it becomes evident that it limits heat transfer in proximity to the heated pipe. However, as one moves away from the heat source, the temperature distribution is similar, whether with or without the grout. Additionally, it is apparent that increasing the thermal conductivity of the grout results in greater heat transfer to the surrounding soil, while the temperature drop at the grout-soil interface remains relatively consistent. Fig. 6-5 emphasizes the significance of accounting for thermal contact resistance in thermal analyses. As demonstrated, the contact of dissimilar materials can result in a noticeable temperature drop. Failing to consider this resistance could introduce inaccuracies into the analysis, emphasizing the critical need for its inclusion in thermal studies. Finally, Fig. 6-6 captures the numerical comparison of the four scenarios, highlighting how the introduction of grout, variations in its thermal conductivity, and the accounting for contact resistance at material interfaces can all potentially give rise to misinterpretations if not subjected to thorough investigation.

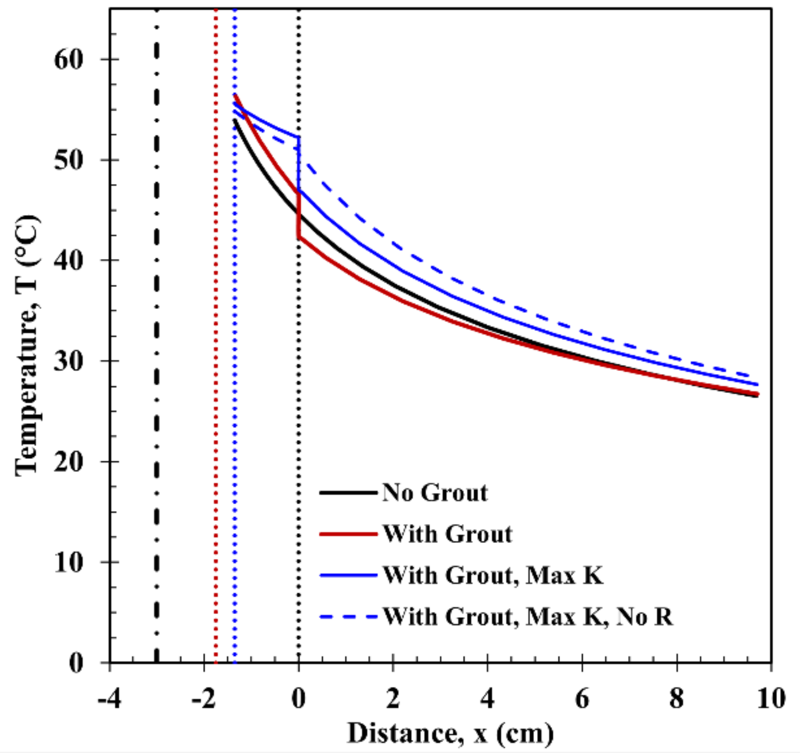

Fig. 6-6. Comparison of the temperature distribution for all four investigated scenarios.

6.5 Conclusion

This study aimed to investigate temperature distribution in a silty sand through experimental and numerical approaches. The soil was subjected to heating using a heated pipe with varying scenarios, including the presence or absence of grout, variation of thermal conductivity and thermal contact resistance of the grout. The presence of grout was observed to significantly affect heat transfer, particularly near the heated pipe, limiting heat dissipation. However, at farther distances from the heat source, temperature distribution remained consistent regardless of grout use. The results highlight the critical role of considering thermal contact resistance, as its omission can introduce analysis inaccuracies. This study emphasizes the importance of conducting comprehensive investigations into factors like grout placement, thermal conductivity variations, and material interfaces in thermal studies to prevent potential result misinterpretations.

6.6 References

Al-Khoury, R. 2011. *Computational Modeling of Shallow Geothermal Systems (Multiphysics Modeling)*.

Bidarmaghz, A. 2014. “3D Numerical Modelling of Vertical Ground Heat Exchangers.” The University of Melbourne.

Bourne-Webb, P. J., J. D. de Sousa Figueira, and T. M. Bodas Freitas. 2020. “On the resistance to heat flow across soil-structure interfaces.” *Energy Build*, 228. Elsevier Ltd. https://doi.org/10.1016/j.enbuild.2020.110488.

Cecinato, F., R. Piglialepre, F. A. Loveridge, and D. Nicholson. 2016. “Numerical analysis of thermal cycling during a multi-stage energy pile thermal response test.” *Energy Geotechnics - Proceedings of the 1st International Conference on Energy Geotechnics, ICEGT 2016*, 593–599. CRC Press/Balkema.

Christodoulides, P., G. Florides, and P. Pouloupatis. 2016. “A practical method for computing the thermal properties of a Ground Heat Exchanger.” *Renew Energy*, 94: 81–89. Pergamon. https://doi.org/10.1016/J.RENENE.2016.03.035.

van Genuchten, M. T. 1980. “closed-form equation for predicting the hydraulic conductivity of unsaturated soils.” *Soil Sci. Soc. Am. J.*, 44(5): 892–898.

Kreith, F., R. M. Manglik, and M. Bohn. 2010. *Principles of Heat Transfer*.

Lamarche, L., and B. Beauchamp. 2007. “A new contribution to the finite line-source model for geothermal boreholes.” *Energy Build*, 39 (2): 188–198. Elsevier. https://doi.org/10.1016/J.ENBUILD.2006.06.003.

Lamarche, L., S. Kajl, and B. Beauchamp. 2010. “A review of methods to evaluate borehole thermal resistances in geothermal heat-pump systems.” *Geothermics*, 39 (2): 187–200.

CNR-Istituto di Geoscienze e Georisorse. https://doi.org/10.1016/j.geothermics.2010.03.003.

Loveridge, F. 2012. *The Thermal Performance of Foundation Piles used as Heat Exchangers in Ground Energy Systems*.

Loveridge, F., and W. Powrie. 2014. “2D thermal resistance of pile heat exchangers.” *Geothermics*, 50: 122–135. Pergamon. https://doi.org/10.1016/J.GEOTHERMICS.2013.09.015.

Man, Y., H. Yang, N. Diao, J. Liu, and Z. Fang. 2010. “A new model and analytical solutions for borehole and pile ground heat exchangers.” *Int J Heat Mass Transf*, 53 (13–14): 2593–2601. Pergamon. https://doi.org/10.1016/J.IJHEATMASSTRANSFER.2010.03.001.

Mualem, Y. 1976. “A new model for predicting the hydraulic conductivity of unsaturated porous media.” *Water Resour Res*, 12 (3): 513–522. https://doi.org/10.1029/WR012i003p00513.

Omer, A. M. 2008. “Energy, environment and sustainable development.” *Renewable and Sustainable Energy Reviews*, 12 (9): 2265–2300. Pergamon. https://doi.org/10.1016/J.RSER.2007.05.001.

Sakashita, H., and T. Kumada. 1998. “Heat Transfer Model for Predicting Thermal Conductivity of Highly Compacted Bentonite.” *Journal of the Atomic Energy Society of Japan / Atomic Energy Society of Japan*, 40 (3): 235–240. https://doi.org/10.3327/jaesj.40.235.

CHAPTER 7. SUMMARY AND CONCLUSIONS

7.1 Summary and Conclusions

This study aimed to comprehensively evaluate the coupling of thermo-hydro (TH) and thermo-hydro-mechanical (THM) processes using a modified soil column testing device. The research involves subjecting soil specimens with varying gradations to static heating and cooling. Additionally, a mock-up model of a geothermal heat exchanger, specifically an energy pile surrounded by unsaturated soil, was designed for heating tests to simulate field conditions and investigate coupled TH processes. The ultimate goal is to gain insights into the complex interactions between thermal, hydraulic, and mechanical processes in soil systems, with practical applications for understanding energy pile behavior and optimizing ground heat exchanger performance. The study was organized into four tasks to achieve its objectives:

- Analyzing the coupled THM behavior of unsaturated soil in a modified soil cell through numerical and experimental approaches.

- Evaluating the impact of gravity on moisture migration under different directions of thermal gradient.

- Determining thermal contact resistance at the interface of a heated pipe surrounded by unsaturated soil and assessing how moisture levels and soil density influence this critical parameter.

- Assessing the influence of applying thermal ground around a ground heat exchanger using a combination of experimental and numerical methods.

Several key findings and conclusions emerged from this research.

In the first task of the dissertation, the study focused on the behavior of sandy silt and silty sand under steady-state temperature conditions. Differences in water movement and moisture flux stabilization were observed, with drier soils requiring more time to reach thermal equilibrium. Experimental measurements and numerical predictions showed some disparities, potentially attributed to material property variations and thermal contact resistance at interfaces. The study highlighted the importance of considering variations in thermal conductivity and moisture retention in numerical models.

The second part of the research involved monitoring volumetric liquid water, air, and water vapor content over 96 hours. The study found that moisture profiles differed between sandy silt and silty sand, mainly due to variations in thermal conductivity and moisture retention. Despite a few discrepancies, the numerical model generally aligned with experimental results, providing insights into fluid flow variations in unsaturated soil.

Soil stress and deformation predictions under various conditions revealed that confined soil specimens experienced high stresses, with sandy silt exhibiting greater stress than silty sand. Unexpectedly, lower moisture content soils showed larger radial and total displacements, emphasizing the complex interplay between moisture, stress, and thermal expansion coefficients.

The second task of this dissertation explored moisture migration in unsaturated sand columns under heating conditions. The research highlighted the role of gravity in moisture movement, influencing temperature profiles and the concavity or convexity of the temperature profile shape. Changes in fluid density and viscosity were identified as factors influencing moisture migration, with gravity affecting the direction and magnitude of moisture movement.

The third task focused on thermal contact resistance between a heated pipe and surrounding soil. Dense soils exhibited higher thermal conductivity, resulting in minimal thermal contact resistance. Moisture migration away from the heat source and its impact on temperature profiles were studied, emphasizing the significance of soil moisture levels in thermal behavior. Experimental and numerical evaluations of thermal contact resistance showed consistent trends, especially in dry soil conditions.

For the fourth task, the study investigated temperature distribution in silty sand using experimental and numerical approaches. The presence of grout significantly affected heat transfer near the heated pipe, highlighting the importance of considering thermal contact resistance in thermal studies. The results emphasized the need for comprehensive investigations into factors such as grout placement, thermal conductivity variations, and material interfaces to ensure accurate analyses.

In conclusion, this dissertation provides valuable insights into the complex interrelationships between thermo-hydro-mechanical behavior in soil. The findings contribute to a deeper understanding of soil responses to heating under various conditions, offering implications for geotechnical and environmental engineering applications. The research underscores the importance of considering factors like material properties, moisture levels, and thermal contact resistance in numerical models and experimental studies to enhance the accuracy of soil behavior predictions.

7.2 Recommendations

This section proposes several recommendations aimed at improving the experimental and numerical investigations and analyses conducted for the examination of coupled thermo-hydro

(TH) and thermos-hydro-mechanical (THM) processes in unsaturated soil:

- Enhancing the characterization of soil properties is advisable to achieve more precise predictions in numerical simulations.
- It is essential to conduct tests on supplementary soil samples with diverse grain sizes, various moisture content levels, and multiple thermal gradients. This will serve to validate this research findings, emphasizing the significance of grain size, initial moisture content, and the magnitude of thermal gradient as crucial factors influencing moisture migration in unsaturated soil.
- Conducting extensive calibration analyses is crucial to thoroughly assess the performance of measuring devices used in experimental programs. Additionally, repeatability tests should be employed to ensure the reliability and precision of measurements.
- A final recommendation suggests a thorough evaluation of additional soil parameters and thermal properties, such as matric suction and other strength parameters. This comprehensive analysis aims to gain a deeper understanding of all the mechanics influencing the coupled thermo-hydro-mechanical processes.